Combined quantum/classical modelling of chemical reactions in enzymes and solution

Turner, Alexander J.

Award date:
1997

Awarding institution:
University of Bath

Combined Quantum/Classical Modelling of Chemical Reactions in Enzymes and Solution

by Alexander J Turner

ProQuest LLC
789 East Eisenhower Parkway
P.O. Box 1346
Ann Arbor, MI 48106-1346

Combined Quantum/Classical Modelling of Chemical Reactions in Enzymes and Solution

Submitted by Alexander J Turner
for the degree of PhD
of the University of Bath
1997

Table of contents:

Summary 6

1. Introduction 7

1.1 Unifying hypothesis 12

2. Definitions 13

2.1 Constants 14

3. Literature review 15

3.1 Structure of reviews 15

3.2 Review of literature pertaining to the thesis as a whole 15

3.2.1 Outline 15

3.2.2 Stationary points 16

3.2.3 Intrinsic reaction co-ordinates 16

3.2.4 Experimental / theoretical comparison using isotope effects 17

3.2.5 Dynamics of rare events and variational transition state theory 18

3.2.7 Conventional transition state theory and potential energy stationary points 19

3.2.8 The use of qm/mm methods 20

3.2.9 State of the art 21

3.2.10 Other modelling 27

3.2.11 Computation of partial atomic charges 27

3.2.12 Optimisation and saddle search algorithms 28

4. Overview of computational experiments 34

4.1 Materials 36

4.2 Table of software contributions 37

5. Computation of point charge distributions by direct fitting to a qm/mm gradient function 40
5.1Orientation to thesis as a whole 40
5.2 Introduction 40
5.3 Method 42
5.3.1 Constrained fitting 43
5.3.2 Off centre point charges 44

6. Solvation of small organic molecules in water 46
6.1 Goals 46
6.2 Introduction 46
6.3 Method 47
6.4 Results 51
6.5 Conclusion 53
6.6 Extension of the technique 54
6.6.1 Non-water and mixed solvents 54
6.6.2 Solvating large solutes 56

7. Ab initio qm/mm modelling 57
7.1 Goals 57
7.2 Introduction 57
7.3 Method 59
7.4 Future extension of the method 62
7.5 The CHARMM semi-empirical qm/mm model 63

8. Computation of fractionation factors for small organic molecules in aqueous solution 65
8.1 Goals 65
8.2 Introduction 65
8.3 Method 67
8.3.1 Initial solvation 67
8.3.2 *Ab initio* optimisations 68
8.3.3 Computation of hessians 69
8.3.4 Comparison of methods 70
8.3.5 Computation of fractionation factors 71
8.3.6 Analysis of electronic polarisation 72
8.3.7 Dihedral effects 73
8.4 Results and discussion 73

8.5 Conclusions 83
8.6 Suggestions for further work 83

9. Methods for computing the qm/mm intrinsic reaction co-ordinate 85
9.1 Goals 85
9.2 Introduction 85
9.2.1 Extending the P-RFO method to thousands of degrees of freedom 91
9.3 Method 94
9.4 Suggestions for further work 100

10. Extension of ab initio qm/mm methods to IRC calculation 102
10.1 Goals 102
10.2 Introduction 102
10.3 Method 103
10.3.1 Construction of a three sub-set qm/mm model 103
10.3.2 Optimisation and IRC techniques using the three sub-set model 104
10.3.3 Improving saddle point location 106
10.5 Suggestions for further work 107

11. Location of transition states in aqueous organic reactions using semi-empirical and ab initio qm/mm modelling 109
11.1 Goals 109
11.2 Introduction 109
11.3 Method 110
11.3.1 AM1 COSMO in detail 110
11.3.2 AM1 qm/mm in detail 111
11.3.3 *Ab initio* qm/mm in detail 113
11.3.4 Gas phase calculations 114
11.3.5 Reduced mass effects 114
11.4 Results and discussion 116
11.5 Conclusions 123
11.6 Suggestions for further work 124

12. QM/MM modelling of lactate dehydrogenase 125
12.1 Goals 125
12.2 Introduction 125
12.3 Method 128
12.4 Results and discussion 135
12.5 Conclusions 143
12.6 Suggestions for further work 146

13. General discussion 147
13.1 Unifying conclusion 151

Appendices:

A. A method for auto-generation of redundant and non-redundant valence co-ordinates 152

B. GRACE 159

References 167

Acknowledgements 183

Summary

Combined Quantum/Classical modelling (qm/mm) is a computational method which allows calculations of chemical properties for very large systems. This thesis develops methods to extend quantum mechanical calculations, which presently can treat only tens of atoms, to qm/mm calculations for models containing thousands of atoms.

The overall target is to model chemical reactions in enzymes and solution by considering only potential energy and vibrational contributions to enthalpy. The purpose of such modelling is to give chemical information directly. It also forms a starting point for future development towards computation of free energy properties by qm/mm methods.

A novel method for generating solvation structures is presented. Included with this is an algorithm for approximation of simple coloumbic equations to quantum-mechanical electrostatic interactions. These methods are used to facilitate the computation of isotopic fractionation factors for hydrogen bound to carbon, for small aqueous organic molecules. This modelling is used to develop the consideration of vibrational-free-energy terms.

Partial-Rational-Function-Operator saddle point searching is extended to systems with thousands of atoms. This technology is used to locate first order saddle points in semi-empirical and *ab initio* based qm/mm models of nucleophilic substitution of halo-methane. This work involves novel methods for accelerating *ab initio* qm/mm calculations and intrinsic reaction co-ordinate following.

Saddle point searching and analysis of intrinsic reaction co-ordinates are used to model lactate dehydrogenase with semi-empirical-based qm/mm techniques. The balance of electrostatic and structural aspects of enzymic catalysis is investigated for the inter-conversion of pyruvate to lactate using this enzyme.

The programming methods used to facilitate these developments are discussed in the appendices. This gives a brief outline of the new code, GRACE, which has been developed for this project.

Chapter 1 - Introduction

Computational chemical modelling (Computational chemistry) attempts to improve understanding of known experimental results and to predict the behaviour of unknown chemical systems.

Many chemical properties are hard to probe by experiment, or the results of such probes are difficult to interpret. Enzymology is an area rich with such examples. A molecular understanding of enzyme catalysis can lead to better artificial catalysts. Modelling of the atom by atom nature of enzyme catalysed reactions can massively improve this molecular understanding. Such insight can also be directed toward molecular biology and pathology. A computer model that accurately describes these, and other, hard-to-probe properties is highly desirable.

Large benefits come from predicting the results of experiments. Such prediction can improve experimental design. For instance, prediction of the effect different solvents will have on reaction rate can prevent wasted laboratory time trying unproductive solvents. Accuracy of prediction by computational chemistry is directly reflected in improved laboratory productivity.

For this discussion, the real chemical system that is being modelled will be called the target. Computational chemistry must make many approximations when attempting to model the target.

It is generally believed that a complete solution to the known quantum mechanical equations, for a chemical system, will completely describe its behaviour. This is not much help because to completely solve the quantum mechanical equations, even for a trivial target, is not possible. This is due to the extremely large amount of computer time required.

One way to overcome this barrier is to solve these equations approximately. In general, the less approximate the solution, the more computational resource is required. A very approximate method may be extremely fast, but lack the accuracy to predict chemical phenomena. A much less approximate method may produce useful results but be out of reach of contemporary computers.

A complementary method of reducing computational cost is to model a chemical system that resembles the target but is much simpler. This may often allow use of less approximate solutions to the quantum chemical problem. A model system that has fewer atoms and fewer electrons may be orders of magnitude faster than one with the full system.

Most of chemistry happens in systems with hundreds or thousands of atoms. *In vacuo* phenomena (in the presence of no other molecules or atoms) represent only a tiny proportion of those observed in chemistry. Simple organic reactivity is usually mediated by solvents. Enzymes contain thousands of atoms and also react in and interact with solvents. Even industrial catalysis involves the interaction of massive numbers of atoms.

Two criteria for judging computational chemistry can now emerge.. There is the similarity between the approximate and exact quantum mechanics and the similarity between the modelled system and the target.

Historically, computational chemistry has addressed these two criteria separately. Two methodological concepts have been generated: Quantum Mechanics and Molecular Mechanics.

Molecular Mechanics:

Molecular mechanics breaks chemical energy down into separate (independent), simple terms. Once a range of terms has been devised, classical mechanical equations are used to represent the energetic contribution for each term. Molecular mechanics approximates the quantum mechanical equations to classical mechanical ones. To make the best match between the two, the classical equations are parameterised so their results reproduce experiment or quantum mechanical results. The resulting set of equations and parameters is referred to as a molecular mechanics potential.

Experience has shown that different terms are important over different inter-atomic distances. High energy terms, like bonding terms, are restricted to short distances whilst lower energy terms, like the electrostatic term, may be effective at long range.

Molecular mechanics is a very fast method of approximating the quantum mechanical equations. Almost more importantly, molecular mechanics can achieve a computational cost that varies almost linearly with the size of a system. This means that the computational cost for a system will double as the number of atoms doubles. This is a very important property. If computational cost scales as a power of the size of system greater than 1, a practical upper limit to the system size rapidly emerges .

The ability of molecular mechanics to scale linearly with size is because *all* terms are truncated after a certain inter-atomic distance. All inter atomic interactions are ignored if the inter atomic distance exceeds some limit.

The development of reliable, inexpensive potentials for molecular mechanics has attracted a lot of attention. As a result, the computation of the energy and its derivatives (gradient, forces etc.) is now very fast, even for systems with

thousands of atoms. Such a fast energy/gradient method has allowed the development of modelling methods mimicking realistic molecular movement and statistical energy distributions. Such methods include Molecular Dynamics (MD) and Monte-Carlo (MC).

Quantum Mechanics:

Not all chemical properties lend themselves to being modelled by molecular mechanics. The most important of these is reactivity. Other examples include inductive effects on vibrations and solvation effects on electronic delocalisation. Molecular mechanics usually lacks terms to handle redistribution of electron density. Even the more complex methods, which contain electrostatic polarisation terms, are still unable to model the electronic changes that occur during bond formation and bond breaking..

Such properties can be modelled by using quantum mechanical methods. The speed of quantum mechanical methods varies enormously. One of the fastest is the semi-empirical molecular orbital method MNDO (Modified Neglect of Differential Overlap, ref. 21). With this method, some of the quantum mechanical properties are approximated by parameters who's values are set to make calculated results mimic experiment. Even this method is orders of magnitude slower than molecular mechanics.

Other methods can be very much more expensive indeed, especially those which scale as the third, fourth or even fith power of the chemical system's size. Even despite the high computational cost, they may be desirable as the only way to get reliable results.

Hybrid quantum mechanics / molecular mechanics:

Hybrid quantum mechanics / molecular mechanical (qm/mm) modelling aims to combine the strengths of both the quantum mechanical and molecular mechanical methods.

A range of such methods can be proposed. The fastest is a two-region approach. A quantum mechanical core is surrounded by a standard molecular mechanics potential and several interaction terms join the two regions. Those atoms that are most influenced by electronic redistribution, in the property under investigation, are included in the quantum mechanical core. The rest of the atoms are placed in the molecular mechanical surroundings.

In this model, an increase in the size of the system generally involves increasing the size of the molecular mechanics component. By constructing the interaction terms between the quantum and molecular mechanical parts correctly, distance truncation of the inter-atomic interactions can be introduced. Such a model scales in the same way as a standard quantum mechanical method as the core size is increased, and like a standard molecular mechanical method as the surroundings size is increased.

At the other end of the range are continuous approaches. At large interatomic distances, the coulombic term in quantum mechanical methods is approximated by a classical term. Once the chemical system size has grown sufficiently big for these approximations to be introduced, the cost of increasing the system size can be made to approach being linear by eventually reducing the terms to zero.

In molecular mechanics the effects of entropy and thermal motion are routinely computed. A very large number of energy calculations are made and statistical properties like Gibbs free energy and averaged atomic interactions are computed.

Despite its near linear scaling, qm/mm modelling is still very much slower than pure molecular mechanics. This makes these methods, that require many energy calculations, extremely expensive computationally.

In small molecule studies using quantum mechanics, several modelling tools have been developed that do not explicitly perform atomic motion. The only treatment of motion is by following thermodynamically reversible pathways or as vibrational information about a single geometry. These can be broadly grouped into minimal-sampling methods.

By applying the large system size ability of qm/mm modelling to the relatively low computational cost of these 'minimal-sampling' methods, computational chemistry of electronic effects in macro and poly* molecular systems may be achieved.

Perhaps the most exciting possibility is to use the information obtained from the zero temperature methods to parameterise or initialise low cost methods (like semi-emprical qm/mm or molecular mechanics) to give an estimation of the entropy contributions. In this way the Gibbs free energy of entire reactions may be computed.

1.1 Unifying hypothesis:

Valuable insights into chemical reactivity of poly/macro-molecular systems can be obtained by minimal-sampling methods, based on a range of quantum/molecular mechanical modelling schemes.

** Poly molecular: A system with many discrete molecules, such as a solute in aqueous solution.*

Chapter 2 - Definitions

For the sake of clarity, some definitions of terms and universal constants are given before the bulk of the thesis.

Gradient vector or matrix:

The vector or matrix of first partial derivatives of a function with respect to a vector or matrix of orthogonal variables.

Gradients and rms gradient:

Where the gradient is a vector, it may be referred to as the 'gradients' or the 'gradient'. 'rms gradient' refers to the root mean square (rms) of the gradient vector or matrix.

Hessian:

The matrix of second partial derivatives of a function with respect to a matrix or vector of orthogonal variables.

Curvature:

The curvature refers to the partial derivatives of order greater than 1 of a function with respect to a vector or matrix of orthogonal variables. Consideration of the hessian as being the curvature is only an approximation.

Vibrational mode:

In the context of studies of molecular vibrations in this thesis, a 'mode' refers to an eigen vector of the hessian of potential energy with respect to geometry, with its associated eigen value.

2.1 Constants:

The constants employed by GRACE (the novel code by which the majority of this work was performed) are uniform with CHARMM24(30) and with Gaussian94(31) and CADPAC6(32) where necessary.

N_a	$= 6.022045 \times 10^{23}$		(Avagadro's number)
ξ	$= 8.85419 \times 10^{-12}$	Fm^{-1}	(Permittivity of free space)
1 kcal	= 4184.0	J	
1 Hartree	= 2625.499748	kJ/mol	
1 amu	$= 1.6605655 \times 10^{-27}$	kg	
1 Ångstrom	$= 1.0 \times 10^{-10}$	m	
1 Bohr	= 0.529177249	Ångstrom	
c	$= 2.99793 \times 10^{8}$	m/sec	
KBoltz	$= 1.380658 \times 10^{-23}$	JK^{-1}	
π	= 3.141592653589793		

All other constants and conversions are derivations of these.

Note: There is a discrepancy, in the 5^{th} decimal place, between **c** in Gaussian 94 and **c** in CHARMM24. This is not considered to be numerically important for this work.

Chapter 3 - Literature review

3.1 Structure of reviews:

To preserve a logical structure to this document as a whole, the literature review is divided into sections. The purpose of the initial section, which follows immediately, is to provide a background for the thesis as a whole. Reviews giving detail behind each new piece of work will be presented in association with that work.

3.2 Review of literature pertaining to the thesis as a whole:

3.2.1 Outline:

- Stationary points

  Potential energy surfaces, minima and saddle points
- Intrinsic reaction co-ordinate

  Initial discussion of the nature of the intrinsic reaction co-ordinate
- Experimental / theoretical comparisons using isotope effects

  The value of isotope effects to this work.
- Dynamics of rare events and variational transition state theory

  Going beyond the scope of research in this thesis to discuss more elaborate uses of intrinsic reaction co-ordinate information.
- Conventional transition state theory and potential energy stationary points

  The method of isotope effect evaluation used in the thesis as a whole.
- Qm/mm methods

  Outline of qm/mm methods and some alternatives.
- State of the art

  Recent publications in qm/mm modelling of chemical systems.
- Computation of partial atomic charges

  Methods for finding atomic/molecular charge distribution.

- Optimisation and saddle point searching

  The background to the developments that are described in this work.

3.2.2 Stationary points:

All the modelling in this thesis is aimed towards the location and characterisation of stationary points on a potential energy surface and the characterisation of the valleys that connect them. An ***n***-dimensional potential energy 'hyper surface' represents the potential energy of a chemical system as a function of its ***n*** geometrical degrees of freedom(1). This defines the potential energy of a chemical system for any complete description of its geometrical co-ordinates.

The words 'stationary point' are from the mathematical definition 'a point at which the first derivative is zero'. When the normal of the gradient vector of the potential energy with respect to the geometrical co-ordinates is zero (*i.e.* the first derivative is zero), the point on the potential energy surface defined by those co-ordinates is a stationary point. In computational chemistry terms, a stationary point is a point on the potential energy surface at which the gradient is zero.

The most interesting stationary points are minima, where the curvature of the surface is positive in all directions, and first order saddle points, where the curvature is negative in one direction. A consequence of a Boltzmann distribution of energy is that energy minima have the greatest significance for chemical equilibrium properties and first order saddle points have the greatest significance for the properties of reactions(2).

3.2.3 Intrinsic Reaction Co-ordinate:

From the minima and saddle points it is a simple matter to compute the Intrinsic Reaction Co-ordinate (IRC) (4,5). This represents the reaction path from the

transition state to products and to reactants, produced under conditions of thermodynamic reversibility(3).

The value of the IRC is especially great when considering reactions occurring at biological temperatures (273-373 K). At these temperatures chemical reactions often resemble the reaction that would occur if the system was thermodynamically reversible (*i.e.* occured infinitely slowly). This is especially true as the system approaches the saddle point. The excess energy is usually so low, that the system 'creeps up' the IRC and over the saddle point. This lack of excess energy allows the geometry to adapt to the changes in the direction of the IRC and so the system follows the bottom of the IRC valley(8).

The IRC is a potential energy function of geometry and contains no contribution from thermally induced motions (vibrations, rotations and translations). Once the reversible reaction path has been found, then contributions resulting from motion can be included. As these contributions are added in, a complete picture of chemical reactivity can be built up.

3.2.4 Experimental / theoretical comparisons using isotope effects:

To obtain a complete picture of chemical reactivity, a stepwise approach can be adopted. At each step, there is a benefit to having a link back to experimental data to investigate the validity of the modelling method being proposed. In this thesis, isotope effects have been used as the major link back to experiment. The reason for this is that these effects reflect bonding changes that are related to electronic structure and so are very revealing about the quality of a model. Another good reason for using isotope effects comes out of the concept of the transition state. If one considers the transition state to be the point of highest free energy along a reaction path from reactants to products, the kinetic isotope effects

(KIEs) for the reaction can be seen as an indication of the electronic and geometric structure of that transition state (13).

Isotopic substitution may affect both the equilibrium constant 'K' and the rate constant 'k' for a reaction. Equilibrium isotope effects (EIEs) are a measure of the change in ΔG for reactions of isotopomeric species. KIEs must be viewed by considering not only the probability of a system having the correct geometry and energy to pass over the reaction barrier, but also the correct motion. This can been seen from the kinetic consideration of chemical reactions (8,10).

If one considers that the maximum point in the free energy path between reactants and products is dominated by the position of the saddle point on the potential energy surface, then the computation of the kinetic isotope effect and elucidation of transition state structure becomes much simpler. Also, if one considers that the minimum potential energy structure is representative of the free energy minima of reactants or products then EIEs can be computed by characterisation of the potential energy minimum structures. It is this approach which has been utilized in the work.

3.2.5 Dynamics of rare events and variational transition state theory:

Before discussing the above approximation in more detail, it is worth discussing the value of the IRC to less approximate methods of attaining KIEs. A much better consideration of the true transition state can be obtained via Variational Transition State Theory (6,7,8). In this approach, the maximum free energy point along the free energy reaction co-ordinate is computed. The simplest method requires that a harmonic approximation to the vibrational structure(11) of the system is computed along the IRC and this can be used to compute the vibrational contribution to free energy. In the gas phase, the contributions to the free energy from translation and rotation must also be considered. For systems which have a

relatively low barrier to reaction (ΔPotential Energy < ~5kT) it has been suggested that variational transition state methods are essential (12).

The ultimate goal of the computational model is to describe all the contributions to the chemical reaction. A major step along this route is now being taken with the 'dynamics of rare events' approaches (9). A Newtonian mechanical approximation to molecular motion is introduced into the model. To make the amount of computational time required to observe a reaction possible, the dynamic motion of the system is biased to follow a pre-determined path. At present it would appear that by far the most appropriate path to follow is the IRC of the reaction.

The equilibrium isotope effect equivalent of the 'dynamics of rare events' is unconstrained free energy perturbation theory (14).

Whilst variational transition state theory and the dynamical approaches are desirable, they require much more computational time than the methods discussed below.

3.2.6 Conventional Transition state theory and potential energy stationary points.

The approach adopted in this thesis is as follows:

Given a point on the potential energy surface one can compute contributions to the free energy from other terms by using the ideal gas, rigid-rotor, harmonic-oscillator approximation (15). Most chemical phenomena under investigation do not take place in these conditions. It would appear that in many cases these approximations will produce reliable results, even where the system under investigation is far from an ideal gas (16,17).

For the computation of an EIE, all that is required is the hessian matrix and geometry at a minimum on the potential energy surface representative of reactants and the same for products. For the computation of a KIE the same is required for the reactants, and a hessian and geometry is required for the saddle point of the IRC. To allow for tunnelling corrections to a KIE, an estimate of the difference in potential energy between reactants and transition state is also required.

3.2.8 The use of qm/mm methods:

As discussed in the introduction, the advantage of the qm/mm method is that it gives access to quantum mechanical properties in systems with thousands of atoms. There are some other methods which attempt to achieve this in a near quantum mechanical way (18) or by taking advantage of the sparse nature of the quantum mechanical terms in large systems to allow full quantum mechanical treatment (19). Such methods are applicable to the *ab initio* (20) and semi-empirical (20,21) quantum mechanical methods. The method of approximating the long-range coulombic interactions to a multipole expansion of the Gaussian functions in DFT theory (18a) can be viewed as a qm/mm approach in that this expansion is into a classical interaction term. It is this concept that is alluded to in the introduction. In all that follows, any reference to qm/mm will be to a quantum core and molecular mechanics environment system, not to such methods as that of ref. 18a.

In this work, the qm/mm approach was chosen over the other methods because of its low computational cost. Especially at *ab initio* levels of quantum mechanical theory, qm/mm approaches remain much more tractable for poly- and macro-molecular systems.

The general approach for coupling the qm and mm terms was laid down by Field, Bash and Karplus (22). This was a development from the seminal paper by

Warshel and Levitt (23). A detailed description of the coupling methods employed will come in chapter 7 of the thesis.

3.2.9 State of the art:

There are 3 basic approaches to qm/mm modelling being employed at present: (1) Minimum region MD and MC; (2) externally derived path following and grid searching; (3) small system energy minimisation. Each area will be discussed in turn.

Minimum region MD and MC.

MD is molecular dynamics, where Newton's laws of motion are applied to the potential energy surface. This yields a lot of information, including thermodynamic properties like free energy differences. MC is Monte Carlo, which may also be used to compute free energy. The range of other properties that can be modelled by MC is much smaller. The advantage of MC is that the computational burden in terms of program complexity and CPU time is generally smaller to yield a given property.

There have been a number of papers published recently discussing the use of MC and MD methods in evaluating the quality of the qm/mm method itself. The effects of the phase change from gas to liquid upon the vibration spectrum of methanol were investigated by Laaksonen et al (24). Periodic boundary conditions were used to mimic bulk methanol. Just one methanol molecule was treated by the Hartree-Fock qm method. Molecular dynamics was used to yield the liquid phase vibrations. By fourier-transforming the motion of the quantum mechanical atoms, the vibrational spectrum for different qm/mm interaction potentials was investigated. This work is very informative as to the importance of the electrostatic perturbation of the quantum-mechanical system by its molecular mechanics environment. The conclusions would appear to be that for proper

hydrogen bond treatment, the electrostatics of the mm molecules must be computed by inclusion into the quantum mechanical electron integrals.

M. F. Ruiz-Lopez *et al.*(25) have used MC to simulate liquid water. A similar system was used to that of Laaksonen, with periodic boundaries and one water treated by Density Functional Theory quantum mechanics. One important aspect of this paper is that it investigates the distance over which it is necessary to include the electrostatic perturbation that was shown to be important in Laaksonen's work. It is demonstrated that for liquid water the error involved in ignoring the polarisation of the qm water by mm waters at distance greater than 5Å is significantly less than other sources of error in the MC simulation. It also contains comparisons of the radial distribution functions of molecular mechanics waters around a single quantum mechanics water. This shows that the qm/mm potential is at least as good as the pure molecular mechanics potential.

J. Gao (26) has been very active in the last two years. This paper extends the use of MC to solvent/solute interactions. The relationship between qm/mm and *ab initio* qm hydrogen bond strengths is computed using free energy perturbation theory. This paper also looks at the size, in energetic terms, of the solvent's polarisation of the solute. The results show this represents up to 20% of the electrostatic energy change on solvation for a number of alcohols, ketones and nucleic acids in water

Work of this type is essential for an accurate understanding of qm/mm models whilst also improving those models. Especially, these papers show the way to a detailed investigation of solvent structure. However, the value of MD and MC approaches to modelling solvation energies is more open to dispute. Whilst it would appear that the methods are of good quality, they require enormous computational effort. Some of the continuum methods now being developed may

give a faster route to solvation enthalpies and free energies (27,28,29). In such models the solvent is treated as being a continuum, not a set of discrete molecules. This avoids the problem of having to take a very large number of solvent structures to obtain time averaged solvation effects. Where these models are parameterised to give free energy, they are very competitive with MC or MD qm/mm simulations(29).

Externally derived path following and grid searching:

In ref.26, Gao leads on to the next category of external path following and grid searching. This is probably the most active area of qm/mm modelling at present, for reasons of interest in chemical reactivity.

In Gao's paper, a MC free energy computation was done over a grid generated by constraining the nucleophile to carbon (N····C) and carbon to leaving group (C····Cl) bond lengths in the Menshutkin reaction ($NH_3 + CH_3Cl \rightarrow CH_3NH_3^+ + Cl^-$). Such a grid search produces an approximation in two dimensional space to the free energy transition state and reaction path. The strength of the approach being that the position of the transition state found is not influenced by factors other than the qm/mm modelling procedure being employed. Its weaknesses are that it requires that the transition state can be located in only two dimensions and has poor resolution (the grid being computed at a 0.1 by 0.2Å step size).

The Menshutkin reaction is a single step, fairly straightforward chemical reaction. For most enzymic processes, the chemistry is much more complex. To appreciate an enzymic mechanism, and then maybe to learn from it or manipulate it, it seems appropriate to break it down into its individual steps. Often the first stage of this is to characterise the intermediates. The idea is to find the reactants and products of each chemical step in the enzyme mechanism.

Merz and Banci (34) have been involved with this form of work on Carbonic Anhydrase. By investigating the binding of CO_2 into the active site, they have demonstrated that the Lipscomb binding mode is favourable to the alternatively proposed Lindskog mode.

To go to the next step of characterising enzymic transition states and reaction paths has not been achieved. Work described in two papers by Lyne, Mulholland and Richards (35) and Mulholland and Richards (36) has come close to this goal for Chorismate Mutase and Citrate Synthase, respectively.

This work has successfully overcome the lack of a saddle point search mechanism that will search in the macro-molecular qm/mm environment. By carefully defining a reaction co-ordinate using gas phase semi-emprical quantum mechanics, an analysis of which internal co-ordinates of the reactive species are most involved in the reaction process was performed. Near rigid internal constraints were placed on those co-ordinates. The values of these co-ordinates were made to follow the gas phase values, in small steps, whilst all other degrees of freedom of the system were minimised. This way, the full qm/mm system was made to follow the gas phase like reaction path.

The reported energy profiles are continuous and smooth. This indicates that these profiles followed a reaction valley and did not jump between valleys. Also, the reported energetics were in reasonable agreement with experiment. One possible concern over this approach is alluded to by Kollman (37), that the use of gas phase or even solution phase data in enzymic reaction studies will bias the results away from a 'true' enzymic result.

Williams and Barnes (38) extended the properties that have been modelled with grid searches to kinetic isotope effects. By using conventional transition state

theory, the ability of the AM1 hamiltonian in qm/mm to model isotope effects was demonstrated. This work also demonstrated the strength of grid searches in revealing unexpected aspects to chemical processes. The two dimensional potential energy surface generated showed possible coexistence of both concerted and stepwise mechanisms for the hydrolysis of AMP.

Harrison, Burton, Hiller and Gould have used similar ideas to investigate transition state like structures in papain catalysed amide hydrolysis (39). This treatment was somewhat less flexible than that by Richards *et al* (35,36) and by Williams and Barnes [38]. The difference was that only a very small proportion of the system was allowed to move. Computation of a grid of potential energies by variation of two degrees of freedom was performed. An approximate saddle point with respect to those two degrees of freedom was found.

This method did yield the correct harmonic vibrational structure for a transition state. However, its reliance on gas phase computed structures, and lack of flexibility, leave it open to the same criticisms of predetermining the result towards gas phase like chemistry. As only a small number of degrees of freedom were optimised, the gradients on the unoptimised atoms were unknown. This means that there was no guarantee that the structure located was close to a first order saddle point with respect to all the possible degrees of freedom.

Small molecule energy minimisation:

This section reviews mainly the work of Morokuma *et al.* (42a,b). In these papers, Morokuma *et al.* extend the concept of qm/mm modelling beyond just the computation of the energy and its geometric gradient. In each case they used *ab initio* quantum mechanics. MM2 (72) molecular mechanics were used in ref. 42a . In ref. 42b MM2 was replaced with MM3 (73).

By utilising the different computational demands of molecular mechanics and quantum mechanics, they accelerated (in terms of time) the optimisation of qm/mm chemical systems. In most qm/mm approaches, the qm/mm gradient vector is considered as a single entity as is the energy function. In ref. 42a Morokuma and Maseras introduce the concept of partitioning, by atom, the computation of the gradient and the energy function. By not polarising the qm atoms by the mm atoms, it was unnecessary to re-evaluate the qm energy and gradient function for a change in just the mm atoms. Optimisations of the mm and qm atoms were then uncoupled producing the acceleration. The mathematical background to this is discussed in detail in chapter 9.

The initial test cases were the geometry of cyclopentene with only the sp^2 carbons and their hydrogens treated using Hartree-Fock(6) quantum mechanics, and the symmetric nucleophilic substitution of chlorine at alkyl chloride with second order Møller Plesset perturbation / Hartree-Fock quantum mechanics (6,71). In both cases good agreement was found between the qm/mm method and the same calculations performed using pure quantum mechanics.

In ref. 42b, Svensson, Humbel, Robert, Froese, Matsubara, Sieber and Morokuma extend these ideas to having a model with multiple layers. Of interest to qm/mm modelling are the models with a core of atoms treated by quantum mechanics and the surrounding atoms by molecular mechanics. For the addition of H_2 to $Pt(P(t\text{-}Bu)_3)_2$ and a range of Diels-Alder reactions, these models were competitive with pure quantum mechanics, in terms of geometry and barrier heights. The significant finding was that such methods often required an order of magnitude less computer time than the pure quantum mechanics for almost the same results.

3.2.10 Other modelling:

The above is in no way exhaustive. In particular, it leaves out discussion of inorganic qm/mm modelling(41) and some extensive work on systems like crown ethers (40). Whilst these areas are of great importance to chemistry, they are not directly in the line of relevance with the work discussed in this thesis.

3.2.11 Computation of partial atomic charges:

Partial atomic charge computation plays a major role in much of the work presented in this thesis. This is a very large area of active computational chemistry research. The papers reviewed below represent a subset of the area which is relevant to the rest of the thesis.

In standard molecular mechanics approaches, such as the CHARMM potential (30), the electrostatic interaction of atoms that are more than two bonds remote from one another is treated using coulomb's law. A point charge is placed at the nuclear centre of each atom and the interaction energy between each point is then computed from $E=q_i.q_j.r^{-1}$ where q=charge and r= inter nuclear distance and the subscripts refer to the particular pair of atoms.

In qm/mm modelling, just as in pure molecular mechanics, there is a desire to have a reliable and fast way of obtaining these point charges. In qm/mm modelling, there are also several schemes which attempt to approximate the qm/mm electrostatic charge interaction to a point charge model(22,24).

For a small molecule, there are a number of ways of obtaining this point charge distribution. For ab-initio quantum mechanics, the favoured method is the least squares fitting of point charges to the electrostatic potential derived from one electron properties (43). Such methods are referred to as potential derived charges. Some concern has recently been raised over the stability of such a

method for assignment of all the partial charges in moderately sized molecules (44). The problem is that the electrostatic potential has insufficient information in it to allow the partial charges to be assigned unambiguously.

Besler, Merz and Kollman (45) have applied the potential derived charge method to semi-empirical wavefunctions. This allows for charge fitting of much larger systems than is possible using *ab initio* wavefunctions. The application of the method to large molecules may cause to it be even more susceptible to ambiguous charge assignment.

Some of the original short comings of the de-orthogonalised method for obtaining potential derived charges from semi-empirical methods have been addressed by Ferenczy, Reynolds and Richards (46a,b). The ZDO method using non-deorthogonalised orbitals would appear to produce results of similar quality to ab-initio potential derived charges.

Bakowies and Thiel (47) have developed a method of using a very simple electro-negativity equalisation method with damping at short (bonded) ranges. With extensive parameterisation, this method shows a way to derive partial charge distributions for macro and poly-molecular systems.

3.2.12 Optimisation and saddle search algorithms:

The initial goal of an optimisation algorithm is to find an extreme optimum value of a function with respect to a set of orthogonal variables. What is defined as optimum depends on the application. For energy minimisation this extreme optimum is easy to define as being a stationary point of minimum potential energy.

Computational chemistry usually defines a saddle point on the potential energy surface with respect to geometry as being a stationary point with one negative

eigen value of the hessian. Under this definition, a saddle point search algorithm is an optimiser that searches for the extreme of low magnitude of the gradient vector where the hessian has one negative eigenvalue. The method of locating this point does not necessarily have to be reduction in the magnitude of the jacobian, but may be some other property leading to that reduction.

The rest of the discussion on optimisers is broken into 5 sections:

- Finding minima and general considerations
- Locating saddle points
- Focal methods
- Reaction co-ordinate methods
- Optimisation - a final note

Finding a minimum and general considerations:

The calculation of potential energy functions and their geometric gradients can be very computationally demanding in chemical applications. Large benefits can be achieved by writing optimisers which require few steps to obtain their goals. It is this driving force that has generated so many approaches to optimisation in computational chemistry.

The background to optimisation is covered extremely well in by Press et al. (48). In qm/mm modelling the jacobian of the energy (with respect to geometry) takes only the same order of time as the computation of the energy alone. This means that it is wise to include computation of the gradients at every optimisation step. Computation of an approximation to the initial hessian can often be done relatively inexpensively. This favours optimisation schemes that keep a continuous record of the hessian and use gradients at every optimisation step (49).

A major difference between small molecule modelling and many macro- or poly-molecular qm/mm models is the large number of variables defining the energy. The storage of the entire hessian matrix can become impossible. In this situation storage of an approximation to the hessian or its inverse can be a better choice (50).

By carefully defining the co-ordinates by which the geometry of the chemical model is defined, it is possible to reduce the number of cycles required by an optimiser (51). It is even possible to optimise using a set of non-orthogonal co-ordinates that over-define the system. These 'redundant' co-ordinate methods are attracting a lot of interest at the present time(52).

Locating saddle points

The location of saddle points is generally much more difficult than the location of minima. Disregarding machine precision problems, if steps are taken of $-\alpha\mathbf{G}$ (where α is a scaling factor and $\mathbf{G}$ is the gradient vector) then as α tends to $1/\infty$ it is inevitable that an algorithm will find a minimum. This 'steepest descent' approach is of value in minimising very difficult functions.

When the optimiser is searching for a stationary point for which the hessian matrix has a single negative eigen value, a simple concept like steepest descents no longer applies. Bell and Crighton (53) discuss the principles of saddle point searching. In this paper two types of methods are discussed. There are the focal methods and the reaction co-ordinate methods. In a focal method, one point on the potential energy surface is moved progressively closer to the saddle point. The reaction co-ordinate methods take the position of the reactants and products into account and try to locate a minimum barrier between them.

Focal methods:

A later development of the focal method by Bell and Crighton (53) is the partial rational function optimisation (P-RFO) method (54). This is derived from an algorithm described by Cerjan and Miller (56). For each step of the Cerjan and Miller algorithm it was necessary to re-calculate the entire hessian matrix. Banerjee, Adams, Simmons and Shepard (55) described a method of improving the stability of the Cerjan Miller algorithm. This allowed the method by Baker (54) to calculate the hessian only once. The hessian for each subsequent step could be estimated from the previous hessian, the gradient vector and the step vector.

The P-RFO method is probably the most used and successful of present saddle point search algorithms. It uses analysis of the eigen values of the approximate or an exact hessian to search for a point with one negative eigen value of the hessian and a zero gradient. It achieves this by minimising along the direction of all but one eigenvector of the hessian matrix and maximising along the remaining vector.

These eigenvectors represent the non mass weighted modes of the chemical system. Another way of viewing the operation of the P-RFO method is that it searches in vibrational space for the property of the hessian having one negative eigenvalue and in energy/gradient space for a stationary point.

Reaction co-ordinate methods:

The simplest form of this approach is to define a reaction co-ordinate as the change in one internal degree of freedom (bond, angle or torsion) whose value varies monotonically between reactants and products. Steps are taken along this co-ordinate whilst all other degrees of freedom are optimised to a minimum. An example of this with cyclohexane is in ref. 52. This method can easily be

extended to more than one degree of freedom, making a relaxed surface scan (38).

Most reaction paths are not adequately described by changes in only one internal degree of freedom. If the changes in value of all co-ordinates between reactants and products are considered as a vector, then scanning along this vector produces an energy profile corresponding to a fixed scan, not a relaxed scan. To allow for relaxation of the system, each point along the line can then be optimised to a minimum either simultaneously (57) or stepwise (58) under some constraint so that the points do not move back towards either reactants or products. Such a method is often referred to as a chain algorithm. The separate points that are being refined are considered to be like the links in a chain.

Such a multi-point approach will not find a saddle point, but will indicate the region of co-ordinates around the saddle point by passing over an energy maximum. As the number of points is increased, the accuracy with which this region of space is located will increase. If a sufficiently finely spaced set of points is used, then a close approximation to the saddle point can be found.

The saddle point found by a fine search like this is guaranteed to be a saddle point with respect to the co-ordinate or path defining the search. If the unconstrained gradient vector of the entire system has a negligible magnitude then this point will also be a stationary point of the whole system (see chapter 9).

Given the reactants and products for an individual elementary step of a reaction mechanism, a different type of reaction co-ordinate method can exactly locate the saddle point. A point between the two points on either side of the saddle is defined. Possible movement of that point through space can be defined by a set of conjugate (mutually non-interfering) directions. If the region of geometric space

at the new point has only one negative eigen value of the hessian, one of these directions will have a local maximum and the rest a local minimum. By searching in these conjugate directions, maximising along that with negative curvature and minimising the rest, the saddle will be found (53).

Conjugate Peaks Refinement, a method that combines the two reaction co-ordinate approaches, has been developed by Fischer and Karplus (59). A chain of points is fed into the algorithm from which it locates approximate positions of local maxima. A conjugate gradients method is then applied to obtain the exact saddle points. By continually updating the positions of the points either side of the expected position of the saddle, this algorithm attempts to become independent of the initial choice of points in the chain. This method is appropriate for very large numbers of degrees of freedom. It does not require the maintenance of a hessian matrix for the focal part of the algorithm. Instead, it can generate the conjugate directions individually as the algorithm proceeds.

Optimisers - a final note:

The P-RFO based methods and methods similar to Conjugate Peaks Refinement represent the present state of the art for saddle point location. The differences between the approaches when applied to qm/mm modelling will be discussed later in the thesis.

The above review does not deal with the question of local and global minima (48) or saddle points. Some consideration of this will be covered in the chapter on solvation. In the presented work, the number of degrees of freedom has largely prevented the application of global optimisation tools, and so their review is redundant to the purpose of the thesis.

Chapter 4 - Overview of computational experiments

To test the unifying hypothesis, the "experimental" work had a unifying target.

> *'Computation of the intrinsic reaction co-ordinate(3) for macro/poly molecular systems with the validation of that co-ordinate through isotope effect calculations and other means.'*

The level of success, and thus support of the unifying hypothesis, will be measured against the following goals.

1. Qm/mm characterisation of aqueous organic transition states and IRCs
   a: Using semi-empirical qm
   b: Using *ab initio* qm
2. Qm/mm characterisation of enzymic transition states and IRCs.
   a: Using semi-empirical qm
   b: Using *ab initio* qm

The path towards these goals followed a route involving the testing of existing methods and the development of new ones. A summary of this route is described below. The use of existing methods and/or development of new ones will be discussed in the separate "experimental" sections.

Chapter 5: ***Charge fitting to the qm/mm function***

Many of the methods in the thesis use charge fitting to the qm/mm function. The ideas behind this are concentrated in one place although the applications and development are spread thoughout the work.

Chapter 6: ***Solvation of small organic molecules in water***

To reach targets 1,a and 1,b it was necessary to have a way of packing water around an organic molecule.

Chapter 7: ***Ab initio qm/mm modelling***

Goals 1b and 2b required an *ab initio* qm/mm method. The semi-empirical method (30) had already been established in macro/poly molecular work (35,36,38).

Chapter 8: ***Computation of fractionation factors of small organic molecules in water***

The characterisation of the IRC's isotope effects necessitated a reliable method for computing isotope effects. To allow this fundamental technique to be developed before the methods for computing the saddle point and IRC, isotopic fractionation factors of small, aqueous organic molecules were investigated.

Chapter 9: ***Methods for computing the qm/mm IRC***

The approach of finding a saddle point on the potential energy surface and computing the IRC from that was investigated.

Chapter 10: ***Extension of the ab initio qm/mm method to IRC computation***

An ab initio qm/mm method capable of efficiently handling large atomic displacements in thousands of degrees of freedom was required.

Chapter 11: ***Application of the IRC methods to aqueous solvolysis of organic molecules***

To test the IRC computation and characterisation by KIEs, the solvolysis of small organic molecules was modelled.

Chapter 12: ***Application of the IRC method to Lactate dehydrogenase***

To move toward goals 2,a and 2,b , the investigation of IRCs in lactate dehydrogenase was performed.

4.1 Materials:

Inventory of computers and their functions:

SG 4D25:

Program development, semi-empirical modelling and molecular visualisation.

DEC AXP 2000 (150 MHz)

Qm/mm and *ab initio* qm modelling.

SG Indigo II - R4400

Ab initio potential derived charge calculations using Gaussian 94 and molecular visualisation.

SG Power Challenge - R8000

Lactate dehydrogenase qm/mm modelling.

None of the reported results have contributions from other machines; a small amount of developmental work was performed on other machines.

Computer software:

Most novel computational procedures have been written into a new code GRACE. As will be discussed in a later chapter, GRACE not only contains its own algorithms, but acts as a communication channel with other software. The following table analyses the contributions to the methods described in the thesis by algorithm. By so doing, it shows the relationship of new and existing work and code.

4.2 Table of software contributions

Symbol	Meaning
***	Totally novel code and algorithm
**	A major development of an existing code or algorithm
*	Standard library code imported into GRACE
-none-	Code or algorithm completely by others

Procedure, Algorithm or method	**Main code of residence**	**Major sub procedures**
Molecular mechanics energy and gradient	CHARMM24b2	
Semi-empirical qm/mm energy and gradient	CHARMM24b2	
ab initio qm/mm energy and gradient ***	GRACE	1. CHARMM24b2 -molecular mechanics 2. CADPAC6 -quantum mechanics
Simulated desublimation	GRACE	1. CHARMM24b2 -molecular mechanics and some mathematical functions. 2. Charge fitting to qm/mm function ***.
Partial rational function and rational function optimisers, configured for sub-set operation. **	GRACE	GETHESS, finite difference hessian generator.***

Adopted Basis Newton Raphson optimiser	CHARMM24b2	
Powell's conjugate gradients optimiser *	GRACE	
Charge fitting to qm/mm function ***	GRACE	1. DGELSS least square fit.*, 2. rfo optimiser *
Transition state location using P-RFO-SS in semi-empirical qm/mm ***	GRACE	1. CHARMM24b2, energy and gradients, ABNR optimiser. 2. GRACE, P-RFO optimiser **
Transition state location using P-RFO-SS in *ab initio* qm/mm ***		1. Energy and gradient, see ab initio qm/m model. 2. CHARMM24b2 ABNR optimiser. 3. GRACE, charge fitting ***. Powell's conjugate gradients optimiser*. P-RFO optimiser **
Valence co-ordinate generation ***	GRACE	VALCOOR***
Relaxed qm/mm, potential energy surface scan	CHARMM24b2	
Intrinsic reaction co-ordinate computation in qm/mm systems ***	GRACE	1. See transition state searching. 2. IRC algorithm from GRACE**

Hessian computation ***	GRACE	
Isotope effect computation	Camvib and Camiso	GRACE , automated generation of valence coordiantes and CAMVIB input ***
General linear algebra*	GRACE	
COSMO solvation of semi-empirical systems	Mopac93	
CHELPG charge fit	Gaussian 94	
Radial distribution function and density analysis ***	GRACE	
Programmable molecular visualisation**	GRACE	1. Rasmol 2. Xmol
Generation of COSMO hessians	Mopac93	

References for code:

DGELSS (74)

Mopac93 (60a)

Cadpac6 (32)

CHARMM24b2 (30a,b)

Rasmol (63)

Xmol (64)

Chapter 5 - Computation of point charge distributions by direct fitting to a qm/mm gradient function.

5.1 Orientation to thesis as a whole:

As discussed in the literature review, there are a number of reasons for computing point charge distributions for both qm/mm application and pure mm applications. Presented here are several novel approaches to finding a point charge distribution based upon the qm/mm energy function. Although the results and analysis of these methods will come in later chapters of the thesis, it seems appropriate to place the description all in one place.

Terminological note:

Generally in computational modelling, the terms jacobian and gradients are considered to be interchangeable. In this section of the thesis they are not. Gradients will refer to the jacobian of the potential energy with respect to geometry. Jacobian will be a general term referring to a set of first partial derivatives. This distinction is to aid clarity in the description.

5.2 Introduction:

A point charge distribution is not an observable quantity in that it cannot be defined as the expectation value of any quantum mechanical operator (47). Point charges are an approximation to true electrostatic charge distributions. Based on this concept, one definition of the 'correct' point charge distribution is: *'the distribution of point charges which best models the interaction of a chemical system with its environment'*. This definition suggests looking for charge distribution by directly analysing the interaction of a chemical system with its environment. This interaction is physically observable and so a point charge distribution defined by it has physical meaning.

Qm/mm models can also be given physical meaning by their predictions of physically observable chemical phenomena. The part of the qm/mm model that is most suitable for modelling these phenomena is the gradient vector. Geometry, temperature, pressure, vibrational spectrum and energy change are all functions of the gradient vector. So it seems desirable to derive the charge distribution from the qm/mm gradient vector.

Gradient-vector derived distributions are likely to reflect those physically observable phenomena that the qm/mm method has modelled. Also, a molecular mechanics force field using point charges derived from the qm/mm gradients is likely to best replicate a qm/mm potential energy function and hence the property prediction of the qm/mm model. The accuracy with which a pure mm model can shadow a qm/mm model defines its usefulness in helping to reduce the computational burden of qm/mm modelling.

An approach that fulfils all the requirements specified is to directly fit a molecular mechanics point charge distribution to a qm/mm potential energy function and its gradients. It is this approach that is discussed here.

5.3 Method:

If one defines the molecular mechanics electrostatic-static term in Cartesian co-ordinates as.

$E_{elec} = \Sigma_{k=x,y,z(i=1,n(j=1,i))} q_i \cdot q_j \cdot r_{ij}^{-2} \cdot rc_{ijk}$ [eqn 5.1]

where the variables are:

r= inter nuclear distance

q=point charge value

rc=cartesian components of the inter nuclear distance

and the subscripts define:

i= the specific atom i

j= the specific atom j

ij= the specific pair of atoms i and j

k= x,y or z cartesian axis

e.g. rc_{ijk} is the distance between atoms i and j along the cartesian axis k

then the gradients are:

$\delta E_{elec}/\delta rc_{ijk} = -q_i \cdot q_j \cdot r_{ij}^{-3} \cdot rc_{ijk}$ [eqn 5.2]

Thus the gradient is linearly dependant upon the charges q_i and q_j.

In the qm/mm model, let atom i is molecular mechanics and j is quantum mechanics. Now $\delta E_{elec}/\delta rc_{ijk}$ is dependent on the interaction of the molecular mechanics point charge distribution with the quantum mechanics wave function.

If q_i is fixed to the molecular mechanics point charge then for pure mm terms $\delta E_{elec}/\delta rc_{ijk}$ becomes linearly dependent upon q_j. Thus an interaction matrix **A** can be generated such that

$\mathbf{A} = -q_j \cdot r_{ij}^{-3} \cdot rc_{ijk}$ [eqn 5.3]

Cycling through specific mm atoms in j and their cartesian axeses in k defines the rows of **A**. Cycling through specific qm atoms in i defines the columns of **A**.

Let:

b= vector of qm/mm gradients, on the mm atoms, due only to the electrostatic term

s= solution vector of mm point charges on the qm atoms

Linear least squares fitting can be performed to minimise | **b-A*s**| thus yielding the best mm point charge distribution to mimic the qm/mm gradients.

In this work, the DGELSS (74) singular values decomposition least squares fit routine was used. This method has the advantage of being stable when **A** underdefines the solution vector **s**. Further, the range of magnitude of the singular values of **A** reports when such underdefinition has occurred.

The unconstrained nature of the fit means that the sum of derived point charges will not have the expected integer charge. In some situations, this may not be a difficulty as the charge distribution is defined as the best mm fit to qm/mm, not by the concept of integer charge.

5.3.1 Constrained fitting:

If the total charge is constrained to give the expected value, the point charge fit becomes non-linear. To solve a constrained charge fit, the following function was defined.

$$f = |\mathbf{b}-\mathbf{b}'| \qquad \text{[eqn 5.4]}$$

b' is the vector of mm electrostatic term gradients on mm atoms given the simple point charge treatment for the 'qm' atoms with point charge distribution **s**.

The constraint is defined as $t=\Sigma s$, *i.e.* the sum of the point charges on the qm atoms must equal t. To constrain, a vector **u** is defined as the unconstrained point charge distribution. From that vectors **c** (correction) and **s** (solution) are defined:

$$\mathbf{c}_i = (t-\Sigma_{j=1,n}\mathbf{u}_j).n^{-1} \qquad \text{[eqn 5.5]}$$

where n is the number of elements in **s**, i.e. the number of point charges being used to approximate the qm electrostatic distribution.

$$\mathbf{s} = \mathbf{u} + \mathbf{c} \qquad \text{[eqn 5.6]}$$

Thus f is a function of **s**, **s** is a function of **u** + **c**, and **c** is a function of **u**. Jacobian vector **j**, of f with respect to **s**, can be computed by finite difference of **u**. f and **j** can then be passed to an optimisation algorithm.

A rational function optimiser (rfo)(54) with updated hessian was used to optimise towards a zero value of f. The updated hessian technique generally made this method twice as efficient as conjugate gradients (61). The values of **u** tend to be highly co-dependent which may explain this advantage of the rfo method.

The solution vector **s**, represents the best point charge distribution for mimicking the qm/mm electrostatic term under the constraint that the sum of point charges of the 'qm' atoms is the provided value t.

5.3.2 Off-centre point charges:

Electron density will not always be well modelled by point charges located at the nuclear positions. A considerable 'off centre' electron density can be produced by factors like π bonds and lone pairs. The non-linear charge fitting procedure provides a mechanism to define off centre point charges to help better match the point charge distribution to the qm/mm electrostatic function.

Whilst chemical intuition can give some clues as to the appropriate location of off centre point charges, no rigorous formula for their *a priori* placement has been devised. To overcome this problem, it is possible to combine the location of optimal position of off-centre points with the general charge fitting.

To achieve this, values for the off centre charges are included in **u** and the corrections for them in **c** {eqn 5.5 and 5.6}. Vector **s** also has added the geometric co-ordinates of the off centre point charges. **s** becomes of the form (in cartesian co-ordinates):

$\mathbf{s} \equiv (u_1+c_1,.....,u_{n+m}+c_{n+m},x_{n+1},y_{n+1},z_{n+1},...,x_{n+m},y_{n+m},z_{n+m})$ [eqn 5.7]

for, n 'qm' atoms and m off-centre point charges.

j is now generated by finite difference of all the elements in $\mathbf{u}_{(1,n)}$ and $\mathbf{s}_{(n+1,m)}$. This approach ensures that the method is a 'combined vector' fitting procedure.

Because there are more point charges involved than in the centre only approach, **f** will generally have a smaller final magnitude than in that approach. The question as to whether the information gained by the location and charges of the off centre points is of value is, as yet, only answerable by the user. This issue is addressed to some extent in chapter 8.

Chapter 6 - Solvation of small organic molecules in water

6.1 Goals:

To allow rapid development of the qm/mm solvation treatment, it was necessary to have a method for generating solvent structures around a solute with minimal computational demand. The generated structure had to be representative of real solvent structure and reproduce observed solvation effects.

6.2 Introduction:

Previous solvation treatments, for all molecule solvation (10), in qm/mm methods, have fallen into one of two categories. Dynamical approaches model a time averaged solvation structure by using molecular dynamics throughout the qm/mm modelling run. The work described in refs. 24,25 and 26 uses this method. For the characterisation of equilibrium geometries, it is unquestionably the most rigorous method.

There are two drawbacks to the dynamics approach. The computational cost is very high indeed, frequently requiring millions of energy and gradient calculations. The second problem is that these methods do not lend themselves to direct transition state searching (as discussed in the main literature review).

The alternative is a minimal sampling solvation treatment. Barnes and Williams have demonstrated the potential of this approach in transition state searching (38). In that work, a solute shaped cavity was removed from the centre of a pre-defined ball of water. The solute was then placed in the cavity and a local energy minimisation technique applied to cause the water to solvate the solute. This method will be referred to as a minimised cavity approach.

One possible criticism of the minimised cavity approach is that the local minimisation technique will be unable to disrupt the existing hydrogen bond matrix of the water. Even where this matrix has been damaged by the cavity formation there is a strong possibility of the water reforming new hydrogen bonds before sufficient molecular displacement has been applied (by the minimiser) to allow solvation of the solute.

One answer to this problem is to use a global minimisation technique (48). This approach is identical to the cavity solvation approach except it would attempt to find the absolute minimum potential energy that the model could adopt. In so doing, the initial approximation of the cavity shape and hydrogen bonding will be obliterated. The drawback of global minimsers is that the computational demands are too high to attain the goal of a rapid method.

After investigation of the cavity solvation method with local and global minimisation, a novel concept was adopted for this work.

6.3 Method

Cavity solvation approaches with local or global minimisation attempt to get realistic solvation by finding a minimum potential energy. The new method attempts to find a realistic solvation structure directly. Solvation shells are built up in a way initially dominated by interactions between the solute and solvent.

The new approach, call *simulated desublimation*, packs water molecules around the solute one at a time. During the formation of the first solvation shell, the positioning of the waters is inevitably dominated by their interaction with the solute. The second and subsequent solvation shells progressively become more bulk water like as the perturbation of the solute becomes more spatially remote.

The 'core' was initially the solute and latterly the solute and already placed waters. For the majority of any one addition step, the unique 'new' water molecule being added to the core. During the last stage of each addition step the new water molecule reached the core and the core relaxed to accommodate it.

Each new water was added by constrained minimisation from starting a point remote from the core. The distance from the origin to each nucleus in the core was computed. The distance of greatest magnitude defined the 'core radius'. A vector of random direction and magnitude 3Å longer than the core radius was then defined. The translation of the origin by the vector defined the remote point for the new water. This can be viewed as the water being placed randomly on a sphere surrounding the origin. New waters were initially tumbled to a random rotational orientation.

To choose a focal point for the initial constraining force, a random number was used to choose any one of the solute (not core) nuclear positions or the origin. A force independent of the displacement from the focal point, of 8.4kJmol^{-1}Å^{-1} (2.0 kcal mol^{-1}Å^{-1}) was then placed on each atom of the new water.

The new water was then placed on the core by optimisation to the constrained minimum potential energy. To avoid numerical problems at the start of the placing, the ABNR(78) algorithm was applied for 150 cycles without being allowed to exit. After these 150 cycles the ABNR minimiser was allowed to exit at a rms gradient of 0.42KJmol^{-1}Å^{-1} (0.1 kcal mol^{-1}Å^{-1}).

To improve packing on the surface of the core, a final constrained minimisation was performed. First the constraint on the new water was removed, making it part of the core. Then a force (towards the origin) of 0.42 kJmol^{-1}Å^{-1}

(0.1 kcal $mol^{-1}Å^{-1}$), independent of distance from the origin, was placed on all core atoms. A minimisation for up to 50 cycles of the ABNR algorithm was then performed with an exit rms gradient tolerance of 0.21 $kJmol^{-1}Å^{-1}$ (0.05 kcal $mol^{-1}Å^{-1}$).

This process was repeated until sufficient water molecules had accumulated in the core. Then a final optimisation, with the only constraint being the continuation of the fixed solute, was performed. The ABNR optimiser was used with an exit rms gradient tolerance of 2.1$kJmol^{-1}Å^{-1}$ (0.5 kcal $mol^{-1}Å^{-1}$).

Removing the initial solute guess:

The solvation structure that was generated at this point was based on the guessed molecular mechanics approximation to the solute. Qm/mm modelling was then used to remove the influence of this guess.

The solute was then treated using semi-empirical, AM1(79) quantum mechanics. The solvent water was treated using molecular mechanics. The ABNR algorithm was then used to optimised towards a minimum until the rms of the energy/geometry gradient vector was less than 0.042$kJmol^{-1}Å^{-1}$ (0.01kcal $mol^{-1}Å^{-1}$). This yielded a solute structure based on the qm/mm function instead of the initial guess. A molecular mechanics point charge distribution was then computed from the resulting qm/mm energy/geometry gradient vector. This fit could have been done with any of the methods described in the previous chapter, yielding a point charge distribution based on the qm/mm function rather than the initial guess. Non-linear constrained charge fitting was used in this work, with and without lone pair location (see chapters 8 and 11 for applications).

Repeating the cycle:

Waters were then added as before, but with the new molecular mechanics approximation. A new qm/mm solvent/solute structure resulted from this. At this point the cycle could be repeated. Such iteration would permit an ever greater removal of any influence of the initial guess. However, in all the work in this thesis, the second qm/mm structure was used without further iteration.

Diagrammatic summary of simulated desublimation

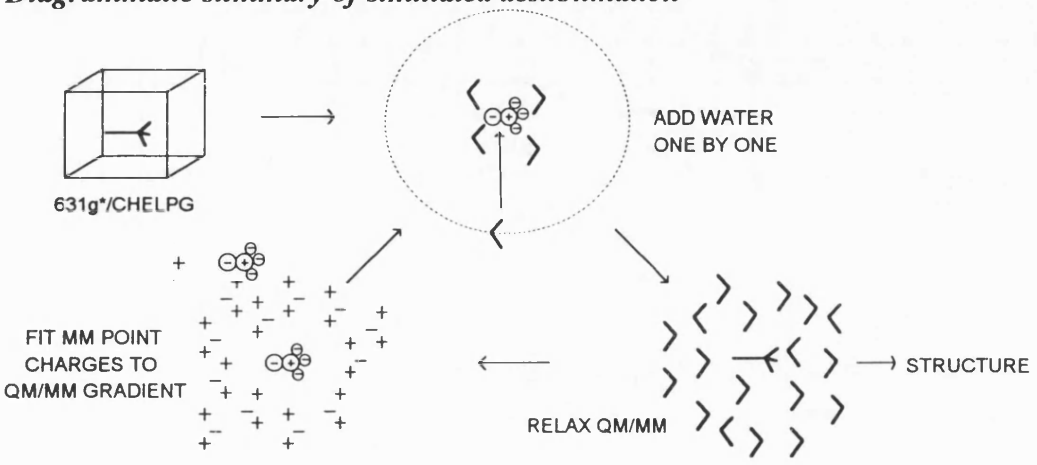

Fig 6.1: Simulated desublimation overview.

6.4 Assessing the accuracy of the desublimation technique (results):

One can measure the success or failure of simulated desublimation from results of models which use its solvation structures. Equilibrium and kinetic results, stemming from simulated desublimation solvation structures, will be presented later in the thesis (chapters 8 and 11). Despite this, independent assessment of simulated desublimation is very desirable. Without such assessment, its suitability for later modelling cannot be gauged.

Two criteria of a solvation method that can be directly compared to experiment are solvent density and radial distribution function (RDF) (10). To assess these two criteria, the simulated desublimation technique was applied to the solvation of a single AM1 (qm) water molecule in 200 TIP3P (mm) water molecules.

The density was calculated by taking several spheres of the resultant water droplet and assessing the mass within that sphere. The density of the system for water with zero exposure of its solvent accessible surface (91) to the surface of the water droplet was approximately 1.2g.cm^{-3}. This figure is in keeping with the slightly short hydrogen bonds found in TIP3P (75) and with the simulation temperature of 0°K.

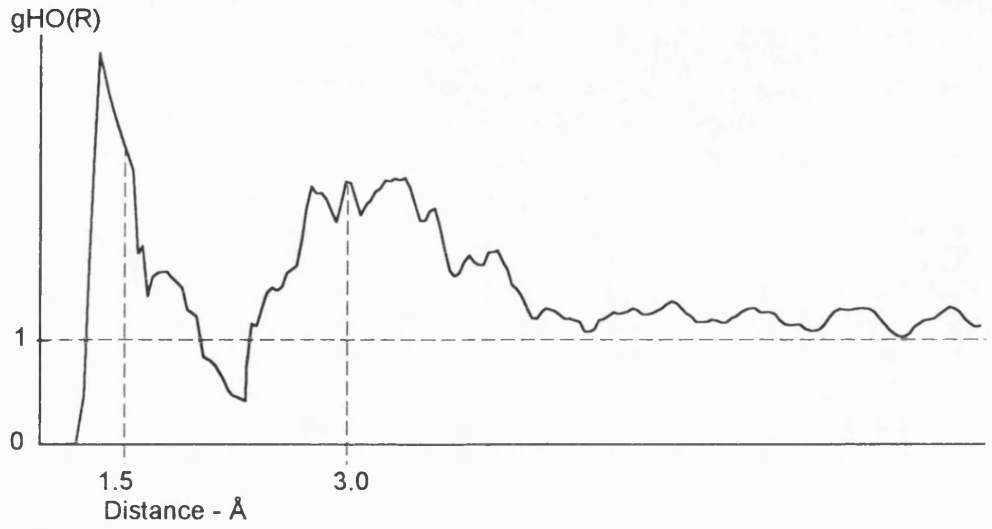

Fig 6.2: Radial Distribution function for H-AM1 to O-TIP3P

From Fig 2 it can been seen that the method is resolving a first and second solvation shell. A comparison with the figures reported for full Monte Carlo with density function theory (DFT) *ab initio* water (25) in table 6.1 shows that the method is performing well. The first solvation shell is at slightly shorter bond length than the DFT/TIP3P model whilst the second is indistinguishable from the DFT/TIP3P model. The position of the second shell's peak is not surprising as this is more dominated by the shared TIP3P potential. An underestimation of hydrogen bond length has been noted in other AM1/TIP3P systems (26).

This graph was generated from three desublimations, each started with a different random number generator seed. Samples were taken at 0.03Å step length and a

window per point of ± 0.1Å. A simple three point moving average of each of the results for the separate desublimations was made. The graph is the numerical sum of these moving averages.

This method of post-processing was chosen to avoid hiding the 'rough' nature of the distribution. As more desublimations are added in, this graph should become more smooth.

Also in ref.(25) it has been noted that the RDF from a AM1/TIP3P dynamics run did not produce a consistent first solvation shell. RDFs for simulated desublimation TIP3P/AM1 solvation show a very clear first and second solvation shell. Whether this anomaly is an artefact of that dynamics run, or a strength of the simulated desublimation method, is not known.

Table 6.1: Comparison of Radial Distribution Function (RDF) peaks in Å

RDF	Exp. ref. 92	TIP3P MC ref. 25	DFT/TIP3P MC ref. 25	AM1/TIP3P SIM/DSB*
Shell 1 Haml-Otip3p	1.85	1.82	1.74	1.5 ±0.05
Shell 2 Haml-Otip3p	3.27	3.21	3.13	3.1 ±0.10
Shell 1 H-H	2.33	2.45	2.38	2.5 ±0.10
Shell 2 H-H	3.84	3.77	3.74	3.7 ±0.10
Shell 1 O-O	2.88	2.76	2.72	2.9 ±0.10
Shell 2 O-O	4.50	-	4.92	4.9 ±0.15

* Simulated Desublimation

6.5 Conclusion:

From density and radial distribution tests, there is no evidence to suggest that simulated desublimation will not produce a representative instantaneous structure

for solvation. The placing of the second solvation shell peak suggests that this method gives solvation packing very similar to the time average packing in a Monte Carlo or molecular dynamics simulation with periodic boundary conditions.

6.6 Extension of the technique:

So far, only simulated desublimation applications that are relevant to other work in the thesis have been presented. Some investigation into further extending the technique was performed, and it seems appropriate to mention those here. The two areas investigated were: (i) the use of different solvents, including mixed solvents, and (ii) the treatment of larger solutes.

6.6.1 Non aqueous and mixed solvents:

Using a different solvent is inherently a simple change from using water. The only complication is that most other solvents have fewer hydrogen bonds than water. Often these bonds are weaker than those in water.

In the case of methanol, exactly the same treatment was tried as with water. As each new methanol contacted with the core it caused methanols that were already part of the core to become detached. Methanol has twice as many atoms as water but only half as many hydrogen bonding opportunities. With the same constraint per atom as with water, methanol had at least four times the ratio of constraint force to hydrogen bonding strength than water. The slightly less polar charges in the methanol model, than in TIP3P, further enhanced this difference. A near complete hydrogen bond saturated methanol structure was achieved by making the acceleration force $25/n$ kJmol^{-1}Å^{-1}, where n is the number atoms in a solvent molecule.

Using the parameters for sugars from CHARMM24b2 (77) and the charge distribution for the molecular mechanics methanol from CHELPG 6-31G**, the simulated desublimation density of methanol in a 200-residue cluster was 1.0g.cm^{-3}. This overestimates the density compared to liquid methanol by a similar amount as the method overestimated the density of water. It seems likely that the same sources of systematic error are responsible for both overestimates.

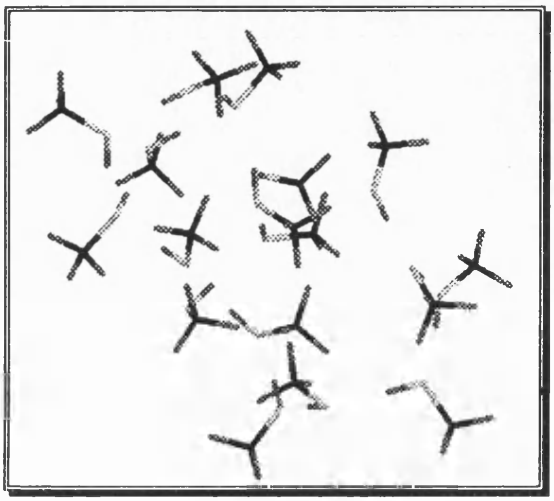

Fig 6.3: The two hydrogen bonds per residue structure of methanol can be seen in this 17 residue cluster.

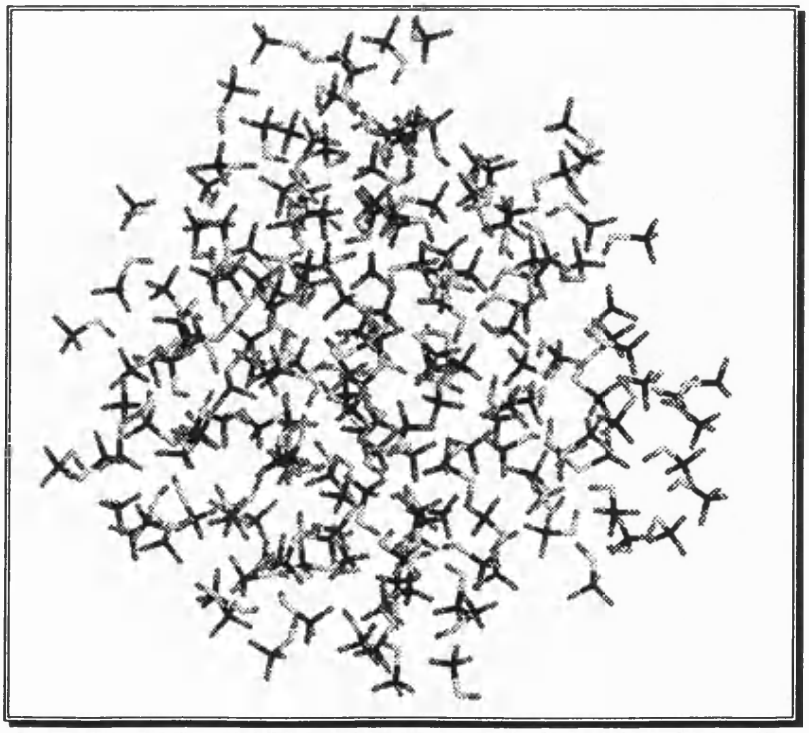

Fig 6.4: This cluster of 200 methanols reveals its open nature. The exposure of the surface methanols accounts for the ease with which they can re-sublime while the cluster is being generated.

A mixture of iso-propanol and methanol was generated. This was achieved by using the same force-per-atom technique as for methanol. To produce a uniform mixture, a random number was used to choose which residue was added at each addition stage of the desublimation.

6.6.2 Desublimation of solvent around large solutes:

Where the solute is large and flexible, making it rigid during the addition of solute may cause the generation of artifactual effects. Dissolution of glucose was used as a test case for the dissolution of large flexible molecules.

A fully parameterised molecular mechanics model of glucose comes with CHARMM24b2. This allowed the non-rigid molecular mechanics treatment of the glucose in the initial addition stage of simulated desublimation. When all degrees of freedom were allowed to relax in the solute, dissolution did not occur. The water clustered around itself and moved the solute out of the way. By fixing one of the ring carbons in position, this effect was eliminated.

Chapter 7 - Ab initio qm/mm modelling

7.1 Goals:

1. To perform fully polarised (see below) qm/mm modelling using ab initio quantum mechanics.
2. To use no more than one order of magnitude more cpu time than the equivalent gas phase modelling.

7.2 Introduction:

One key concern in developing an *ab initio* qm/mm model, for macro molecular modelling, is computational efficiency. The high computational cost of each calculation of the qm potential energy function, and its geometric gradients, generates considerations that are not present for semi-empirical qm/mm modelling. Taking the qm/mm approach in ref. 22 as a base line, this thesis contains two methods to reduce the computational burden when performing *ab initio* qm/mm modelling.

The first of these is relevant to the calculation of equilibrium geometries, where the *ab initio* and semi-empirical structures are thought to be very similar. It is this approach that is described in this section. A method relevant to the search for transition structure and intrinsic reaction co-ordinates is discussed in the chapter 'Extension of the *ab initio* qm/mm method to IRC computation'.

One approach to qm/mm modelling is to include in the quantum mechanics Hamiltonian fractional point charges on the molecular mechanics atoms. Such methods are referred to as 'polarised' qm/mm. 'Unpolarised' models use molecular mechanics terms to model the electrostatic interaction between quantum and molecular mechanical atoms; the molecular mechanics point charges are not then included in the quantum mechanical hamiltonian.

Purely as an aid to understanding, it is helpful to break the interaction of the molecular mechanics point charges and the quantum mechanical atoms into two terms. The electrostatic interaction between the electrons and nuclei with a point charge can be referred to as the 'coulombic term' Q. The reorganisation of the electron density due to the presence of the point charges can be called the 'polarisation term' P. Even though P and Q are non-orthogonal, they form useful references in discussion of qm/mm modelling.

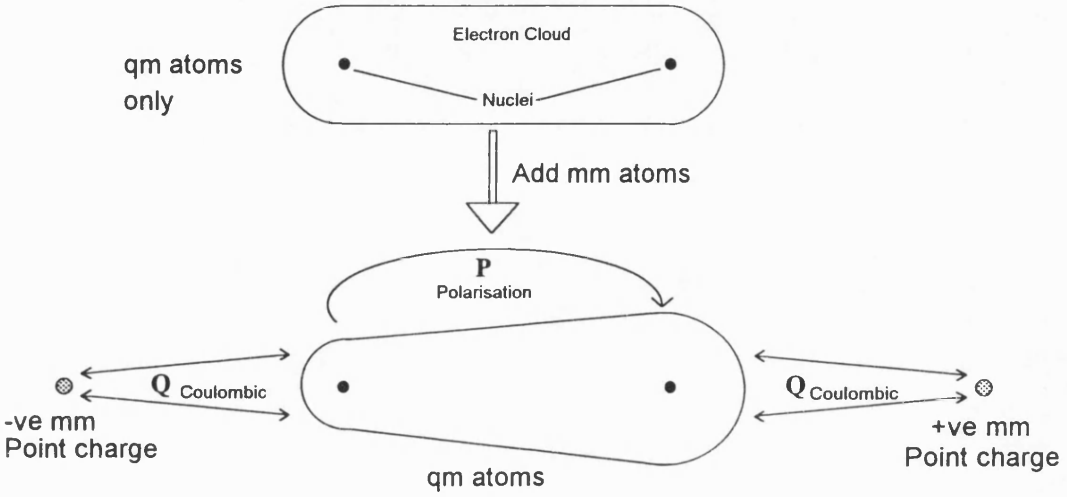

Fig 7.1: Diagrammatic representation of the origin of P and Q terms

There is considerable evidence building up for the preference of polarised qm/mm modelling over non-polarised (24,26). This consideration led to the adoption of fully polarised qm/mm modelling in this work. The major drawback to this approach is that P can only be obtained by performing a full quantum mechanical calculation. Therefore, any change in geometry in either the qm atoms or the mm atoms will require a call to the quantum mechanics code.

Ab initio quantum mechanics geometry optimisations can be significantly speeded up by using an algorithm with a full record or either the hessian† or its inverse. The greatest again comes from computing the hessian† using a less computationally demanding level of quantum mechanics. 'Hessian inheritance'

then allows this hessian to be used as the initial hessian for the optimisation algorithm. That algorithm then 'updates' this hessian from the jacobian vectors generated during the optimisation (49,60).

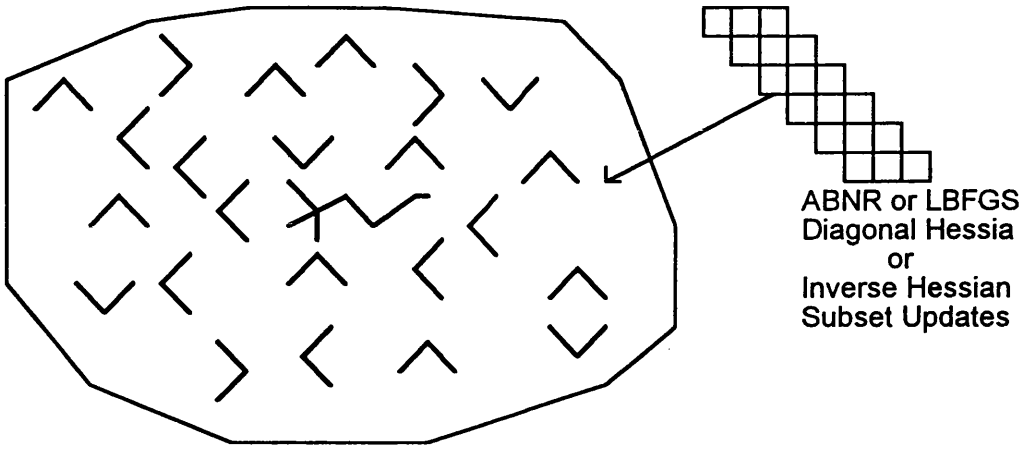

Fig 7.2: Everything optimised, nothing fixed

For the majority of macro/poly molecular systems the total number of geometric variables is so great that storage and manipulation of a hessian is not viable. Optimisation strategies overcome this problem either by storing an approximation to the hessian† (65,66) or by using a conjugate gradient technique that does not require any hessian information (64). Unfortunately, by removing the use of a hessian, hessian inheritance is also made unavailable.

7.3 Method:

The fully optimised, 'nothing fixed' approach, with approximate hessian†, was adopted for the semi-empirical qm/mm modelling of equilibrium geometries; *i.e.* geometric degrees of freedom were optimised to minimum potential energy. The assumption was then made that the *ab initio* qm/m geometry would be very similar to the semi-empirical one. Under this condition, only a sub-set of all the degrees of freedom needed be optimised in the *ab initio* qm/mm model. The rest were left at the semi-empirical qm/mm geometry.

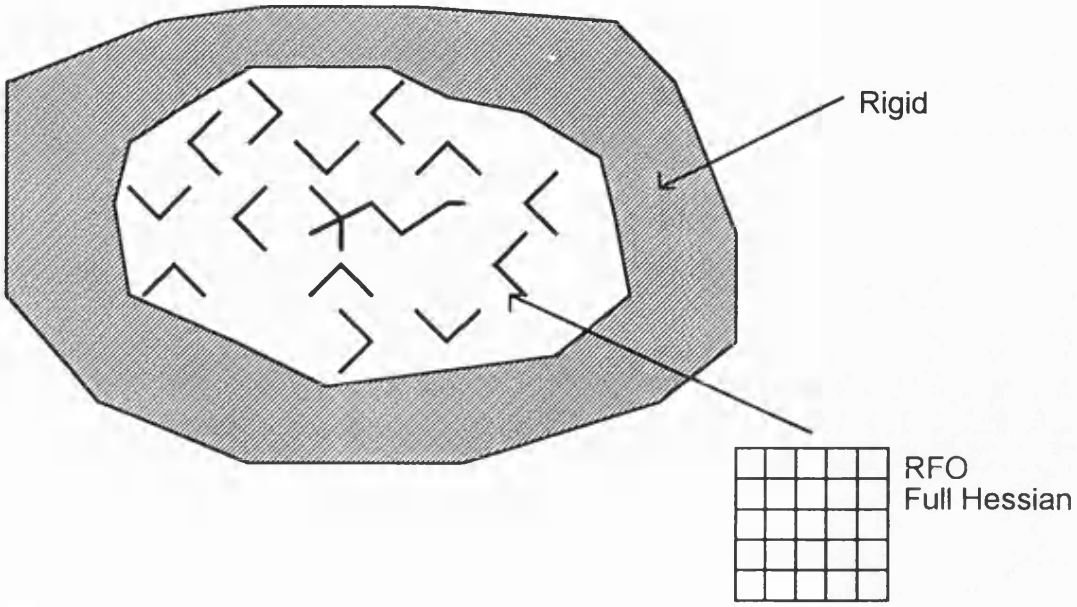

Fig 7.3: Core only optimised, outer zone fixed

Hessian inheritance then became viable due to the much reduced number of degrees of freedom. The choice of sub-set for optimisation will be discussed in the chapter on aqueous fractionation factors. An RFO (54) optimiser was used to optimise the sub-set of cartesian co-ordinates to a minimum potential energy.

Breakdown of the construction of the qm/mm potential energy function:

The qm/mm potential energy function algorithm was specifically designed to take advantage of the sub-set number of degrees of freedom. For this reason, and for completeness, a description of this qm/mm function is included. The potential energy was built up from the following terms:

Quantum mechanical

Hartree Fock molecular orbital theory with or without second order Møller Plesset perturbation theory (32,61,67).

Electrostatic

From inclusion of molecular mechanics point charges in one electron integrals of the quantum mechanics (22). Then the electrostatic terms which are ignored by the molecular mechanics part of the system (1,2, 1,3

and 1,4 terms) are computed (where necessary) using Coloumb's law and subtracted from the electrostatic term generated by the quantum mechanics.

Van der Waals

Sometimes referred to as Leonard-Jones terms. These terms were computed by the molecular mechanics package. All normal interactions in the molecular mechanics part of the system, and interactions between the molecular mechanics section and the quantum mechanics section, were included.

Bonds, angles, dihedrals, improper torsions *etc.*

All bonded terms for the molecular mechanics section were computed by the molecular mechanics code. None of the *ab initio* qm/mm modelling had bonds crossing between the quantum and molecular mechanics sections, therefore specific treatment of this eventuality was not coded.

Constraint terms

Full access to all of CHARMM's internal and cartesian co-ordinate constraints was permitted by including their contributions into the qm/mm function.

Each qm/mm function evaluation required a call to CADPAC6 to acquire the quantum mechanical terms, a call to GRACE's coulombic term algorithm to remove unwanted coulombic interaction energy and two calls to CHARMM24b2 to get the rest of the molecular mechanics terms and any constraint terms.

CADPAC6 was edited to allow an extension to its method of including point charges in the qm hamiltonian. This involved changes to the input reading and geometry computation routines.

The non-standard approach was to permit the existence of these nuclei, they were only included in the one electron integrals and the nuclear repulsion calculation. The energy and gradients* for their interaction with the normal quantum nuclei and with each other could also be computed. It is this method that was used for those molecular mechanics atoms which had their degrees of geometric freedom optimised.

Standard CADPAC6 allows the inclusion of point charges *via* the 'LATTICE' key word. These fractional point charges are included in the one-electron integrals. The gradients* on them and the interaction energy between them are not computed. This method was used for the non-optimised molecular mechanics atoms. This method is computationally more efficient in terms of cpu time and memory requirement.

7.4 Future extension of the method:

As discussed in the chapter on extension of the *ab initio* method later in this thesis, the above method is limited in scope. However, the gains in efficiency by using the 'LATTICE' method of point charge handling over the 'nucleus' method are of more general application.

If all the mm point charges were to be included via the 'LATTICE' method, then no gradients* for these point charges' electrostatic term would be computed. For Monte Carlo calculations, and some global-minimum searching methods, these gradients are not required. The 'missing' electrostatic energy from point-charge / point-charge interaction energy could be computed from Coulombs law and added

in. Such models would benefit greatly from the 'LATTICE' approach to point charge handling.

* Gradient vector of potential energy with respect to geometry.
† Hessian of potential energy with respect to geometry.

7.5 The CHARMM semi-empirical qm/mm model:

This section describes the semi-empirical qm/mm method in CHARMM(22,30a,30b). It is placed here, instead of in the literature review, because many of the ideas in this section have already been discussed in the earlier sections of this chapter.

The MNDO(21) and AM1(79) semi-empirical methods are included in the qm/mm method. These are coupled to the CHARMM (30a) force field. The qm/mm model allows the partial charges on the molecular mechanics atoms to polarise the electronic distribution of the quantum mechanical atoms. Molecular mechanics point charges are treated as if they are *s* orbitals by the quantum mechanics. Rather than containing electrons, these orbitals only contain partial charges. This allows point charges to be included in the semi-empirical scf and so polarise it. This introduces one electron integral and core/core terms in keeping with the NDDO (neglect of diatomic differential overlap) methodology. The exact mathematical construction of the energy terms are described in ref. 22.

The CHARMM qm/mm method handles 'link atoms' that make it possible for covalent bonds to link mm atoms to qm atoms. The link atoms are given no Van der Waals, bonding, angle or torsion parameters. This means that they interact in the standard semi-empirical way with the qm atoms and with the partial charges of the MM atoms. The purpose of link atoms is to maintain the correct charge and hybridisation of the qm atoms. Where bonds link qm and mm atoms, energies

from the bond, the angles with the bond and the torsions about the bond are generated from mm parameters. By default, the charge on the mm atom at the end of a bond that has a link atom is set to zero.

Breakdown of the construction of the CHARMM qm/mm energy function:

Quantum mechanical:

Semi-empirical AM1 or MNDO quantum mechanical energies and forces for all qm atoms and link atoms.

Electrostatic:

The electrostatic interactions of mm atoms with other mm atoms are handled using the molecular mechanics routines. The electrostatic interactions between mm partial charges and the qm atoms are treated as part of the quantum mechanics in the manner described previously.

Everything else:

All other parts of the energy function are calculated using the molecular mechanics routines. Charmm must prevent the molecular mechanics routines from calculating parts of the energy that are calculated by the quantum mechanics. Failure to do so would cause these components to be 'double counted'. CHARMM deletes the appropriated elements from the lists of components of the molecular mechanics energy function.

Chapter 8 - Computation of fractionation factors for small organic molecules in aqueous solution

8.1 Goals:

1. Formulation and testing of methods for computing isotope effects in qm/mm systems.
2. Computation of deuterium fractionation factors for solvated organic species.
3. Investigation of the microscopic nature of solvation and its effects on isotope effects.
4. Comparison of semi-empirical, 2nd order Møller Plesset (MP2) and Hartree Fock qm/mm methods.

8.2 Introduction:

A knowledge of equilibrium and kinetic isotope effects is a vital tool for understanding reaction mechanism (see main literature review). Fractionation factors offer an excellent first step towards development of techniques to compute kinetic isotope effects. Representing the equilibrium isotope effect for deuterium exchange from one species to another, they require only a knowledge of the equilibrium properties of the species. In general, equilibrium properties are easier to compute than transition state properties in chemical modelling.

The isotopic fractionation factor ϕ for deuteration of XH, relative to a standard YH, is the equilibrium constant for the reaction:

$$XH + YD \rightleftharpoons XD + YH$$

In ref (17) Williams showed some success in computing fractionation factors for deuteration of hydrogen bound to carbon. The method was using *ab initio* restricted Hartree-Fock (6) quantum mechanics in the gas phase using the 4-31G (39) basis set. The fractionation factors were computed from the hessian matrix of potential energy with respect to geometry using the rigid-rotor / harmonic-

oscillator approximations. By the author's admission, this work suffered from the calculations being in the gas phase whilst the experimental data to which they were compared being in the aqueous phase.

Williams and Barnes (38) extended the rigid-rotor / harmonic-oscillator approximation to a qm/mm treatment of aqueous hydrolysis of an analogue of adenine mono phosphate. The solvent water was treated in an all-molecule fashion, *i.e.* all discrete water molecules were modelled. The computed kinetic isotope effects were accurate to within the experimental error. This suggests that the approximations used were valid for aqueous solution.

An alternative to the all-molecule model of water is a continuum model. AMSOL(89) and COSMO(27) are two widely used examples in which the solvent water is treated as a polarisable continuum with a defined dielectric constant. By wrapping a polyhedral surface around the solute, and allowing the properties of that surface to mimic the polarisible continuum, a treatment of solvent effects on the solute is provided.

This work repeats some of the computation of fractionation factors for deuteration of hydrogen bound to carbon in ref(17), but using an all molecule solvent model of water as in ref(38). In this case the all-molecule treatment of water as the solvent is achieved using qm/mm modelling, allowing comparisons to the gas phase methods, *ab initio* qm/mm models and the COSMO continuum representation of water.

3.3 Method:

3.3.1 Initial solvation:

Each organic species was dissolved in TIP3P(75) water using the simulated desublimation technique (chapter 6). The AM1(79) hamiltonian was used for the qm/mm part of the desublimation process. Two hundred waters were added in each case. Once a satisfactory AM1 structure had been computed, the method was changed to *ab initio* quantum mechanics.

Point charge fitting for the second water-addition iteration of simulated desublimation (see chapter 5) was done using non-linear constrained charge fitting. For species with lone pairs, an attempt was made to improve the fit by including a point for each lone pair. These points were retained where they remained in the vicinity of the expected positions of the lone pairs and stayed negatively charged. Of the molecules fitted, only methoxide, acetaldehyde and methylcyanide met both these two criteria. For the other molecules (*e.g.* methanol) only the nuclear centres had point charges for the second water-addition iteration. Lone pairs could not be located for oxygen or nitrogen bound to hydrogen, or for fluorine.

The resultant structure and charge distribution from the first water addition stage of simulated desublimation is generally asymmetric. This will tend to be the case even if the equivalent gas-phase structure would be symmetric, due to the asymmetry of the solvation shell. If this asymmetry persisted to the second water-addition iteration, it could be compounded. This would result in a grossly asymmetric solute structure. The internal co-ordinates, which would be symmetrically equivalent in the gas phase were therefore set to the mean of the asymmetric values. The charge for gas phase symmetrically equivalent centres were also reset to their mean. This averaging removed any tendency to compound asymmetry on the second desublimation iteration. A tiny Van der

Waals radius parameter of 10^{-3} Å was placed on the lone pair point charges. This was to prevent exact overlap of an atom with the lone pair, which would cause the system to fall into a catastrophic well, during the water addition process. Once the water was added, and before the AM1 qm/mm optimisation, the lone pair points were deleted from the model.

The effect of inclusion of lone pairs on charge distribution is illustrated in table 8.1. The lone pairs (3 points) for methoxide were at 1.78Å from the oxygen, those for acetaldehyde were at 1.20Å (2 points) and the one on the nitrogen of methylcyanide was at 1.66Å.

Table 8.1: Changes in charge distribution upon inclusion of lone pair points for methoxyde and methylisocyanide

Species	Atom Type	symmetrised charge in atomic units		
		CHELPG 6-31G* refs 39,43a & b	QM/MM AM1 no lone pairs	QM/MM AM1 with lone pairs
CH_3O^-	O	-1.02	-1.02	-0.62
	C	0.68	0.59	-0.11
	H	-0.22	-0.21	-0.02
	Lone Pairs	-	-	-0.07
CH_3CN	C	-0.24	-0.17	-0.08
	H	0.11	0.08	0.07
	C from CN	0.41	0.38	0.26
	N	-0.50	-0.45	-0.35
	Lone Pair	-	-	-0.03

The qm/mm charges were computed from a constrained least squares fit of a molecular mechanics potential to the qm/mm gradients generated on exit from the first simulated desublimation iteration

8.3.2 Ab initio optimisations

The qm/mm system with the AM1 qm section was optimised toward a minimum until the gradient of potential energy with respect to geometry was less than 0.042 kJ.mol^{-1}Å^{-1} (0.01kcal mol^{-1}Å^{-1}). An *ab initio* qm section was then used, utilising CADPAC6(32). The method was as described in chapter 3, with all the solute and all water molecules - any part of which was within 4.0Å of any part of

the solute - being free to move. The 6-311G** (39,32) basis set was used with 2nd-order Møller-Plesset perturbation theory(71) for the final calculations. No orbitals were frozen, and the scf was converged until the root mean square difference in the density matrix between two scf iterations was less than 10^{-7}. The initial density guess was the superposition of atomic densities.

The initial approximate hessian for the optimisation was generated by forward difference numerical differentiation of the gradients using the 3-21G (39) basis set. This was then used to initiate an optimisation, in cartesian co-ordinates with the RFO optimiser (54), using the 6-311G* basis set with the Hartree-Fock calculation. The exit hessian of this optimisation was then used as an initial approximate hessian for the final electron-correlated optimisation to a minimum, with the largest component of the gradients of potential energy with respect to geometry less than 0.126 $kJmol^{-1}Å^{-1}$ (0.03 $kcal\ mol^{-1}Å^{-1}$) and the rms gradient less than one third of that figure. These gradients only refer to that section of the system that was being optimised, see chapter 7.

8.3.3 Computation of hessians:

Once the AM1 and *ab initio* qm/mm structures had been computed, it was necessary to compute hessian matrices of potential energy with respect to geometry. Computation of the hessian was by finite difference numerical differentiation of the gradients. A two-point algorithm was employed to yield high accuracy.

Even using the AM1 qm section, computation and then diagonalisation of a hessian matrix for all the cartesian co-ordinates of the systems was not computationally viable. Two approaches were tested in an attempt to avoid this problem. Firstly, the hessian for only the solute was computed using a 'relaxed environment' method. In relaxed environment, finite difference displacements

were only made for the co-ordinates defining the position of solute atoms. Before each energy and gradient evaluation for these displacements, all the solvent was optimised to a local minimum with the solute fixed at the displaced position.

The second approach was a 'sub-set' method. Finite difference steps were taken for the co-ordinates defining a sub-set of the atoms of the system. This sub-set contained the solute and some of the solvent. A catchment distance was defined. All waters any part of which was within the catchment distance from any part of the solute, were included in the hessian. As the catchment distance was increased, the vibrational coupling to the solute of atoms at the outer edge of the catchment decreased. This meant that, as the catchment was increased, any error due to the interaction between atoms in the sub-set and those outside it became less and less significant to those atoms responsible for the isotope effect.

Initial tests using the sub-set approach, with AM1 based qm/mm, showed that the computed fractionation factors were invariant in the second decimal place for increasing the catchment distance above 2.5Å. Similar tests using the relaxed environment method reproduced almost exactly the same fractionation factors as the sub-set method. To achieve this, the environment had to be minimised to the numerical limit of the machine, thus making the method computationally demanding. Even with such tight convergence, the relaxed environment proved to be numerically unstable by introducing convergence error from the environmental optimiser (see chapter 9 for more details). For these reasons, the sub-set method with a 2.5Å catchment was adopted.

8.3.4 Comparison of methods:

To allow comparison of the qm/mm methods with alternative approaches, fractionation factors in the gas phase and using COSMO(27) were also computed. Gas phase AM1 and COSMO (ε =78.4 for water) were computed using

MOPAC93. The structures were entered as z-matrices and optimised to MOPAC93's 'PRECISE' standard using the RFO optimiser (60a,54). Hessians were then computed using a four-point algorithm for numerical differentiation of the gradients.

Gas phase *ab initio* hessians were computed using CADPAC6 (32)and GAMESS_UK (33) with a mixture of analytical and central-difference numerical hessian computation methods (for machine resource reasons) after optimisation to a minimum potential energy using the BFGS(93) algorithm. All settings for these computations were those recommended in the manuals. MP2 electron correlation was used with restricted Hartree-Fock self consistent field theory with the 6-311G** basis set and correlation of all orbitals.

8.3.5 Computation of fractionation factors:

The cartesian hessian matrices contained contamination from rotation and translation modes for the entire system of atoms which they represented. To ensure the complete removal of these contributions, the hessians were transformed into internal co-ordinates and then back into cartesian co-ordinates using the CAMVIB (62) program. The internal 'valence' co-ordinates were similar in nature to those used in infra-red spectrometry. To define manually the hundreds of valence co-ordinates required to transform the qm/mm hessians would have been unreasonably labour intensive. Instead a novel algorithm for the generation of non-redundant valence co-ordinates was employed. A full description of this algorithm is given in appendix A. The resultant hessian matrices had six zero eigenvalues, with no rotational or translational contamination of the vibrational modes.

The fractionation factors were computed using the CAMISO (62) program from the hessians generated by CAMVIB. The rigid-rotor / harmonic-oscillator

calculations were performed with the temperature set to 25°C. The deuterium fractionation factor for species X, relative to standard Y, was computed as the equilibrium constant for the reaction: X-H + Y-D $\rightleftharpoons$ X-D Y-H .

The hessian employed for the species on both sides of this formal equation were identical, but the isotopic masses differed. For species containing sites related by rotation, the fractionation factor was determined as the Boltzmann-weighted average of the values found for isotopic substitution in each unique position.

8.3.6 Analysis of electronic polarisation:

The aim of this analysis was to determine the relative extent to which each solvent atom polarised the electron distribution of the solute. The method consisted of changing to zero (zeroing) the charge on a given solvent atom and re-calculating the qm/mm gradient vector. Because the nuclear positions of the solvent atoms were not allowed to move between gradient vector re-calculations, the solvent had no mechanism to 'screen' any effect this charge change would have on the self consistent field. It is important to note that the dielectric effects of the solvent only affected the effect of charge zeroing in so far as they determined the electrostatic and geometric structure of the initial system.

The effect of the charge zeroing on the self constent field was analysed by comparison of the point charge fit to the electrostatic properties of the qm atoms with and without having been charge zeroed. The unconstrained charge fit method (see chapter 5) was used to compute a point charge fit to the solute's charge density at the AM1 level of theory.

The rms (root mean square) difference, in the point charges fitted, between the initial system and that with the zeroed charge gave an indication of the polarisation of the solute's charge density by that particular solvent atom. The

magnitude of this rms deviation was then plotted against the distance between the altered solvent atom and the geometric centroid of the solute (see results).

8.3.7 Dihedral effects:

For many biological applications, deuteration is on a carbon with a hydroxyl substituent. Most of the fractionation factors reported here are the Boltzman weighted mean fractionation factors for sites that would be rotationally equivalent in solution. In some bio-molecules, such as sugars, the structure of the rest of the molecule generates hydroxyl dihedral angle rotamers (the angle of the C-O-H plane to the H*-C-O plane where H* is the isotopomeric site) that are not symmetrically equivalent. The same argument can be extended to hydrogens that are beta to the hydroxyl group. It is desirable to quantify the differences between the various computation methods in the extent of deviation of fractionation factors between substitution at these sites.

To assess these dihedral effects at hydroxylated carbon and upon a methyl substituent of the hydroxylated carbon, the results for ethanol were used. Fractionation factors for the reactions

$$HOD + CH_3CH_2OH \rightleftharpoons H_2O + CH_3CH(OH)D$$

and

$$HOD + CH_3CH_2OH \rightleftharpoons H_2O + DCH_2CH_2OH$$

were considered for deuteration at each of the sites (H1 to H5) in figure 8.7 (see results p82). This yielded five distinct sites as the C_1 rotomer of the hydroxyl group was found to be of lower energy than the C_s.

8.4 Results and discussion:

Table 8.2 shows the fractionation factors for $CH_3D + XCH_3 \rightleftharpoons CH_4 + XCDH_2$ where X is some substituent. The mean deviation of the computed fractionation

factors from experiment is quoted at the bottom of each column (CH_3NH_2 was not included as the MP2 result is missing).

Table 8.2: Aqueous phase deuterium fractionation factors for hydrogen bound to sp^3 hybridised carbon at 298.15K, determined as the equilibrium constant for $XCH_3 + CH_3D \rightleftharpoons XCH_2D + CH_4$, where X is the substituent group listed below.

X	Experiment (ref 94)	AM1 Gas	AM1 COSMO	AM1 qm/mm	MP2* Gas	MP2* qm/mm
$-CHOH^+$	0.97	0.97	0.99	0.98	1.02	1.03
$-CH^+CH3$	1.02	0.93	0.97	0.94	0.98	0.99
-CN	1.04	1.05	1.02	1.03	1.08	1.08
-CHO	1.05	1.07	1.04	1.04	1.04	1.04
-NH2	1.09	1.08	1.08	1.07	-	-
$-O^-$	1.11	0.97	1.11	1.11	0.71	1.03
$-NH_3^+$	1.13	1.05	1.08	1.05	1.21	1.18
-F	1.17	1.14	1.13	1.09	1.22	1.21
-OH	1.18	1.17	1.17	1.15	1.15	1.19
mean absolute error	0.0	0.049	0.025	0.036	0.088	0.043

* Using 6-311G** basis set Restricted Hartree Fock.

For each quantum mechanical method, a treatment of solvation has been successful in improving the match with experiment. The improvement is greatest for the MP2/6-311G** quantum mechanical method. As this method produced the most erroneous gas phase results, consequently the qm/mm improvement did not yield the most overall successful method. AM1/COSMO and AM1 qm/mm (TIP3P water) proved to give very similar results. The COSMO approach produced the overall best results. The reason for the poor performance of MP2/6-311G** is the treatment of methoxide. This method becomes competitive with AM1/COSMO if methoxide is not considered (see suggestion for further work at the end of this chapter).

Table 8.3: Aqueous phase deuterium fractionation factors for hydrogen bound to sp^3 hybridised carbon at 298.15K, determined as the equilibrium constant for XH +HOD $\rightleftharpoons$ XD + HOH , where X is the substituent group listed below.

X (H bound at bold face **C**)	Experiment (ref 94)	AM1 Gas	AM1 Gas§	AM1 COSMO	AM1 qm/mm	MP2* Gas	MP2* Gas§	MP2* qm/mm
CH_3-**C**=O	0.83	1.03	0.95	1.10	0.97	0.85	0.79	0.68
O=CH-CH_2†	0.84	1.03	0.96	1.07	0.96	0.90	0.83	0.72
HO-CH_2	-	1.13	1.05	1.20	1.06	0.98	0.91	0.83
CH_3**C**H(OH)	1.04	1.22	1.13	1.28	1.14	1.08	1.00	0.89
$HOCH_2$-CH_2‡	0.88	1.06	0.98	1.12	0.97	0.92	0.85	0.74

† experimental model = pyruvate

‡ experimental model = lactate

* Using 6311g** basis set Restricted Hartree Fock.

§ Divided by vapour pressure isotope effect for water as in ref(17)

One method for obtaining these fractionation factors is to divide the gas phase factor by the vapour pressure isotope effect for deuteration of water (1.0793 at 25°C). The other results in table 8.3 were generated by treating both the water and the XCH3 by a solvation treatment of COSMO or qm/mm in the same manner as the fractionation factor with respect to methane.

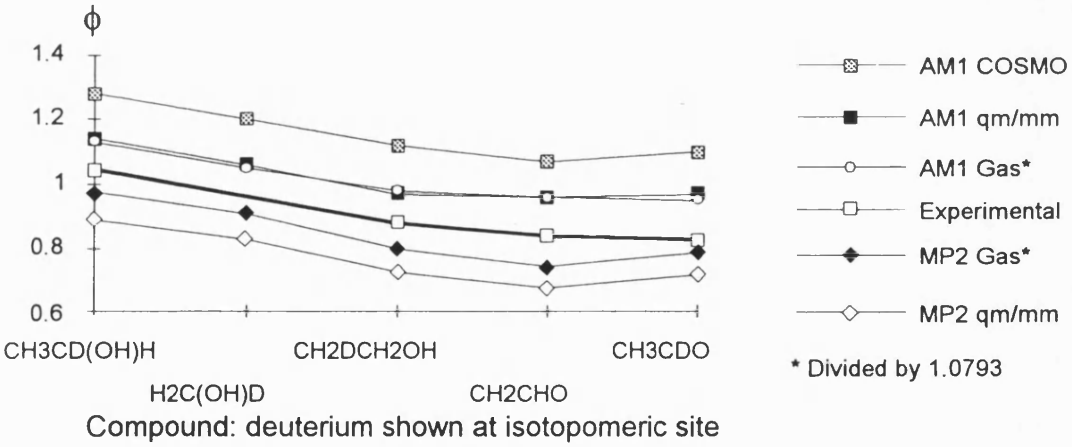

Fig 8.1: Fractionation factors relative to deuterated water for several isotopic substitution sites of ethanol, methanol and protonated acetaldehyde. The graph compares different computational methods.

For the qm/mm methods, three separate simulated desublimations were performed on the water, with different random number seeds. The resultant fractionation factors, using the different water structures, produced results invariant in the second decimal place. As there was no obvious method to compute an

equilibrium constant between the different water structures, the reported results are from the first structure generated.

The computed fractionation factors with respect to HOD are totally dominated by the vibrational partition function for the water. Gas phase results scaled down by 1.0793 prove to be the most accurate, with MP2/6-311G** treating the water molecule better than AM1. In sharp contrast to the fractionation factors with respect to methane, COSMO did not perform well. The mismatch between experiment and calculation for CH_3CDO may be due to acetaldehyde being a poor model for pyruvate.

Molecular arrangements of solvation:

One of the advantages of the qm/mm method is its ability to reveal molecular insights into the solvation structures. Whilst the experimental solvation structures are time averaged, the ability of the qm/mm methods to predict solvation effects on fractionation factors would suggest that the computed solvation structures may be indicative of the dominant experimental solvation structure.

The figs. 8.2 - 8.5 were generated directly from the qm/mm co-ordinates and have been altered only by the deletion of atoms that are not salient to the discussion. All distances are in Å.

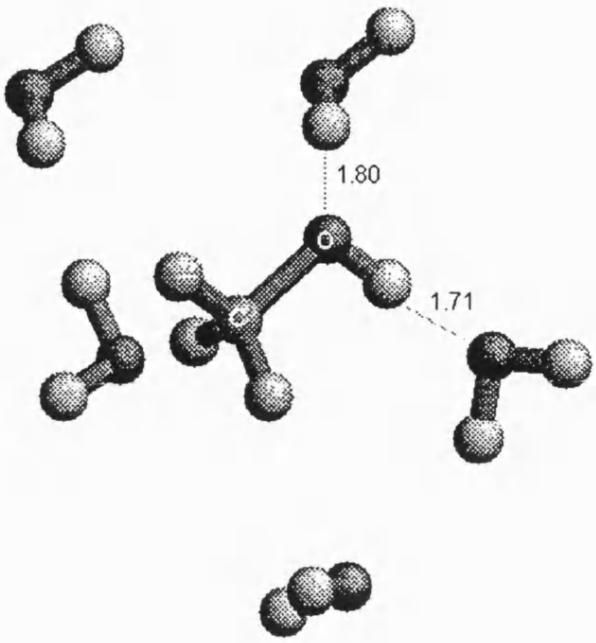

Fig 8.2: The first solvation shell of methanol in TIP3P water using MP2/6-311G** *ab initio* quantum mechanics.

Fig 8.2 is methanol and all those waters any part of which are within 2.5A of the methanol molecule. The model was generated using the 6-311G** basis set with MP2 electron correlation for the methanol and TIP3P for the water. The one hydrogen bond to the methanol oxygen is in accordance with the hydrogen bonds in liquid methanol (see fig 6.3).

Generated as for methanol, methoxide has five waters forming close hydrogen bonds to the oxygen. Four are approximately co-planar with one approaching from the top.

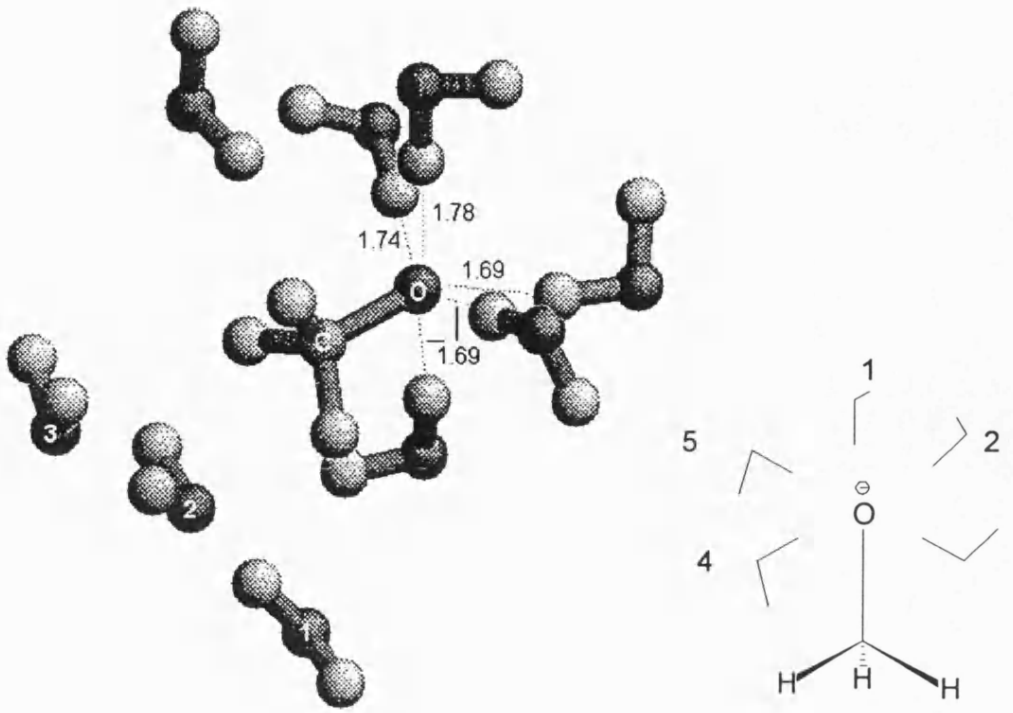

Fig 8.3: Shows the first solvation shell of methoxide, from the MP2/6-311g** qm/mm model. The left hand image shows all waters any part of which are within 2.5Å of the solute. The numbers show which waters make up part of the first solvation shell around the hydrophobic end of methoxide. The right hand diagram shows the scheme of hydrogen bonding to the methoxide. The numbers of the right hand diagram relate to table 8.4 on hydrogen bond lengths.

In the left hand picture of fig 8.3, waters marked 1, 2 and 3 are forming the start of the solvation shell around the hydrophobic end of the methoxide. The three waters around the base of the methanol are the equivalent for that system.

Table 8.4: Hydrogen bond lengths for solvated methoxide in Å using AM1 and MP2/6-311G** quantum mechanical methods. See fig 8.3 for the numbering of the bonds.

BOND	AM1	MP2
1-O hbond	1.80	1.69
2-O "	1.91	1.74
3-O "	1.81	1.69
4-O "	1.82	1.69
5-O "	1.95	1.78
C-O	1.35	1.39

$(CH_3)_2CH^+$ (fig 8.4, 8.5)shows strong interactions of hydrogen bond length with the two 'axial' hydrogens and the solvent. The hydrogen of the sp^2 carbon shows a similar interaction. The two hydrogens co-planar with that hydrogen have weaker, but still significant hydrogen bond like interaction. The only candidate for a dipolar interaction between a water oxygen and the sp^2 carbon is 3.19 Å distant.

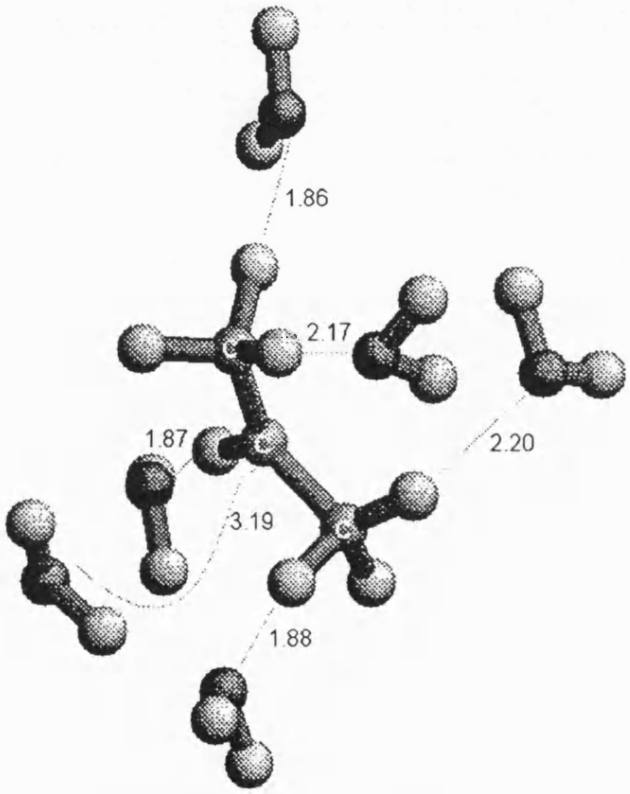

Fig 8.4: A selection from the first solvation shell of $(CH_3)_2CH^+$ at MP2/6-311G**. See discussion for details.

Solvation of this species appears to be due to hydrogen bonding to the protons of the solute. There is little evidence for strong dipolar interactions between water oxygen and the sp^2 carbon. The improvement upon solvation of the agreement between the computed and experimental fractionation factors, using either AM1 or MP2/6-311G**, suggests that this result is not an artefact of the qm/mm method.

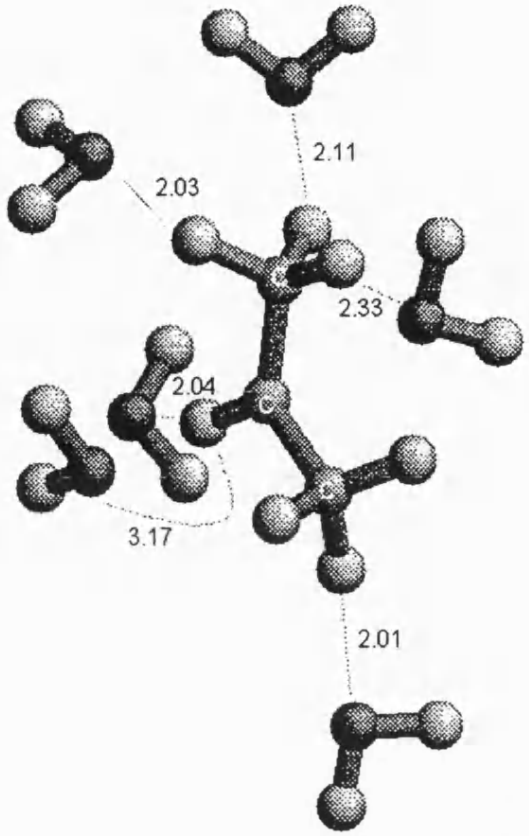

Fig 8.5: A selection of the AM1 first solvation shell of $(CH_3)_2CH^+$ showing the close interactions of solute protons with solvent oxygen atoms and a possible dipolar interaction between a solvent oxygen and the sp^2 carbon of the solute.

Electronic polarisation of solute by solvent:

Estimates of the relative magnitude of the polarisation of the solute electrostatic distribution by the solvent were obtained for CH_3O^- and CH_3CHOH^+ . Both species are charged and so a large solvation effect is to be expected. Whilst the methoxide shows a big change in fractionation factor upon solvation, the protonated aldehyde shows very little change.

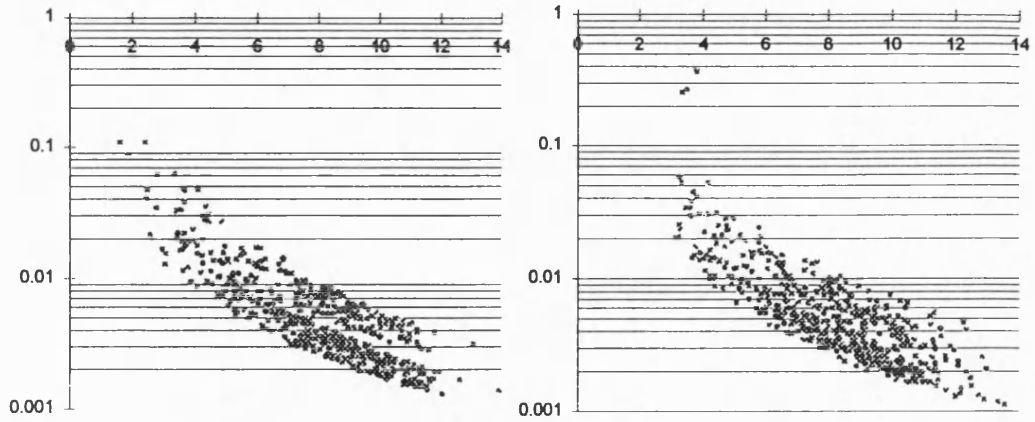

Fig 8.6:

Electronic polarisation of
CH_3O^- and CH_3CHOH^+

Vertical: RMS change in fitted charge distribution in atomic units.
This is a measure of the polarisation of the solute by a particular solvent atom.

Horizontal: Distance of removed point charge from solute centroid in Å.

For details see 'analysis of electronic polarisation' in methods.

The construction of the graphs in fig 8.6 is decribed in methods under 'analysis of electronic polarisation'. The graphs indicate that for CH_3CHOH^+, there are some solvent atoms that polarise the electronic distribution of the solute even more than the maximum solvent polarisation for CH_3O^-. Consequently, the lack of change in fractionation factor for the protonated aldehyde cannot be explained as being due to small solvent polarisation of its electronic structure.

A possible explanation for the difference is in the nature and extent of orbital overlap. The location of point charge centres for the lone pairs of CH_3O^- showed them to lie antiperiplanar to the hydrogens. This offers perfect overlap between the lone pair sp^3 orbitals and the C-H σ^* anti bonding orbitals. The donation of electron density into these orbitals probably accounts for the large inverse fractionation factor in the gas phase. Once solvated, the lone pairs' electron density shifts to interact with the water and so no longer delocalises into the C-H anti-bonding orbitals, making the system much more methanol-like. For CH_3CHOH^+, the orbital overlap between the C-O π system and the C-H bonds is not so good. The co-planar C-H bond of the methyl group and the π system are

orthogonal and thus have no overlap; the axial C-H bonds are ~30° away from perfect overlap. With the positive charge delocalised over both the C and O of the C-O bond, the necessity to delocalise further will also be small.

Dihedral effects:

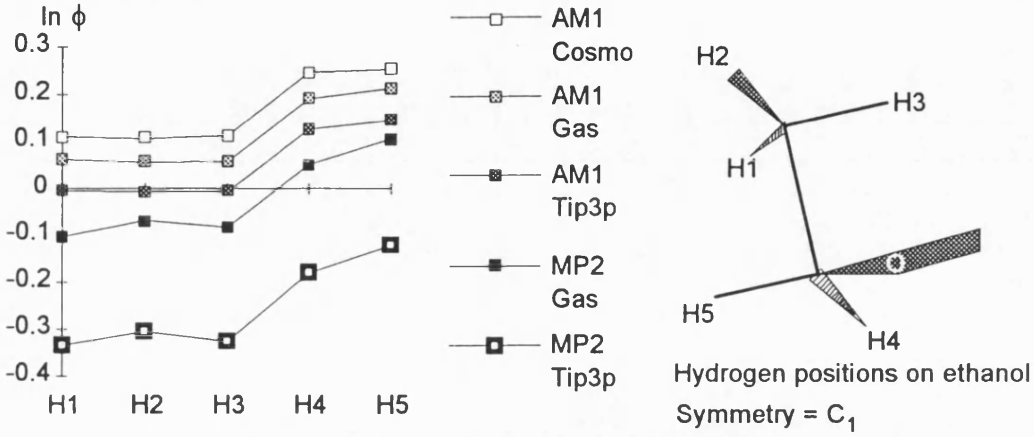

Fig 8.7: The natural log of the fractionation factors with respect to deuterated water at different isotopomeric sites on ethanol. H1 to H5 on the graph relate to sites H1 to H5 on the ethanol. *E.g.* the first vertical set of points on the graph give the natural log of the fractionation factor for the hydrogen that is *beta* and anti-periplanar to the hydroxyl.

The MP2/6-311G** results show a markedly larger variation in fractionation factor upon change of isotopomeric site compared to AM1. As this difference is seen in both gas and aqueous phase results, it can be assumed to be due to the quantum mechanical method rather than the coupling of that method to the molecular mechanics. The AM1-COSMO method would seem to slightly reduce the differences in sites compared to AM1-qm/mm or AM1 gas phase.

The difference in lnϕ (natural log of fractionation factor) between H4 and H5 with MP2-qm/mm is 0.058 which is greater than the natural log of the β deuterium kinetic isotope effect for the hydrolysis of β-D-methylglycoside (13a). Also, the difference in lnϕ between H2 and H1 ,at the same level of theory, is greater than the natural log of the γ deuterium kinetic isotope (-0.030 > -0.029). This indicates that the assessment of the isotope effects of hydroxylated systems is critically dependent on obtaining the correct dihedral angles of the hydroxyl

groups unless these dihedral angles are largely invariant between isotopically substituted species.

8.5 Conclusions:

Deuterium fractionation factors for hydrogen connected to carbon can be computed with a reasonable degree of accuracy using the AM1 and MP2/6-311G** quantum mechanical methods with solvation effect included by either qm/mm methods or (for AM1) the COSMO method. For AM1, the very much lower computational cost of COSMO, compared to qm/mm, makes this the method of choice unless the qm/mm model is required to investigate features unavailable to COSMO.

For MP2, the increase in cost going from gas phase to qm/mm (less than one order of magnitude) is much smaller than for AM1. For computation of fractionation factors in aqueous solution, the qm/mm method seems highly desirable for high levels of *ab initio* theory.

The analysis of the structure of the solvent yields valuable insight into the nature of solvation. This, coupled with the electronic polarisation by solvent analysis, gives considerable functionality to the qm/mm methods that is not available to other modelling techniques such as COSMO.

The use of the AM1 hamiltonian for computation of deuterium fractionation factors for hydrogen bound to carbon is justifiable for systems containing atoms for which AM1 is known to be well parameterised.

8.6 Suggestions for further work:

The use of diffuse basis functions for the computation of fractionation factors for methoxide using the MP2 method should be investigated.

There is often a significant systematic error in computed vibrational frequencies. (The standard deviation of the difference between computed and experimental frequencies gives a measure of the non-systematic error in the computed frequencies). Systematic error can be removed by scaling of the computed frequencies. Therefore, it is the magnitude of the standard deviation of the error between computed and experimental frequencies that governs the accuracy calculated frequencies after scaling.

Comparing the vibrational frequencies of gas phase methanol with the computed frequencies by the harmonic oscillator approximation, the standard deviation of the errors for MP2/6-311G** is 1.128 whilst those for BLYP/6-311G** (24) is 1.116. These results suggest the density functional approach (BLYP) is more accurate than the Møller Plesset method. This indicates the merit of repeating some of these calculations using BLYP/6-311G** *ab initio* qm/mm modelling. This is achievable using GRACE and CADPAC6, but not on the platform used for the presently computed fractionation factors (due to a code bug in CADPAC6).

The interaction of solvent with the protons in $(CH_3)_2CH^+$ is curious. Once computational technology has developed enough to permit it, the treatment of the first solvation shell of this system by ab-initio quantum mechanics may elucidate whether these hydrogen bond like interactions are artifacts of the qm/mm potential or related to the underlying chemistry.

Chapter 9 - Methods for computing the qm/mm intrinsic reaction co-ordinate

9.1 Goals:

1: To either find an existing technique or create a novel technique for finding first order saddle points for bond making and bond breaking processes in qm/mm models of high dimensionallity.

2: To apply the information obtained whilst attaining goal 1 in the calculation of intrinsic reaction co-ordinates from first order saddle points to reactants and products.

9.2 Introduction:

Intrinsic reaction co-ordinates are generated by following the mass-weighted 'steepest descents' path from a first order saddle point, on the potential energy surface, (for the rest of this section referred to as 'saddle point') to the reactants and products (59). Location of this saddle point is necessarily the first step in calculating the intrinsic reaction co-ordinate. As discussed in the main literature review, the P-RFO(54) and conjugate peaks refinement(59) methods are nearly, if not exactly, state-of-the-art in saddle point location. Conjugate peaks refinement is a representative of the largest class of saddle search algorithms that has been applied to systems with hundreds or thousands of degrees of freedom. To the author's knowledge, P-RFO has never before been applied to such system.

A formal discussion of each method can be found in ref.(59) for conjugate peaks refinement (CPR) and in ref.(54) for P-RFO. To develop a frame of reference for the following discussion, a description of their physical (rather than formally mathematical) methodology is included here.

Conjugate Peaks Refinement:

The method attempts to locate saddle points by considering two aspects of their nature. The first aspect is that the saddle point is a maximum on the minimum potential energy 'valley' that connects reactants and products on a potential energy surface. Where intermediates exist, these become reactants and products of a sub-reaction within this terminology. The second aspect is that a set of conjugate vectors describing instantaneous motion (in the sense used by calculus) about the saddle point will be, with respect to potential energy, a stationary maximum in one vector and stationary minima in all other vectors. As a hessian matrix of potential energy with respect to geometry (for the rest of this section referred to as a hessian) is Hermitian, its eigenvectors describe a set of conjugate vectors of instantaneous motion. Consequently, another way of looking at this second property of saddle points is that the hessian has one negative eigenvalue and the rest positive (or zero) at a saddle point. The harmonic oscillator approximation to vibrational frequencies derives these frequencies from the square root of the eigenvalues of the mass-weighted hessian. This produces the commonly reported property of a saddle point having one imaginary frequency.

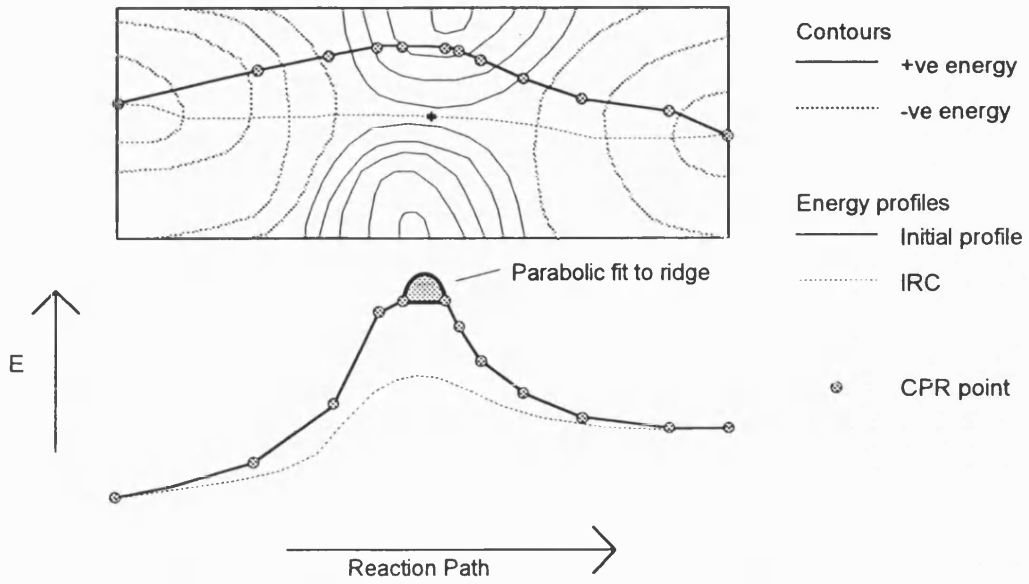

Fig 9.1: A drawing illustrating the two aspects of CPR. CPR places a set of points on the potential energy surface (top) and refines the position of those around an energy maximum along the chain of points whilst performing a parabolic fit to the space linking the highest two points.

CPR attempts to locate the region of space in which to use the second property for saddle searching, by utilising the first property (see diagram). CPR is initiated with a set of points that should approximate the minimum potential energy valley connecting reactants to products. The vector describing geometric motion between the two points of highest potential energy is taken to be the conjugate vector of instantaneous motion about the saddle point that is a stationary maximum. Maximisation along this vector and minimisation along a number of the other conjugate vectors is performed. A new energy maximum along the resultant set of points is then found and the process repeated.

In ref. 59 the authors explain the drawback to this process when applied to a grossly non quadratic potential energy surface. The line minimisations are performed after the line maximisation and in tandem with one another. The direction for each line minimisation is generated as being conjugate to the last direction minimised and starting at the point on the potential energy surface that was the result of the previous line minimisation. If the surface is quadratic, then each minimisation will remain conjugate to the original maximisation direction.

Where the surface is non-quadratic, this may not be so. As a consequence, line minimisations will interfere with the maximisation direction (*i.e.* be non conjugate to it) and the algorithm will converge toward a minimum not a saddle point.

To overcome this problem, it would be necessary to maximise along one conjugate direction and minimise along all others simultaneously. This should ensure that the minimisations were all conjugate to the maximisation. This is how the Partial Rational Function Operator (P-RFO) method operates.

P-RFO:

As mentioned above, the eigenvectors of the hessian represent a set of conjugate vectors of instantaneous motion about a point. The Partial Rational Function Optimisation algorithm constructs a step that represents maximisation in the direction of one of these vectors and minimisation in the others. Repeated application of this approach should lead to the maximised direction being at a stationary maximum and all other directions being at stationary minima, i.e. a saddle point.

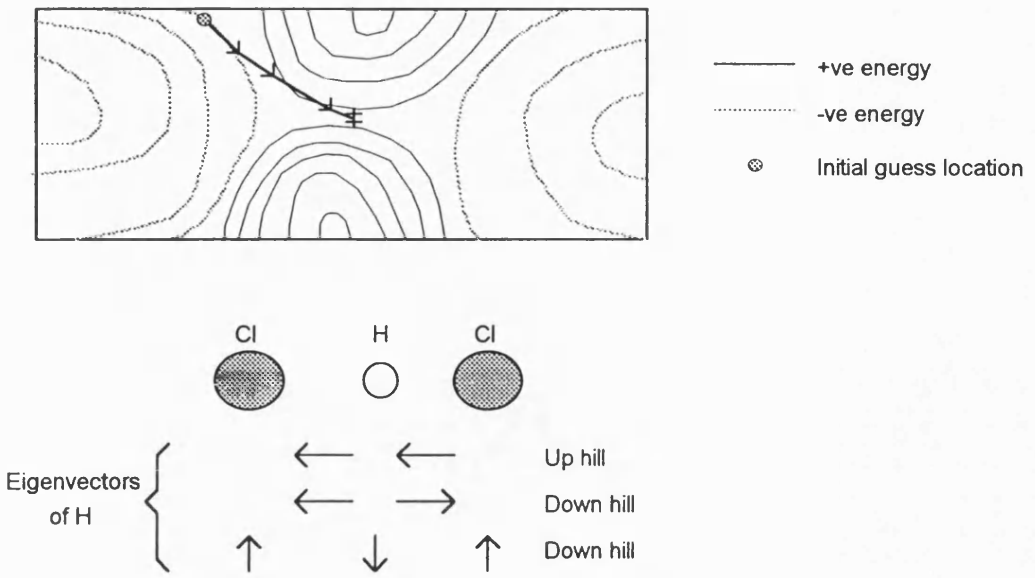

Fig 6.2: A drawing illustrating the P-RFO method for saddle point searching. The eigenvectors of the hessian (H) define a set of conjugate vectors, a step is taken which simultaneously goes uphill (maximisation) along one root and downhill (minimisation) along all the others. This leads in a series of steps towards the saddle point marked ‡. The potential energy surface (top) shows how these steps move towards the saddle. The simpler surface generated for proton transfer between chlorine atoms can be described (in 2D) by three conjugate vectors (bottom).

For qm/mm systems, computation of the hessian is extremely demanding of computer time. If the potential energy surface is quadratic, then the hessian would only need to be computed once. For a non-quadratic surface, the hessian must be re-computed after each step taken by the optimiser. A compromise to avoid this re-computation is to estimate the new hessian from the old one, the step taken and the gradient at the old and new points. Such methods are referred to as 'hessian update schemes'. For saddle point searching, the preferred update scheme is the one by Powell (96). For a saddle point search, a computed hessian is always used to start the search. From then on, more computed hessians can be used, or update scheme, or a mixture of both.

Whatever method is used to maintain a hessian, it will not be an exact representation of the curvature of a non-quadratic surface. If the gradient vector is divided by the hessian matrix, the result gives a vector defining the step direction and length of step to a stationary point under the quadratic

approximation to the curvature of the potential energy surface. The estimated change in the function value (in this case potential energy) can also be obtained by a quadratic fit to the function, Gradient and hessian. Where the surface is non-quadratic, the predicted function change will be incorrect. In this case, a 'trust-radius' can be defined as the maximum step length in which the predicted and actual function changes match to within pre-defined limits. Culot *et al.* defined a mechanism for estimating this trust radius (65).

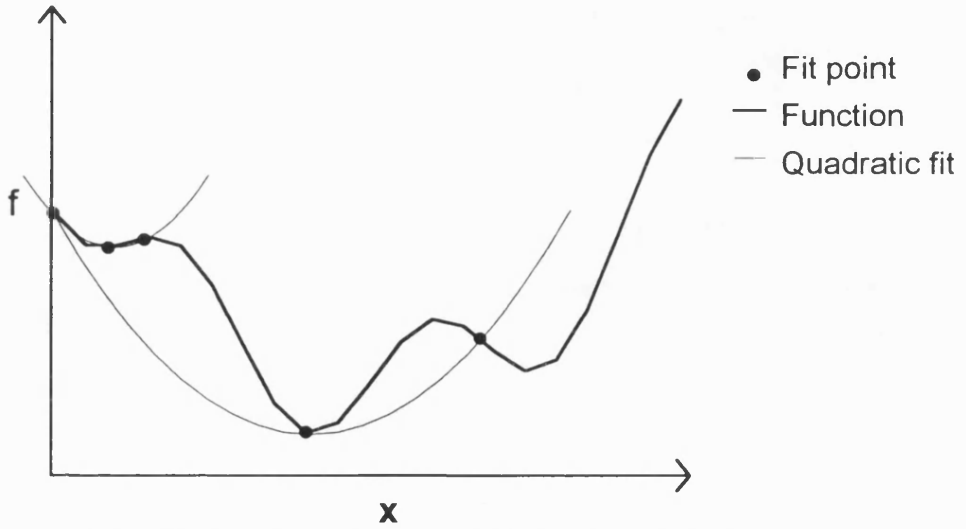

Fig 6.3: A diagram showing how a quadratic fit to function f with respect to variable x can become totally invalid as higher order terms move the function away from quadratic. The quality of the quadratic fit generally improves as the distance it is used over is reduced. The large parabola would not permit accurate prediction of function **f** with respect to variable **x** whereas the small parabola would.

In CPR, the vector defining that direction which was to be maximised was explicitly defined as the translation vector between two points on either side of a maximum. Such an approach cannot work for P-RFO as there is only one point defined. The mechanism for defining the maximised direction is to pick one of the eigenvectors of the hessian. Most matrix diagonalisation routines report the eigenvectors of the matrix in order of the magnitude of the eigenvalues. If these eigenvectors are to represent direction, the ordering that emerges from the diagonaliser has nothing to do with this direction. After each hessian re-

computation or update, there is a need to find which eigenvector is most similar, in terms of direction, to the eigenvector maximised in the last optimisation step. This concept is called mode following, where the name mode represents an eigenvector of the hessian.

Maximisation in the direction of a mode should make the eigenvalue associated with that mode more negative (or less positive) . If the followed mode is the one with the lowest eigenvalue, then it may be possible to assume that the algorithm can continue to follow the mode with the lowest associated eigenvalue. If the mode for maximisation is not the lowest mode to start with, it will be at the end of the saddle point search. The optimiser must be able to track which mode to follow as its position in the ordering of eigenvalues changes. The normally adopted method is to find the scalar product of the previously followed normalised mode with each of the new normalised modes. The absolute value of the result of this calculation is called the overlap. The new mode which produces the largest overlap from this calculation is the one that is followed.

The overlap value can be used to manipulate the trust radius. In the form of P-RFO by Jensen in MOPAC6 (60b) (which was ported into GRACE), there is a minimum overlap criterion. Should the overlap fall below this, the step that was taken is rejected and the trust radius halved in an attempt to improve overlap. For hessians maintained by an update scheme, the overlap generally will not be perfect even for an infinitesimal step length. To accommodate this, a minimum trust radius is defined below which the step will not be rejected on the overlap criterion.

9.2.1 Extending P-RFO optimisation to thousands of degrees of freedom:

There is no mathematical reason that the P-RFO method cannot be extended to an arbitrarily large number of degrees of freedom. The algorithm does have two

practical limits. Each calculation of each P-RFO step vector requires diagonalisation of the hessian matrix. The computational cost of a diagonalisation scales as the cube of the number of degrees of freedom being optimised. For qm/mm schemes that scale near linearly or as the square of the number of degrees of freedom, this diagonalisation starts to take longer than the computation of the potential energy and its geometric gradient! Where extremely time consuming quantum mechanical methods are used in qm/mm modelling, the size of hessian to diagonalise, before it would become the time limiting factor, can be quite large (thousands of degrees of freedom). In this case, storage of the hessian matrix, which scales as the square the number of degrees of freedom, would become a problem.

Morokuma and Maseras (42) suggest a method for dividing an optimisation into sections. Below is a discussion of this formalism and an extension of it to second derivatives. Such a method allows the P-RFO algorithm to operate on a sub-set of the total number of degrees of freedom of the system whilst locating a saddle point with respect to all the degrees of freedom. This removes the scaling problems of the P-RFO algorithm.

The system is divided into two sub-sets referred to as A and B. Let E be the potential energy of the system and **G** be the gradient vector of potential energy with respect to geometry. E_A is the energy due to interactions between atoms in sub-set A and themselves. $\mathbf{G}_A$ is the gradient vector of E_A with respect to the geometry of sub-set A. Substitution of subscript A for B refers to sub-set B.

Within this frame of reference one can define the total gradient vector **G**:

$$\mathbf{G} = \delta E_{AB}/\delta \mathbf{AB} = \delta E_A/\delta \mathbf{A} + \delta E_B/\delta \mathbf{B} + \delta E_B/\delta \mathbf{A} + \delta E_A/\delta \mathbf{B} \qquad \text{[eqn 9.1]}$$

let

$$\mathbf{G}_B = \delta E_{AB}/\delta \mathbf{B} = 0 \qquad \text{[eqn 9.2]}$$

=>

$$\delta E_B/\delta \mathbf{B} = 0 \;\; \& \;\; \delta E_A/\delta \mathbf{B} = 0$$

$\therefore$

$$\mathbf{G} = \delta E_{AB}/\delta \mathbf{AB} = \delta E_A/\delta \mathbf{A} + \delta E_B/\delta \mathbf{A} \qquad \text{[eqn 9.3]}$$

Equation 9.3 shows that under the condition that the gradient $\mathbf{G}_B$ has zero magnitude, the co-ordinates of sub-set A and gradient $\mathbf{G}_A$ completely define the system for the purposes of optimisation. The practical realisation of this idea is to optimise to zero gradient sub-set B with sub-set A fixed, before each step of optimisation of sub-set A is taken. This will make the optimiser controlling sub-set A in fact control the entire system AB. In general, as the gradient is zero at a minimum, sub-set B is optimised to a minimum at each step of the optimiser controlling the co-ordinates of sub-set A.

The relationship does not work for $\delta^2 E_{AB}/\delta \mathbf{AB}^2$ which defines the hessian **H** of potential energy with respect to geometry. All eigenvalues of **H** are not necessarily (in fact rarely) zero at a stationary point on the energy surface. This means that a simple extension of zeroing $\mathbf{H}_B$ will not produce a useful relationship between the co-ordinates of sub-set A and an optimisation of the entire system. The solution is to compute a finite difference approximation to **H**.

Let **A'** be **A+D,** where **D** is a small displacement vector for the finite difference.

For **A'** compute a new vector **B'** , such that

$\delta E_{AB}/\delta \mathbf{B} = \delta E_{A'B'}/\delta \mathbf{B'} = 0$ [eqn 9.4]

=>

$\delta^2 E_{AB}/\delta \mathbf{AB}^2 \approx ((\delta E_A/\delta \mathbf{A'} + \delta E_B/\delta \mathbf{A'}) - (\delta E_A/\delta \mathbf{A} + \delta E_B/\delta \mathbf{A}))/\mathbf{D}$

(in direction D) [eqn 9.5]

Equation 9.5 shows that the finite difference hessian will be correct for the second derivatives of equation 9.3 under the condition that equation 9.2 is true. The practical realisation of this is that, if sub-set B is optimised to a minimum for each finite difference step of computation of H_A, H_A will be correct with respect to the entire system defined by only the degrees of freedom of sub-set A. Also, a hessian update scheme based only upon $\mathbf{G}_A$, the geometry of A and the step taken by the optimiser controlling the geometry of A, will be correct with respect to the entire system defined by only the degrees of freedom of sub-set A

9.3 Method:

To implement the above ideas, the optimisation and IRC calculations were divided into two sub-sections: a fast-cycling sub-section and a slow-cycling sub-section. The fast-cycling sub-section represents section B in the above mathematical discussion and can be thought of as an 'environment' to the slow cycling sub-section A, which can then be referred to as the 'core'. The algorithm attempts to maintain the gradient of the environment at zero and the potential energy at a minimum. The algorithm then searches for a saddle point (or minimum) in the degrees of geometric freedom defining the core.

Before each evaluation of energy and gradient used for core, the environment is optimised to a minimum. This means that the number of cycles of the optimiser

acting on the environment is much greater than that for the core. This is why the environment can be described as a fast cycling sub-section.

A hessian matrix needs only to be stored and maintained for the core. Because the environment is being minimised, the ABNR (78) or LBFGS (50) optimisers can be used. These optimisers store only a diagonal hessian and small number of previous steps and gradient vectors. The alternative conjugate gradient method by Powell(68) was found to be less efficient. In this application, as the ABNR optimiser was resident in CHARMM rather than in GRACE, it proved to be slightly more efficient that LBFGS due to lower inter-process communications and so was the optimiser of choice for minimising the fast cycling sub-set.

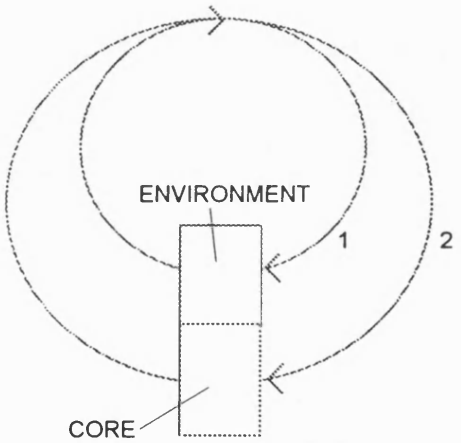

Fig 9.4: Summary of the two loop, core environment approach to transition state searching. Outer loop 1 optimises the core atoms towards a saddle point. For each cycle of loop 2, loop1 performs sufficient optimisation cycles to minimise the environment until the root mean square of the gradient is less than $0.0126 kJmol^{-1}Å^{-1}$ ($0.003\ kcalÅ^{-1}mol^{-1}$). Loop 2 cycles until the maximum component of the gradient vector of the entire system is less than $1.26 kJÅ^{-1}mol^{-1}$ ($0.3\ kcalÅ^{-1}mol^{-1}$) and the root mean square of the entire system is 1/3 this exit criterion. In cases where it proves hard to obtain only one negative eigenvalue of the hessian, an exit criterion of $0.42 kJlÅ^{-1}mol^{-1}$ ($0.1\ kcalÅ^{-1}mol^{-1}$) has been used.

Unfortunately, the mathematics describing the two sub-section method cannot be fully realised computationally. One major reason is that the environment cannot be minimised to a gradient that is truly zero. The best the algorithm can do is to converge to within machine precision of zero. Uncertainty in the exit potential

energy of the environment minimisation is passed on to the core optimiser. The resultant potential energy after each step of the slow-cycling optimiser is then uncertain. The effect of this is to reduce the accuracy with which the gradient vector presented to the slow cycling optimiser represents the derivatives of the potential energy with respect to geometry. This effect can be referred to as 'converger error' and resembles the effects caused by poor convergence of the self consistent field in optimisation of quantum mechanical models..

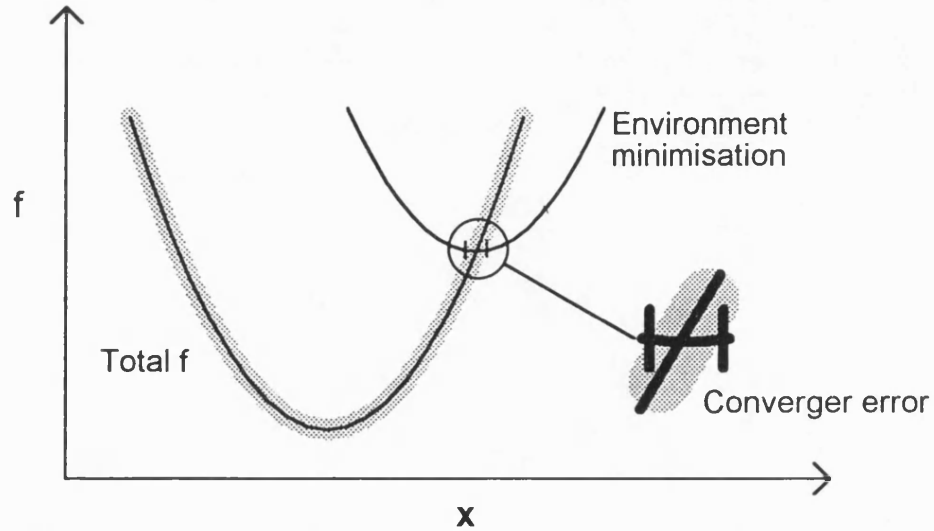

Fig 9.5: Diagram showing how numerical uncertainty in the point of convergence (**converger error**) of the environment minimisation is passed on as errors in the gradient experienced by the slow cycling optimiser. Function **f** is being minimised with respect to variable **x** (e.g. a reaction co-ordinate) in the presence of a continually minimised environment. For any value of **x**, **f** can only be defined within the uncertainty of the environment optimiser's exit point (the uncertainty is represented by the grey zone in the diagram).

A second problem is that there may be more than one viable structure for the environment. *i.e.* there may be two or more local minima for the environment for any given structure of the core. After a step of the slow-cycling optimiser there may be no new structure for the environment that resembles the previous one, and is a minimum. This will cause the environment to move to a different minimum structure. Such a move is instantaneous and irreversible with respect to the optimiser controlling the core.

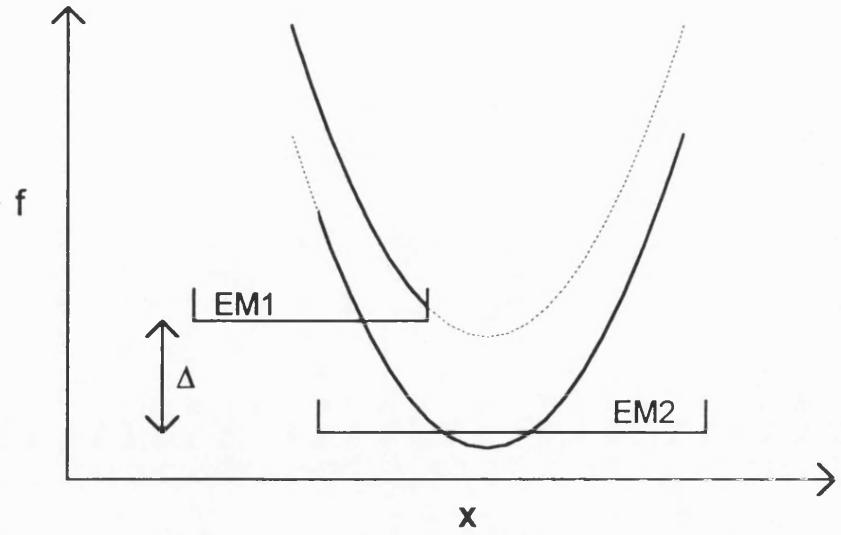

Fig 9.6: Diagram showing how, in a sub-set optimisation, different local minima in the environment can cause instantaneous irreversible change in the energy function **f** when searching in variable **x** (e.g. a reaction co-ordinate) that define the geometry of the core. The environment has two local minima (EM1 and EM2) structures. At small **x** only EM1 (energy minimum one)-like structures are viable for the environment. As **x** increases, structures like either EM2 or EM1 are viable for the environment. Eventually, only EM2 like structures become viable for the environment. The environment instantaneously (within one cycle of the core optimisation algorithm) moves from an EM1 to EM2 like structure. As EM2 is viable for the majority of values of **x** the new environment structure persists even if **x** is reduced.

The effect of converger error is to reduce the accuracy to which the slow cycling optimiser can converge. Experience would indicate that it does not become a problem unless an overall gradient of less than 10 times the numerical accuracy of the potential energy/gradient function is required. In chapter 10, a method by which sub-set B is represented by pure molecular mechanics is presented. In this case, the molecular mechanics generates a gradient accurate to 10^{-12} $kJ\text{Å}^{-1}mol^{-1}$ and so the environmental optimiser can minimise to an extremely low gradient. The result is that converger error between core and environment is less than the error introduced by convergence of the self consistent field.

The effect of the discontinuity is to disrupt the trust radius mechanism in the slow cycling optimiser. The instantaneous change in potential energy makes the predicted and actual energy change very different for the optimisation step in

which the change occurs. The trust radius method will reject that step and try a shorter step. Unfortunately that will not help because the new environment structure persists. This causes the trust radius to be continually reduced until the step length becomes so short that the algorithm becomes numerically unstable. To avoid this problem, the P-RFO algorithm has been amended to accept the step once the trust radius has dropped below a minimum criterion. See table 9.1 for a summary of the changes made to Jensen's P-RFO algorithm after it was imported into GRACE.

IRC calculation:

A standard IRC calculation can be performed in the core with the environment continually minimised. The result will not be a true IRC. If the core is of sufficient size to ensure the velocities of the atoms in the environment would have been trivial, should they have been included explicitly, then the error introduced by the approximation will also be trivial.

One drawback with this approach is that discontinuous changes in the environment (as discussed above) can cause the potential energy to rise during a step of the IRC algorithm. Energy rise during the IRC is one of the exit criteria of the algorithm. This effect can produce a premature end to the IRC calculation. It would seem that a core / environment approach to IRC computation can only be justified where there is some significant computational advantage to using this method (see chapter 10).

Table 9.1: Summary of the new and pre-existing features controlling the P-RFO optimiser in GRACE

Features in MOPAC & GRACE	Purpose of feature and comments
Update/recalculate	Choose between BFGS and Powell update schemes and/or periodic recalculation of the hessian
Minimum overlap criterion	Reject step and halve trust radius if the new mode and previous have an overlap less than this criterion.
Initial trust radius	Set the initial trust radius. Too large a setting produces a non convergent optimisation and/or poor mode following. Too small a value wastes cycles.
Minimum reducible trust radius for overlap criterion	If the trust radius is this size or smaller, the overlap criterion cannot cause it to be further reduced
Maximum and minimum ratio of predicted and actual energy change	The trust radius is reduced if the predicted and actual energy change lie outside these criteria. Setting these near to unity should improve the accuracy of the hessian in update schemes
Maximum trust radius	Trust radius cannot exceed this value. Setting this small reduces step rejection and improves overlap between steps. A small value might also require more calls to the potential energy and gradient algorithm.
Features new to GRACE	
Minimum step criterion	If the trust radius drops below this value, instead of exiting (as in MOPAC version) the step is accepted. The 'minimum reducible trust radius for overlap criterion' is set to this value also.
Mode animation during optimisation	Ensures that the structure of the followed mode is chemically relevant and permits restart and other actions if it is not.
Overlap viewing	The overlap (see text) between the last mode and each of the new modes can be viewed at each step to check for near identical modes.

Features new to GRACE *cont.*	Purpose of feature and comments
Convergence criterion	The criterion of convergence was changed from the norm of the gradient to the maximum absolute value of any element of the gradient. Also, the root mean square of the gradient must not exceed 1/3 the exit criterion.
Square root of minimum overlap	To avoid oscillations between accepted steps allowing trust radius increase followed by step rejection, the step is accepted but the trust radius halved if the overlap between the new and previous mode is less than the square root of the overlap criterion and the trust radius is greater than the minimum step criterion. This can be seen as a simple integration method in the control mechanism for the trust radius

9.4 Suggestions for further work:

The implementation of the core / environment method in GRACE has no intercommunication between the fast and slow-cycling optimisers. If the fast cycling optimiser was to reject the entire previous minimisation when the slow cycling one rejects a step there might be a significant efficiency improvement. Considering diagram 9.6, after a discontinuous change in environment structure, instead of the environment staying at an EM2 like structure upon trust radius reduction, it will return to the EM1 like structure. This means the trust radius may not have to be reduced to the minimum criterion level before a step can be made. However, if the discontinuous change must occur at some point anyway, the advantage would be lost.

Where optimisation of the environment is the dominant computational burden of the algorithm, improvements in this optimisation would be worthwhile. The present method starts the environment minimisation from 'scratch' for each cycle of the slow cycling optimiser. If the `LBFGS` algorithm was employed for the environment optimiser, it could be initiated with the diagonal inverse hessian from the exit of the previous environment optimisation. This could significantly reduce

the number of steps taken by the fast cycling optimiser for each step of the slow cycling one.

Changing the co-ordinates defining the geometry of the system from the present cartesian to redundant internal co-ordinates may be of advantage. Where the environment is a pure molecular mechanics function, the extra cost of the redundant co-ordinate manipulations would probably not be justified for the environment.

Chapter 10 - Extension of *ab initio* qm/mm methods to IRC calculation

10.1 Goals:

1: To reduce the amount of computer time required to locate first order saddle points and to calculate intrinsic reaction co-ordinates (IRCs) with *ab initio* qm/mm modelling.

2: To obtain this reduction without reducing the number of degrees of freedom by which the saddle points and IRCs are defined.

10.2 Introduction:

In chapter 6 a method of partitioning an optimisation or IRC calculation into fast-cycling and slow-cycling sub-sections was discussed. For saddle-point searching, where a hessian matrix of potential energy with respect to geometry must be maintained and diagonalised, this sub-set approach has an immediate benefit. IRC calculations (once the saddle point has been found) only require storage and manipulation of vectors, therefore having these two sub-sets is not any advantage in itself.

In chapter 4 - fig. 4.6, the polarisation of a self consistent field by atoms at varying distances is plotted. From this it is clear that most of the polarisation effect comes from only a few atoms. If the polarisation effect is ignored, and the mm electrostatics treated using point charges to represent the qm atoms, computation of the energy contribution from the mm atoms no longer requires a quantum mechanical calculation. Morokuma *et al.* (42) have used this concept. They have made all the mm atoms non-polarising, *i.e.* their electrostatics are computed with point charges for the qm atoms. This means that the mm atoms can be placed in the fast-cycling sub-set. Consequently, their degrees of freedom require only trivial amounts of computer time to optimise. The work here

represents a novel approach for extending this idea to polarising qm/mm modelling.

10.3 Method:

A qm/mm system can be broken into three sub-sets: qm, mm polarising (mmp) and mm non-polarising (mmnp). If all those mm atoms that would have a significant polarising effect are included in the mmp atom sub-set, this three sub-set model will be very similar indeed to having all mm atoms polarising. To take account of the change in charge on the qm atoms during an optimisation (or IRC), the non-constrained charge fit procedure described in chapter 2 can be employed to fit the qm atomic partial charges to the gradient of energy with respect to geometry for the mmp atoms. This fit can be repeated periodically to ensure that partial charges represent the current qm electrostatic structure.

The final step is to place the mmnp atoms in a fast-cycling sub-set of the optimiser. This way the number of degrees of freedom for which the optimiser must make quantum mechanics calculations is greatly reduced. This method also lends itself to the use of non-bonded cut-off schemes. The non-bonded interactions between mm atoms can be ignored after a given inter-atomic distance, as is normal practice in pure mm methods. As long as the distance at which the non-bonded cut-off scheme starts to work is greater than the maximum radius of the mmp region, a standard non-bonded cut-off scheme will operate without modification. Such a method will achieve the near linear scaling of pure mm methods. This extends its usefulness to applications where the 'fast-cycle / slow-cycle' optimiser (or IRC calculator) was not being employed.

10.3.1 Construction of a three sub-set qm/mm model:

The qm/mm potential energy function is generated from three main components, namely electrostatic/quantum, bonded/ Van der Waals, and 'ignored'. The

'ignored' refers to those atoms whose electrostatic point charges are ignored by the quantum mechanical calculation.

The electrostatic/quantum and bonded Van der Waals components represent the qm/mm model described in chapter 7 and are computed in exactly the same way in this work. Constraint terms are included as in chapter 7.

Summary of the construction of a three layered qm/mm model:

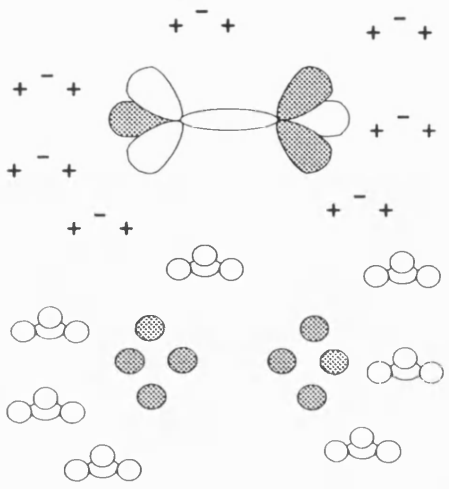

Fig 10.1: Quantum/electrostatic contributions for the polarising molecular mechanics interactions with itself and the quantum atoms, plus the qm atoms interaction with themselves.

Fig 10.2: Bonded/ Van der Waals component of the qm/mm energy function contains all the bonded mm interactions between the polarising mm atoms with themselves and all the Van der Waals interaction between the polarising mm atoms with themselves and with the qm atoms.

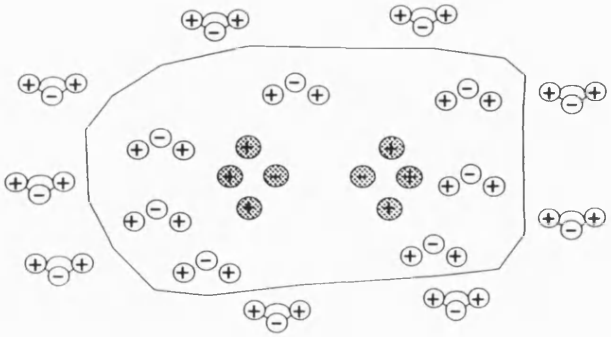

Fig 10.3: The 'ignore' contribution to the potential energy function contains all point charge electrostatic interactions and all Van der Waals interactions between the 'ignore' atoms (outside the line) and the polarising mm and qm atoms (inside the line). It also contains the entire molecular mechanics force field components for interactions between the 'ignore' atoms and themselves.

10.3.2 Optimisation and IRC techniques using the three sub-set model:

Minimisation and saddle searching is similar to the two sub-set model described in chapter 9. Both the quantum mechanics and polarising molecular mechanics atoms are placed in the slow-cycling sub-set. The 'ignore' are placed in the fast

cycling sub-set and the charge fit is performed every iteration of the slow cycle.In this work the P-RFO optimiser was used for the slow-cycling sub-set and the ABNR optimiser (78) for the fast- cycling sub-set.

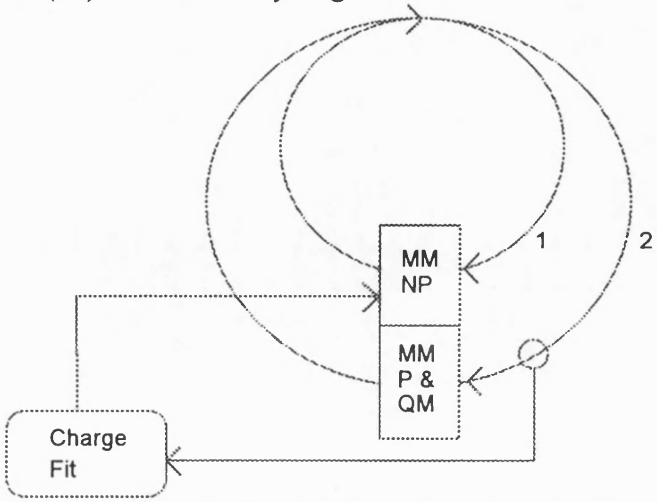

Fig 10.4: Summary of the two loop approach to qm/mm saddle point searching with a non polarising environment and charge fitting.

Fast-cycling loop 1. This loop must completely optimise to a minimum the mmnp atoms for each iteration of loop 2. The exit criterion of loop 2 is that the root mean square (rms) of the gradient is less than 0.0126 $kJÅ^{-1}mol^{-1}$ ($0.003kcalÅ^{-1}mol^{-1}$).

Slow-cycling loop 2 is optimised to a saddle point or minimum by manipulating the sub-set of geometry variables defining the qm and mmp atoms. The exit criterion is that the maximum component of the entire system's gradient (i.e. qm, mmp and mmnp) is less than $0.126kJÅ^{-1}mol^{-1}$ ($0.003kcalÅ^{-1}mol^{-1}$) or if it proves difficult to remove all but one negative eigenvalue from the hessian of the qm/mmp atoms, $0.042\ kJÅ^{-1}mol^{-1}$ ($0.001kcalÅ^{-1}mol^{-1}$). The rms of the gradient must be no more than 1/3 the maximum component.

This method has the drawback that the computed gradient of potential energy with respect to geometry is incorrect. The true gradient vector of potential energy with respect to geometry would be constructed from contributions from two gradient vectors. The first being the gradient of potential energy with respect to geometry, given that the fitted charges did not change. The second being the gradient of potential energy with respect to change in fitted charges, where the change in fitted charges is some function of the charge in geometry of the qm and mmp atoms. The reported gradient is only the first of these two and ignores the second.

In practice this is not a problem. As the magnitude of the gradient vector decreases, the step length of the optimiser also decreases. As the step length decreases, the change in fitted charges decreases. So, as more accurate gradients are required, (i.e. when the magnitude of the gradient vector is small) the error decreases towards zero.

10.3.3 Improving saddle point location:

Whilst the above 'two loop' approach has proven satisfactory for optimisations to minima and for IRC calculations, it has been less stable when applied to location of saddle points. The semi-empirical qm/mm models located saddle points by only including the qm atoms in the core (slow-cycling sub-set). Simply including all the mmp and qm atoms in the core was not satisfactory for *ab initio* applications. Doing so significantly increased the size of the hessian matrix; the optimiser proved less able to follow the correct mode when it was using these larger hessians.

The solution was to include a third optimisation loop. This allowed the core to contain just the qm atoms. The conjugate gradients optimiser by Powell (68) was used to optimise the mmp atoms to a minimum for each step of the slow-cycling optimiser. For each step of the mmp optimiser, the mmnp atoms were optimised to a minimum using the ABNR(78) optimiser.

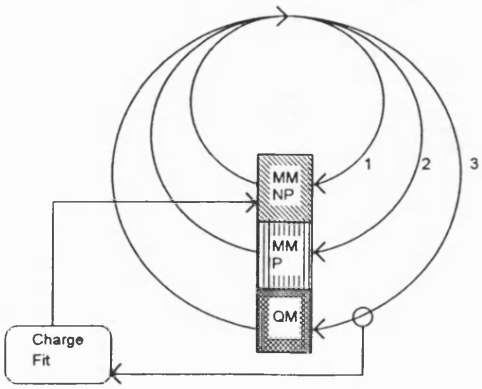

Fig 10.5:
Loop 1: Optimise core towards a saddle point using P-RFO optimiser. Charge fit qm region to point charges, for interaction with mmnp, every cycle.
Loop 2: Optimise mmp to a minimum for each cycle of loop 1. The exit potential energy and gradient of this optimiser are reported to the optimiser running loop 1 as the result of the step.
Loop 3: Optimise the environment (mmnp) to a minimum for each cycle of loop 2 using pure molecular mechanics.

10.7 Suggestions for further work:

The method needs to be extended to semi-empirical qm/mm modelling. It would seem likely that the charge fitting would have to occur less often than for the *ab initio* qm/mm method. Charge fitting at every quantum mechanical calculation could well take up a comparable time to the semi-empirical quantum mechanical calculation itself.

In some cases it is likely that the fitted charges on the qm atoms would be under-defined by the elements of the potential energy / geometry gradient of the mmp atoms. This will be detected by a large ratio between the maximum and minimum singular value reported by the DGLESS algorithm (74). This is not necessarily a problem in itself; the fitted charges will still represent the best fit available. The problem may be that the charge distribution will change significantly between charge fittings. Some investigation into these points and treatments of potential difficulties must be performed before the method can be considered to be generally applicable.

The near-linear scaling property of this method (with non-bonded cut-offs) makes it attractive for molecular dynamics of very large systems. The error in the gradient (as discussed above) will adversely affect the velocity integration of a molecular dynamics algorithm. To prevent this, the available knowledge of what the gradient would have been if the charges had not been fitted could be used to correct the temperature after each charge fit. This would help avoid having to resort to arbitrary velocity scaling. Such considerations are not necessary for Monte Carlo modelling, where the gradient is not required.

The use of a variable metric (*e.g.* P-RFO) optimiser for the mmp loop in the 'three loop' method, with the exit hessian of one optimisation starting the next, may well

improve efficiency. The reason for using the conjugate gradients method was to do with program construction.

Chapter 11 - Location of transition states in aqueous organic reactions using semi-empirical and *ab initio* qm/mm modelling

11.1 Goals:

1: To locate first order saddle points for organic substitution reactions in aqueous solution using semi-empirical and *ab initio* qm/mm modelling.

2: To use transition state theory to characterise these saddle points in terms of kinetic isotope effects and reaction barrier heights .

11.2 Introduction:

The logical extension of the calculation of fractionation factors for aqueous organic molecules was the location and characterisation of transition states for aqueous organic molecules. Use of a small (no more than three heavy atom) qm sub-section was desirable to allow use of electron correlated methods.

Leffek and Maclean reported the kinetic isotope effect for deuteration of the methyl group in the nucleophilic attack of methyl iodide by substituted ammonia(66). The free energy barrier for the equivalent nucleophilic attack of chloromethane by ammonia was computed by Monte Carlo qm/mm modelling by Gao (26) using the semi-empirical AM1 qm/mm method in CHARMM. The availability of these data makes the latter reaction a good candidate for modelling. Llewellyn, Robertson and Scott reported kinetic isotope effects for solvolysis of methyl chloride in water (67), making this reaction another good candidate for qm/mm modelling.

11.3 Method:

The kinetic isotope effect for the deuteration of all the hydrogens on the methyl group was computed for the following reactions:

$$CH_3Cl + H_2O \underset{\text{aqueous @ 363.15K}}{\rightleftharpoons} CH_3OH_2^+ + Cl^-$$

$$CH_3X + NH_3 \underset{\text{aqueous @ 323.15K}}{\rightleftharpoons} CH_3NH_3^+ + X^- \qquad X=I \ \& \ Cl$$

Calculations were performed using the AM1 (79) quantum mechanical method with COSMO(27) treatment of solvation. The results of these calculations were used to initiate qm/mm modelling with the AM1 quantum mechanical method and with the Restricted Hartree Fock method and 3-21G , 6-31G* and MP2/6-31G* basis sets (refs. for MP2(71), for RHF (6), for basis sets (39)). The TIP3P(75) molecular mechanics model was used for all water except that involved in nucleophilic attack. Kinetic isotope effects were computed using the rigid-rotor / harmonic-oscillator approximations by the CAMVIB and CAMISO (62) programs using the Bell(95) tunnelling correction. Modelling of the iodomethane containing reactions was limited to non-qm/mm methods due to a limitation in the CHARMM24 program and the computational cost of *ab initio* modelling of iodine.

11.3.1 AM1/COSMO in detail:

MOPAC93 (60a) was used for all calculations. The COSMO method was implemented with default settings and ε=78.4 for water. All calculations were performed with the 'Precise' setting in MOPAC. A 10 by 10 point grid of relaxations was performed with the carbon to leaving group bond length in one axis and the carbon to nucleophile bond length in the other. The grid spacing was 0.1Å. Grids were repeated over different ranges of bond lengths until a saddle point was located on the three dimensional surface of bond lengths against potential energy. The geometry from the point on the grid closest to the

interpolated position of the saddle was then used to initiate a saddle search, with all internal co-ordinates free to move, using the partial rational function optimiser (54) in MOPAC. An initial hessian of potential energy with respect to geometry, for the optimiser, was computed by forward-difference numerical differentiation. The symmetrical hessian update by Powell(96) was then used to maintain the hessian through the optimisation. The four–point numerical differentiation of geometric gradients scheme in MOPAC was then employed to compute the hessian for the saddle point once it was located.

The CH_3X (X=I or Cl) compounds were optimised from an initially guessed z-matrix using the partial rational function optimiser with a guessed diagonal initial hessian matrix. The four–point numerical differentiation scheme was employed again to compute the hessian for the equilibrium geometry once it was located. No final hessian matrix for the nucleophile equilibrium geometry was required for the computation of the changes in relative vibrational partition function involved in the isotope effects. Consequently, the equilibrium geometry of the nucleophile was not computed in the aqueous solution.

A set of 'valence' internal co-ordinates was generated by hand and passed to CAMVIB to remove the rotational and translational contamination from the hessian before the kinetic isotope effects were computed by CAMISO.

11.3.2 AM1 qm/mm in detail:

Two hundred water molecules, using the TIP3P potential (75), were packed around the AM1/COSMO derived saddle point structure using simulated desublimation. The method was identical to that for the fractionation factors work in chapter 8 and so will not be repeated here, except that there was no re-optimisation of the quantum mechanical atoms after the first addition of water. The geometry of the solute was kept fixed to the AM1/COSMO saddle point

geometry. No lone pairs were located for the Cl or I atoms during charge fitting in the simulated desublimation process.

The qm/mm model was the default AM1 based model in CHARMM24(30) by Field, Bash and Karplus ref.(22). The two sub-set optimiser described in chapter 9 was used to locate the saddle point from the result of the simulated desublimation. The atoms of the solute were placed in the core sub-set and the water atoms in the environment. First the environment was optimised to a minimum with the core fixed then an initial hessian of the core atoms was computed by forward difference without relaxation of the environment. This hessian was then used to start the saddle point search optimiser on the core, with environment continually optimised to a minimum. For all the molecules, the optimiser found a first order saddle point to a maximum component of the gradient vector of energy with respect to geometry of $0.42 kJmol^{-1}Å^{-1}$ ($0.1 kcalmol^{-1}Å^{-1}$) and the rms of the gradient one third that value.

A hessian matrix of energy with respect to geometry was then computed by bi-directional finite difference numerical differentiation for the solute and all atoms of any water any part of which was within 2.5Å of any part of the solute. The method employed was identical to the 'sub-set' approach discussed in the methods section of chapter 8.

A smaller hessian, for just the core atoms, was then used to start an intrinsic reaction co-ordinate calculation(3) with the environment continually relaxed and the core atoms following the mass weighted reaction co-ordinate down from the saddle point to reactants. The intrinsic reaction co-ordinate calculation exited when the energy increased after a step had been taken. The rms gradient at this point was not sufficiently low, for any of the species tested, for accurate vibrational analysis. A few steps of the ABNR(78) optimiser were used to lower

the gradient to an rms of 0.042kJmol^{-1}Å^{-1} (0.01kcalmol^{-1}Å^{-1}). The very demanding exit criterion was required because the ABNR optimiser, in CHARMM24, did not have a maximum gradient component exit criterion, only the rms was checked. The resultant structure was used to compute a hessian matrix in the same manner as for the saddle point.

11.3.3 Ab initio qm/mm in detail:

The located structures for the saddle point for the AM1 qm/mm calculations were used to initiate the *ab initio* calculations. The *ab initio* qm/mm model was that in GRACE using CADPAC6 (32) and CHARMM24b2 in conjunction with the three layer qm/mm approach detailed in chapter 10. The solute atoms were treated quantum mechanically, all those water molecules any part of which were within 3.5 Å of the solute (in the starting structure) were treated as polarising molecular mechanics (mmp) atoms, the rest were treated as unpolarising molecular mechanics (mmnp) atoms. The superimposition of atomic densities was used as the guess for the density matrices. The density matrices were converged until the rms difference in the density matrix between two successive iterations was less than 10^{-7} au. Saddle searching was performed using the three layer search algorithm described in chapter 10.

After a very considerable effort (a total of about one thousand cpu hours on the DEC AXP2000) no saddle point was found for the solvolysis of chloromethane using any of the 3-21G, 3-21G* 4-31G or 6-31G* basis sets with restricted Hartree Fock quantum mechanics. Several grid searches were tried and different selections of atoms in the core part of the optimiser were also tried. However, when second-order Møller-Plesset perturbation theory was applied to all the orbitals using the 6-31G* basis set (MP2/6-31G*), a saddle point was found starting from the saddle point structure from the AM1 qm/mm system.

Saddle points were found for the nucleophilic attack of chloromethane by ammonia using restricted Hartree Fock (with no electron correlation) with the 3-21G* and 6-31G* basis sets and using MP2/6-31G*.

Because the less computationally expensive methods were available for the saddle point for the reaction with ammonia as nucleophile, the structure located using the 3–21G* method was used to start the 6-31G* search, and this location was used to start the MP2/6-31G* search. This approach reduced the computational burden of finding the MP2/6-31G* saddle point by about an order of magnitude compared to performing the saddle search entirely at MP2/6-31G* (as had to be done for the reaction with water as nucleophile).

Once the saddle points had been located, the intrinsic reaction co-ordinates were computed and hessian matrices found in the same manner as for the AM1 qm/mm calculations, with the only difference being the use of the three layer instead of two layer qm/mm model.

11.3.4 Gas-phase calculations:

Some gas-phase calculations were performed using MOPAC93 and CADPAC6 with default settings to obtain indications of bond energies; see results, tables 8.3 and 8.4.

11.3.5 Reduced mass effects:

Using transition state theory, the cause of kinetic isotope effects can be simplified to the difference in the change in the vibrational partition function (zv) of the reactants and transition state upon isotopic substitution. This change in zv (Δzv) will be different for different reactions.

One can consider two major contributions to this difference in $\Delta z\nu$ ($\Delta\Delta z\nu$). 'Force constant effects' are caused by differences between the non-mass weighted force constants experienced by the isotopomeric species in different reactions. Vibrational frequencies, and hence $z\nu$, are affected by the mass of the vibrating species. The mathematical term used to describe this relationship is 'reduced mass'. The other contributions to $\Delta\Delta z\nu$ are 'reduced mass effects'. These are where the differences in the reduced mass of the vibrating system contribute to $\Delta\Delta z\nu$.

A good example would be the reaction $ICH_3 + NH_3 \rightleftharpoons CH_3NH_3 + I$ with a transition state $I—CH_3—NH_3$. The kinetic isotope effect for deuteration of the methyl hydrogens comes from $\Delta z\nu$ on going from ICH_3 to $I—CH_3—NH_3$. A comparison of the kinetic isotope effects for the equivalent chloromethane reaction could be broken down into reduced-mass and force-constant effects. The force constant effects would be due to the change in force constants describing the vibrations of the methyl hydrogens. The reduced mass effects would be due to the difference between the mass of ICH_3 and $ClCH_3$ and between $I—CH_3—NH_3$ and $I—CH_3—NH_3$. If the two reactions were electronically and geometrically similar, the reduced mass effects would be the major contributor to the difference in kinetic isotope effect between the two reactions.

When comparing the computed and experimental kinetic isotope effects for $ICH_3 + NH_3 \rightleftharpoons CH_3NH_3 + I$ with the equivalent chloromethane reaction, it was desirable to find out if the difference was a reduced-mass or force-constant effect. To do this an altered version of CAMISO was used to re-compute the isotope effects but with the atomic mass of chlorine replaced with that for iodine. Several other comparisons between computed and experimental results were performed in the same way. *E.g.* comparisons between substituents H and CH_3 involved setting the atomic mass of H to 15 a.m.u..

11.4 Results and discussion:

Comparison of free energy perturbation results to present work:

Gao reported the free energy of activation for the aqueous nucleophilic substitution of chloromethane by ammonia ref(26). The calculation was done by Monte Carlo modelling of the CHARMM24 AM1 qm/mm force field in TIP3P water. The computed figure of 110.1±0.1 $kJmol^{-1}$ agrees very closely with the enthalpy and potential energy barriers computed in this work (see table 8.1). Given the closeness of the barrier height calculated here using the same qm/mm model, but by saddle location and intrinsic reaction co-ordinate, it would appear that the change in entropy between reactants and transition state is very small. The magnitude of the error in estimating ΔG as being the same as ΔH is not significant compared to other sources of error, such as using the AM1 method.

Table 11.1: Calculated kinetic isotope effects for triple deuteration of the methyl group, and barrier height for the reactions

$$CH_3X + NH_3 \rightleftharpoons CH_3NH_3^+ + X^-$$ [aqueous 323.15K], X= I or Cl

The property of the chemical reaction to which the figures refer	AM1 COSMO CH_3Cl	AM1 COSMO CH_3I	AM1 qm/mm CH_3Cl	RHF qm/mm 3-21g* CH_3Cl	RHF qm/mm 6-31g* CH_3Cl	MP2 qm/mm CH_3Cl
KIE 3D*	0.929	0.857	0.921	0.945	0.952	0.932
" Cl Weighted† to I	0.930	-	0.921	0.946	0.952	0.932
" I Weighted to Cl	-	0.858	-	-	-	-
" H Weighted to Ethyl	0.928	0.851	0.921	0.945	0.952	0.932
" H Weighted to ^{t}But	0.928	0.851	0.921	0.945	0.951	0.932
$\Delta E^{\ddagger}$ ($kJmol^{-1}$)	107.3	155.2	106.4	39.7	55.54	66.0

RHF: 3-21G* basis set (39) restricted Hartree Fock

MP2: 6-31G* basis set (39) restricted Hartree Fock , MP2 electron correlation on all orbitals

$\Delta E^{\ddagger}$: The energy difference between the reactants and transition state. For AM1 qm/mm this is the difference in mm relaxation energy plus the difference in heat of formation from the qm calculation . For *ab initio* qm/mm this represents the difference in relaxation energy of the mm force field and the difference in total electronic + nuclear repulsion energy for the quantum mechanical force field and the qm/mm interaction energy.

KIE 3D*: Kinetic isotope effect for deuteration of all three methyl hydrogens.

Weighted†: Weighting of the computed substituents with the mass of experimental substituents, see 'reduced mass effects' in methods.

Using chloromethane as an analogue of iodomethane:

Gao went on to suggest that the experimentally derived barrier (26) of 98.3kJmol^{-1} for the iodomethane equivalent of this reaction is in good agreement with his results. In the absence of other data, this might seem reasonable. The close similarity of the results obtained by use of the COSMO solvation to those obtained by the qm/mm method, seems to indicate that AM1/COSMO results can be used to predict AM1/TIP3P qm/mm results. This being the case, the calculated figures (table 8.1) show that the correlation between the $ClCH_3 + NH_3$ calculated barrier and the $CH_3I + NH_3$ experimental barrier is coincidence. The AM1/COSMO calculated barrier height for the iodomethane reaction is 155.2kJmol^{-1} (table 8.1).

The comparison of ΔH to ΔG for the entropically similar chloromethane reaction shows that the very small entropy component of the barrier cannot account for the difference between AM1/COSMO and experimental results for the iodomethane reaction. However, AM1/COSMO calculated secondary α-deuterium kinetic isotope effects for the iodomethane reaction with ammonia in aqueous solution (k_{H3}/k_{D3}=0.86) agree very well with those observed experimentally for reaction of iodomethane with triethylamine in benzene of 0.87 (66) and for solvolysis of iodomethane in water 0.87 (67).

The calculated kinetic isotope effect for the chloromethane reaction is not in agreement with the experimental iodomethane effect (AM1/COSMO calculated k_{H3}/k_{D3}=0.93, AM1/TIP3P calculated k_{H3}/k_{D3}=0.92). If the argument that the computed chloromethane reaction is a good model of the experimental iodomethane reaction is to be pursued, this difference would have to be accounted for by reduced mass effects. By substituting the mass of iodine at the atomic centre of the chlorine and re-computing the isotope effects (table 11.1) it is clear that the difference is not a reduced mass effect; the change in isotope effect upon

change in mass is trivial. A similar approach applied to the substitution on the nucleophilic ammonia (table 11.1) indicates that the series of kinetic isotope effects reported in ref(66) are not reduced mass effects either. The computed effects show a trend opposite to that found experimentally as the molecular weight of the nucleophile is increased (see table 11.1 and 11.2).

Table 11.2: Results for secondary α-deuterium kinetic isotope effect (k_H/k_d) for: $CH_3I + NR_3 \rightleftharpoons CH_3NR_3^+ + I^-$, at 323.15K ref (66)

Tri-ethylamine	0.87
Tri-n-propylamine	0.89
Tri-n-butylamine	0.89
Pyridine	0.91

These results must be accounted for by steric effects on the out of plane bending modes of the hydrogen on the methyl group, and by electronic effects on the bond stretching and angle bending force constants.

Comparison of the calculated kinetic isotope effects for the different methods:

In agreement with the results for fractionation factors in chapter 8, the COSMO and qm/mm methods are in close agreement with one another. For the reaction with H_2O as nucleophile, the MP2/6-31G* qm/mm result is in very good agreement with experiment, whilst the AM1/COSMO and AM1 qm/mm results are incorrect. The AM1/COSMO result for the displacement of iodide by ammonia agrees well with experiment (as discussed above) whereas the chloromethane result does not agree with the iodomethane result. This makes it hard to compare the *ab initio* methods to the AM1 because there are no experimental values for ammonia attacking chloromethane. The close agreement of the kinetic isotope effects results for ammonia as nucleophile with MP2/6-31G* and with AM1 suggest that the failure of AM1 for the water as nucleophile was due to its treatment of the C-O bond.

Table 11.3: Calculated kinetic isotope effect for triple deuteration of the methyl group, and barrier height for the reaction:

$CH_3Cl + H_2O \rightleftharpoons CH_3OH_2^+ + Cl^-$ [aqueous 323.15K]

Property modelled	AM1/COSMO CH_3Cl	AM1 qm/mm CH_3Cl	MP2 qm/mm CH_3Cl
KIE - 3D	0.87	0.86	0.92
$\Delta E^{\ddagger}$ (kJ/mol^{-1})	134.6	159.0	59.8

MP2: 6-31G* basis set restricted Hartree Fock , MP2 electron correlation on all orbitals

$\Delta E^{\ddagger}$: see table 11.1 for details.

Reasons for not finding RHF saddle points of solvolysis of chloromethane:

It is not clear why the saddle point for the aqueous solvolysis of chloromethane was not located at the restricted Hartree Fock level of quantum mechanical theory. Simple observation of the energies of the O-C bond in the gas-phase products (table 8.4) shows a relatively large bond energy for the MP2/6-31G* quantum mechanical method, compared to restricted Hartree-Fock methods. This would give a more S_N2-like saddle point for MP2/631G*. It would seem likely that an S_N2-like transition state will have a greater negative curvature, and thus become less prone to numerical problems in the saddle location algorithms. The greater magnitude of the imaginary frequency for the AM1 qm/mm method and the greater ease of finding the saddle point, lends weight to this argument (see table 8.6). This argument is further supported by the larger C-N bond energies, in $CH_3NH_3^+$, associated with the much more easily found saddle point for nucleophilic attack by ammonia (see table 11.5).

Table 11.4: Heterolytic bond energy ($kJmol^{-1}$) for O-C bond in protonated methanol calculated using a range of quantum mechanical methods.

Theory	C-O length Å	Energy CH_3^+	Energy H_2O	Energy $CH_3OH_2^+$	Bond energy
AM1	1.496	1055.8	-247.0	578.5	230.3
PM3	1.476	1073.4	-223.6	655.0	194.8
6-31G*	1.511	-103000.1	-199566.2	-302822.5	256.2
MP2/6-31G*	1.508	-103259.4	-200061.1	-303646.8	326.5

Energy: Heat of formation for semi-empirical methods and total electronic + nuclear repulsion energy for *ab initio* methods.

Table 11.5: Heterolytic bond energy ($kJmol^{-1}$) for N-C bond in protonated methylamine calculated using a range of quantum mechanical methods.

Theory	C-O length Å	Energy CH_3^+	Energy NH_3	Energy $CH_3NH_3^+$	Bond energy
AM1	1.479	1055.8	-30.5	622.2	403.1
PM3	1.495	1073.4	-12.9	641.4	419.1
6-31G*	1.507	-103000.1	-147512.0	-250928.2	417.1
MP2/6-31G*	1.511	-103259.4	-147966.3	-251722.9	497.2

Energy: Heat of formation for semi-empirical methods and total electronic + nuclear repulsion energy for *ab initio* methods.

Table 11.6: Calculated imaginary frequencies in icm^{-1} for the saddle point structures for the reactions:

$CH_3X + Nu \rightleftharpoons CH_3Nu^+ + X^-$ [aqueous], X= I or Cl, Nu= H_2O or NH_3

Saddle point	AM1/COSMO	AM1/qm/mm	3-21G*	MP2/6-31G*
$Cl\text{-}CH_3\text{-}OH_2$	791.0	504.2	-	450.2
$I\text{-}CH_3\text{-}NH_3$	837.8	-	-	-
$Cl\text{-}CH_3\text{-}NH_3$	791.8	785.2	680.1	724.6

Comparison of the differences in barrier height and saddle point structure for the different methods:

The AM1 qm/mm and AM1/COSMO method are in less agreement in saddle point structure than they are in energies and isotope effects (see table 11.7). For the displacement of chloride by ammonia, the AM1/COSMO structure agrees almost as closely with MP2/6-31g* qm/mm as it does with AM1 qm/mm. For the water as nucleophile, it appears that AM1 estimates the O-C bond at the saddle

point to be considerably shorter than does MP2/6-31G*, with either the COSMO or qm/mm solvation method for the AM1.

Table 11.7: Distances (Å) from the methyl carbon to the leaving group and methyl carbon to the nucleophile at the saddle point which approximates to the transition state for the reactions:

$CH_3X + Nu \rightleftharpoons CH_3Nu^+ + X^-$ [aqueous], X= I or Cl, Nu= H_2O or NH_3

Bond reported	AM1/COSMO	AM1/qm/mm	3-21G*	6-31G*	MP2/6-31G*
$I\text{-}CH_3NH_3^+$	2.341	-	-	-	-
$ICH_3\text{-}NH_3^+$	1.917	-	-	-	-
$Cl\text{-}CH_3NH_3^+$	2.123	2.104	2.190	2.242	2.198
$ClCH_3\text{-}NH_3^+$	2.067	2.022	2.238	2.215	2.095
$Cl\text{-}CH_3OH_2^+$	2.295	2.304	-	-	2.180
$ClCH_3\text{-}OH_2^+$	1.832	1.756	-	-	2.059

The number and length of hydrogen bonds to the solute changes much more for the AM1 based methods, than the MP2/6-31G*, between saddle point and reactants. This might be an indication that the solvation of the solute is greater at MP2/6-31G*. Semi-empirical methods are known to underestimate charge movement, and so a greater polarisation and solvation by the water can be expected for the *ab initio* methods. Such a difference in solvation may account for part of the reduction in barrier height with *ab initio* methods as compared to AM1. In the gas phase, it was not possible to locate a saddle point for nucleophilic substitution of H_2O for Cl^- on chloromethane. The saddle point for similar attack by ammonia (Gao (26)) is very different from that in water. This prevents the comparison of aqueous and gas-phase results being a valid probe of the solvation effect on barrier height for different quantum mechanical approaches.

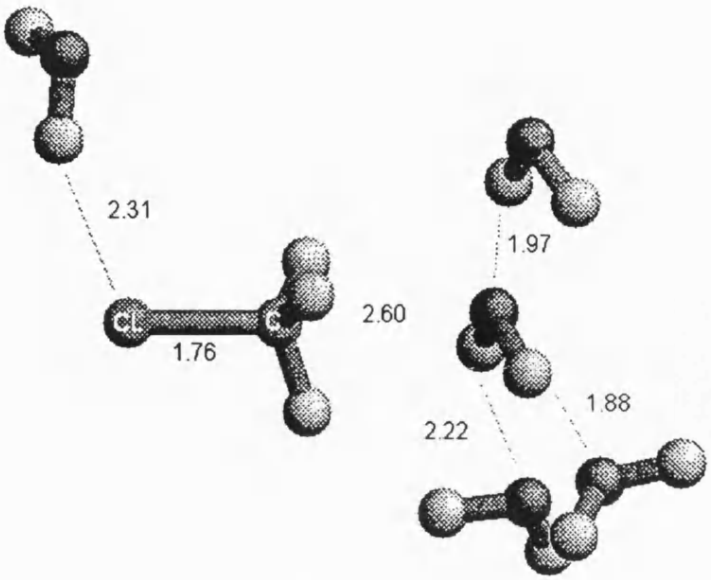

Fig 11.1: A selection of the first solvation shell of the reactants modelled at AM1 qm/mm for aqueous solvolysis of chloromethane. Inter atomic distances in Å

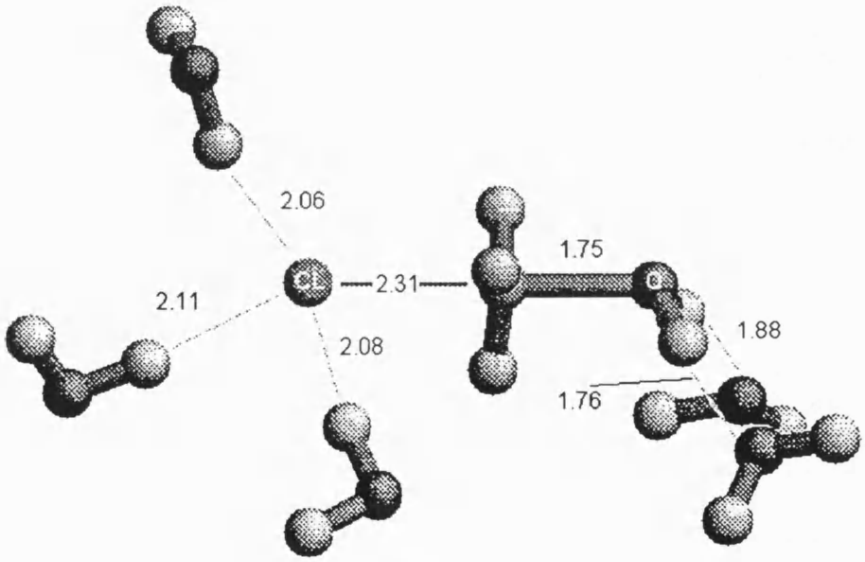

Fig 11.2: A selection of the first solvation shell of the saddle point modelled at AM1 qm/mm for aqueous solvolysis of chloromethane. Inter atomic distances in Å

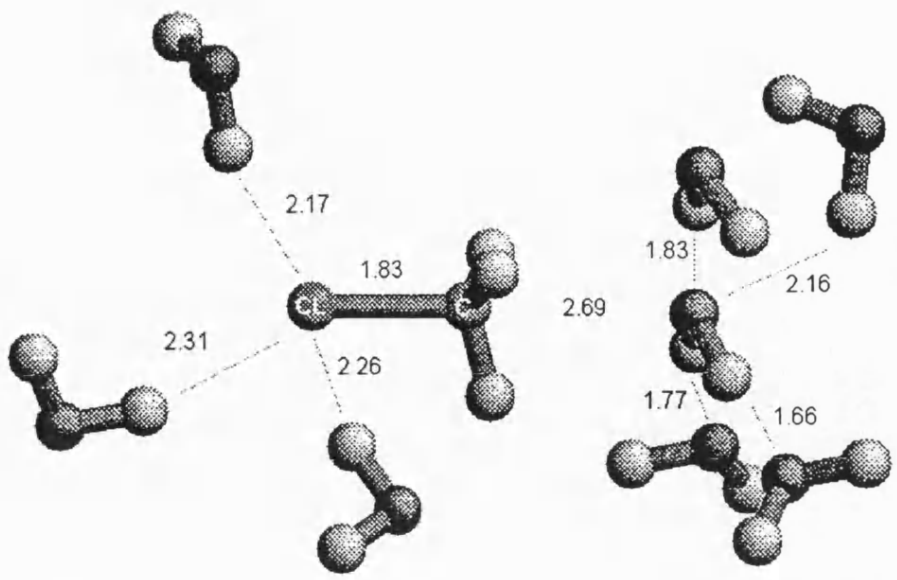

Fig 11.3: A selection of the first solvation shell of the reactants modelled at MP2/6-31G* qm/mm for aqueous solvolysis of chloromethane. Interatomic distances in Å

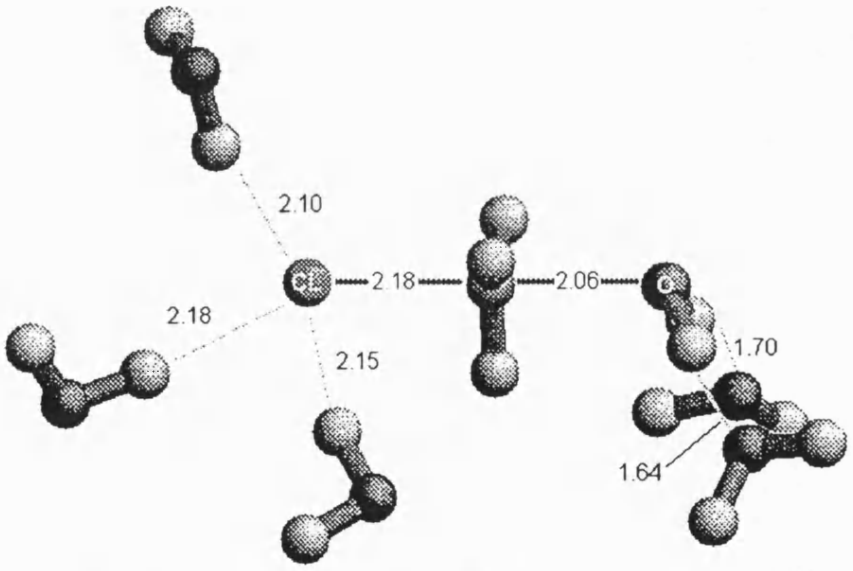

Fig 11.4: A selection of the first solvation shell of the saddle point modelled at MP2/6-31G* qm/mm for aqueous solvolysis of chloromethane. Interatomic distances in Å

11.5 Conclusions:

These results conclusively demonstrate the ability of the present algorithms to locate saddle points in qm/mm models of high dimensionality. The success of the 3-layer *ab initio* qm/mm model in predicting kinetic isotope effects goes a long way to supporting this modelling method. It would appear that the use of semi-

empirical methods must be treated with much more caution for saddle points than for equilibrium geometries.

Despite the very much greater cost of the *ab initio* methods compared to semi-empirical, it would appear that for these reactions they are justifiable for the calculation of experimentally reproducible results.

11.6 Suggestions for further work:

The major suggestion for further work is to improve the efficiency of the optimisation scheme so that more time can be sent on each quantum mechanical calculation and hence larger molecules can be treated. Chapter 10 gives some specific suggestions for improvements to the algorithms used here. The use of internal rather than of cartesian co-ordinates for the 'core' part of the optimisation may improve efficiency further.

These results do not include an analysis of the entropy components of the reaction barriers for *ab initio* methods. The first step to investigating this area would be to perform Monte Carlo free energy perturbation calculations along the IRC to find the change in entropy for these reactions. By applying the Monte Carlo algorithm only to the mmp and qm atoms, and maintaining the mmnp atoms minimised, the dimensionallity of the geometry space that must be sampled would be massively reduced (compared to conventional Monte Carlo). This approximation should not significantly reduce the validity of the simulation, but may bring such free-energy perturbation calculations within reach of moderate workstations, even at the MP2/6-31G* level of quantum mechanical theory.

Chapter 12 - Qm/mm modelling of lactate dehydrogenase

12.1 Goals:

The goal of the work described in this chapter was to investigate the strengths and weaknesses of the qm/mm and minimal sampling methods for modelling enzymes. It did this by using semi-empirical based qm/mm modelling on the lactate dehyrogenase enzyme. Unfortunately, *ab initio* qm/mm modelling of enzymic reactions was not possible for lack of computational resource.

Division of contributions:

This section of the thesis refers to work carried out in collaboration with Dr V. Moliner who was a visiting fellow at the University of Bath during 1996/97.. Whilst the strongest emphasis is given to those parts of the work for which the author was principally responsible, no one piece of the work was purely the result of one individual's effort.

The majority of the algorithmic development was the work of the author. The bulk of the code operation was performed by Dr Moliner, as was the initial setting up of the enzymic model. The analyses of the results, as presented here, were evenly split between the author and Dr Moliner.

12.2 Introduction:

Proton and hydride transfers are known to play a leading role in biological systems; they occur in the course of many enzyme reactions. The enzyme lactate dehydrogenase (LDH) (EC 1.1.1.27) catalyses the inter-conversion of lactate and pyruvate by employing nicotinamide adenine dinucleotide (NAD) as cofactor. For the reduction of pyruvate, the substrate interacts with the active site residues in such a way that a hydride ion is transferred from the reduced nicotinamide ring, while a

histidine residue is the proton donor (see fig 12.0). The mechanism by which these transfers occur is a matter of topical debate. A good example of this would be the work by Andrés, Moliner, Krechl and Silla (80), by Williams and Wilkie (81b) and by Yadav, Jackson, Holbrook and Warshel (82). The first two suggest a concerted mechanism whilst the latter suggests a stepwise mechanism with hydride transfer preceding proton transfer.

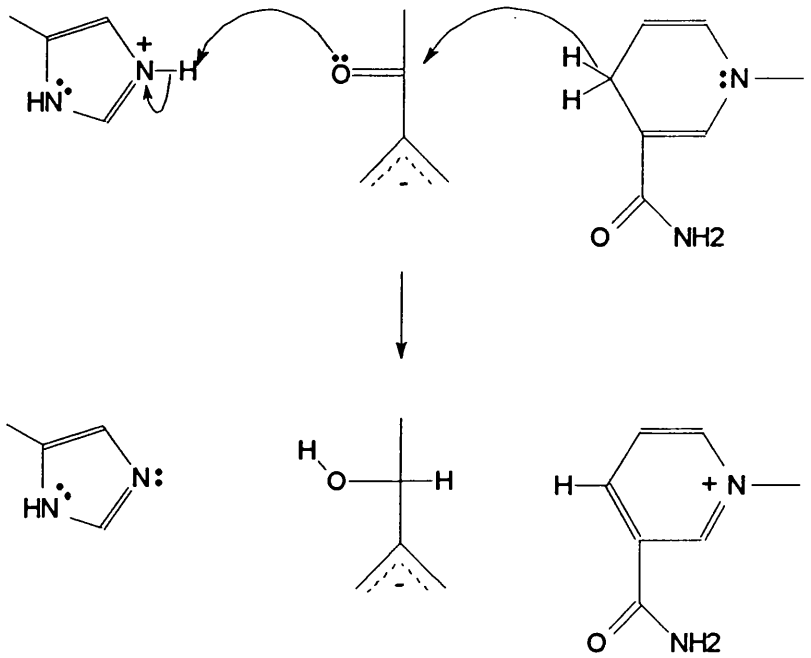

Fig 12.0: The reduction of pyruvate to lactate by a concerted mechanism. There is hydride transfer from the nicotinamide (right) to the alpha carbon of the pyruvate and proton transfer from the histidine (left) to the carbonyl oxygen of the pyruvate.

One key question, which theoretical studies have attempted to address, can be summarised as 'what is the origin of the catalysis'. The concept that the enzyme aligns the substrate and reacting residues in a similar conformation to that of the transition states has been explored in the work by Andrés *et al.* (80) and by Williams and Wilkie (81a,b). Williams and Wilkie located *in vacuo* first order saddle points for various truncated analogues of the acid catalysed reduction of pyruvate. These transition states proved to be of similar geometry across a range of quantum mechanical methods and a variety of truncated reactants. The located transition states suggested a concerted mechanism with the proton transfer very nearly

completed and the hydride transfer about 50% completed at the saddle point. The work by Andrés *et al.* came to similar findings using semi-empirical quantum mechanics and also using the AMSOL (89) continuum model for aqueous solution. All these transition states show remarkable similarity to the reactant state structure of LDH as resolved by x-ray crystallography (85).

The concept that electrostatic effects may be responsible for the catalytic abilities of LDH has been addressed by Williams and Wilkie(81). They altered the acidity of the proton donor by electrostatic interaction with a variable strength dipole. The effect of the dipole on the primary kinetic isotope effect for protide *vs.* to deuteride transfer was computed. This work indicated that increasing strength of the acid catalyst increased the isotope effect.

Warshel *et al.* (82) suggest that reducing solvent reorganisation energies is a significant contribution to the catalytic effect of the enzyme. This concept can be viewed as the unification of the structural and electrostatic catalytic hypothesis. The aqueous transition states discussed in chapter 11 give a simple example of this idea. The structure of the first solvation shell around the transition state is dominated by the charge and geometric structure of the transition state. The alignment of the water dipoles is such as to reduce $\Delta G^{\ddagger}$ (the energy barrier for going from reactants to transition state). The reorganisation of the solvent on going from a reactant solvation structure to a transition state solvation structure is referred to as λ_S, the 'solvent reorganisation energy'. λ_S may well require energy and so increase $\Delta G^{\ddagger}$. If the enzymic active site has dipoles which are held in the transition state stabilising orientation then λ_S will be reduced. Reducing λ_S will reduce $\Delta G^{\ddagger}$. This is a structural catalytic effect where the active site structure is held at that which favours the transition state. This structural effect is combined with the catalytic action of these 'held' dipoles, which is an electrostatic stabilisation effect.

The work described in ref. 82, by Warshel *et al.*, used the 'empirical valence bond' (EVB) modelling method (10). As discussed in the literature review (chapter 3), this method has the tendency to 'pre-determine' the result of a modelling exercise. The purpose of this qm/mm model is similar to EVB in that it requires much less truncation of the chemical system than did the studies by Andrés *et al.* (80) or Williams and Wilkie (81b). The semi-empirical molecular orbital qm/mm approach used here (21,79) has the advantage of making less *a priori* assumptions about the reaction mechanism than EVB does. Consequently, it is complementary to the previous studies.

12.3 Method:

Work by others (Dr Tim Dafforn - University of Bristol):

The initial LDH structure has been derived from the X-ray structure of the ternary complex oxamate-NADH-LDH and fructose-1,6-bisphosphate (allosteric agonist) at 2.5 Å resolution (85). Owing to the great size of tetrameric LDH molecules, and because of the independence of sub-units, only one sub-unit was considered. The substrate pyruvate was constructed from the oxamate structure by making the appropriate atom and angle changes. Hydrogens were added, with all ionizable groups set at a state complementary to pH 7. The entire system was hydrated within a pre-formed 20Å sphere of water, centred on His-195. Once the system was prepared an extensive conformational search was carried out. This search had initial minimisation of the water molecules with the protein atoms fixed. Then a series of minimisations were performed to remove bad contacts whilst using harmonic constraint terms to prevent the system undergoing gross conformational changes due to the bad contacts. Then a very brief period of 4 picoseconds of equilibration at 300K was performed using molecular dynamics with the Verlet algorithm (88). The conformational analysis then consisted of taking individual structures from a further 30 picoseconds dynamics trajectory at 6 picosecond intervals (76).

Novel work:

Our group was then supplied with the six structures from the second dynamics trajectory. Each of these structures was treated separately, producing six sets of results. The procedures performed on each structure will be referred to as 'jobs'. The work carried out on structure number 1 and the consequent results will be referred to as job number one *etc.*.

The qm/mm treatment was performed by the CHARMM 24b2 (30) program. The memory requirement for the semi-empirical qm/mm method in this program scales as the square of the number of atoms in the entire system. In order to make the memory requirement small enough to fit on the available machines, several truncations were performed.

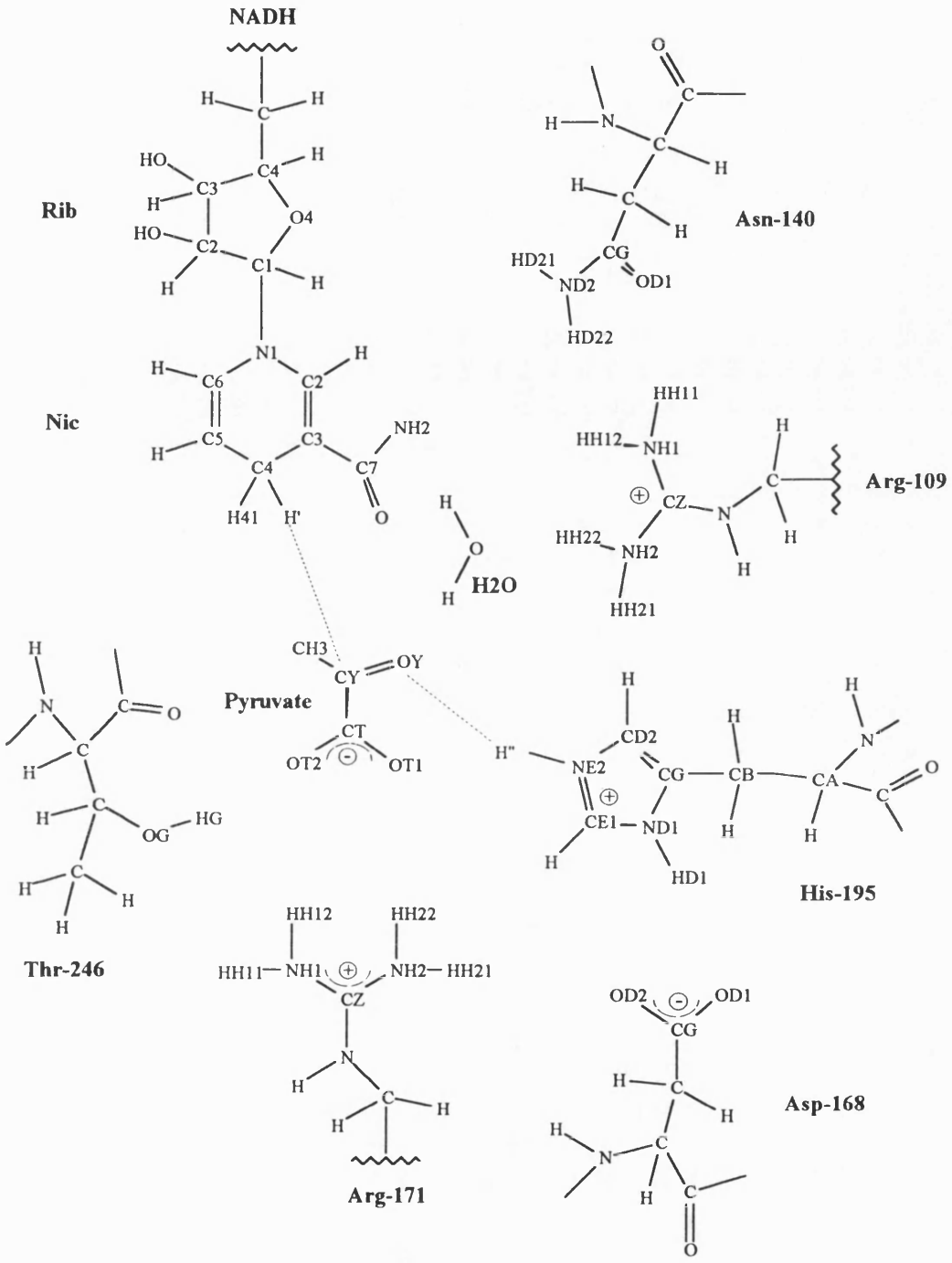

Fig 12.1: The residues that make up the region considered in this work to be the active site (AS). H' is the transferring hydride and H" is the transferring proton. The dotted lines indicate the atoms to which these species transfer. Elsewhere **Pyr** may be used to abbreviate **pyruvate**.

It was important that the truncated structures contained enough atoms to incorporate all residues that were likely either to have a significant effect on the reaction or be required for substrate binding. After several tests, a system formed by all residues with an atom within a distance of 12 Å of the carbonyl carbon of pyruvate

(CY in fig 12.1), the donor carbon of the nicotinamide ring of NADH (C4 in fig 12.1) or of the nitrogen donor atom of the His-195 (NE2 in fig 12.1) was chosen. All other atoms were deleted.

The geometric centroid of the system was moved to the origin. The remaining atoms were placed in a cavity that was deleted from a pre-formed sphere of waters of 17Å radius. This water sphere was also centred on the origin. A solvent boundary potential (83) was applied to the water molecules in order to maintain the structure of the water at the edges of the system. The resulting molecular system was a pseudo-sphere containing about 2000 atoms.

Harmonic restraints were applied to the heavy atoms further than 12 Å away from the origin (ca. 500 atoms), which means a mass weighted penalty function proportional to the square of the displacement of the atoms from their reference positions was included in the mm hamiltonian (84). This served to retain the structure of the enzyme, especially where loops of protein were disconnected from the main chain by the truncation.

The entire chemical system was divided into quantum mechanical (qm) and molecular mechanical (mm) regions. After some experimentation with different partitioning schemes, it was decided to treat the pyruvate molecule, the nicotinamide ring of the NADH and part of the His-195 as qm. The rest of the protein and all the water molecules were treated as mm. Fig 12.2 depicts a schematic representation of the qm atoms. The qm region consisted of 39 atoms. This was chosen as the best compromise between the requirement to represent the reaction region accurately and the need to minimise the number of qm atoms to keep the calculations tractable. Two link atoms (22) were inserted where the qm/mm boundary intersected covalent bonds They were placed between atoms C1 and N1 of NADH and CB and CA of His-195 (see fig 12.1).

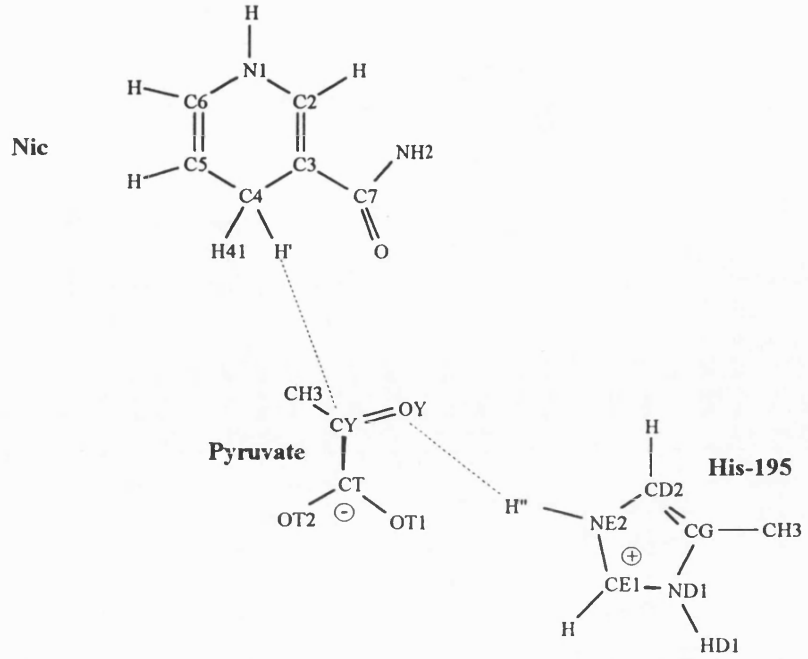

Fig 12.2: The atoms that are treated using quantum mechanics (qm atoms). Where a covalent bond connected a qm atom with an mm atom, a hydrogen atom was added to the qm region. These 'link' atoms were included in the gas phase and aqueous calculations and so the qm atoms for each type of calculation were identical.

Once the system was prepared, qm/mm optimisations were carried out, where the qm atoms of the reacting system were treated by the AM1 semi-empirical molecular orbital method (79) and the mm atoms by the CHARMM24b2 protein parameter set (77). The CHARMM24b2 (30) program was used for all calculations of the qm/mm energy, and its geometric gradient, using the method by Field, Bash and Karplus (22, and chapter 3).

Grid scanning was used for the initial phase of the saddle point search procedure. One advantage of the qm/mm method was its ability to model saddle points without any *a priori* information as to their location. Because of this, the grids were scanned over a large range of geometric values, rather than a small range near the values predicted by the gas phase calculations. Grids were generated that were defined by both parameters CY···H′ and OY···H′′ (see fig 12.1). *i.e.* the distances between carbonyl C atom of pyruvate and the H′ atom of the nicotinamide ring (hydride donor), and between the O atom of pyruvate and the H′′ atom of His-195 (proton donor), respectively. These internal co-ordinates were fixed at each point by internal

co-ordinate harmonic constraints with a force constant of 4.184×10^7 kJmol^{-1}Å^{-1} (10^7 kcal mol^{-1}Å^{-1}). The ABNR algorithm (78) was then used to optimise the system to the minimum of the constrained qm/mm energy. The exit criterion of the optimiser was set such that it exited only when machine errors prevented the optimiser from minimising the system any further. By using this very stringent exit criterion, smooth energy surfaces were generated.

The surfaces generated for all six jobs by the grid scan contained a single saddle shaped region. By performing finer grid searches around these regions, initial approximations as to the saddle point structures were generated.

A two sub-set partial rational function operator optimiser (chapter 9) was then used to exactly locate the transition states. The 'core' region, for which a hessian matrix was maintained, contained all the quantum mechanical atoms (see fig 12.2) including the link atoms. Whilst it was possible to locate the saddle points using larger cores (97), these small cores provided a more rapid convergence of the optimiser. The rest of the enzyme was treated as environment and continually optimised to a minimum rms of the gradient vector of 0.0042 kJmol^{-1}Å^{-1} (0.001 kcal mol^{-1}Å^{-1}). The core was optimised to a first order saddle point until no element of the gradient vector of the entire system (core plus environment) was larger than 0.42 kJmol^{-1}Å^{-1} (0.01 kcal mol^{-1}Å^{-1}).

All those atoms in fig 12.1 plus the quantum mechanical link atoms were defined as the 'active site' (AS) atoms. The remainder of the system was defined as 'bulk'. To confirm the exact first order nature of the located saddle points, hessian matrices were computed for the AS atoms by central finite difference differentiation of the geometry gradient vector. All the resultant hessians had only one negative eigenvalue.

The intrinsic reaction co-ordinate (IRC) was calculated in both directions from the saddle points. This confirmed that the located saddle points were for the reduction of pyruvate to lactate. The reactant structures from the IRC calculations were further optimised to a minimum. The hessian matrices of the AS atoms were computed for these reactant structures in the same way as for the saddle points. The rigid-rotor/ harmonic-oscillator approximations (15) were then used in the CAMVIB/CAMISO package (62) to calculate the primary kinetic isotope effects for replacing the transferring protide with deuteride. A comparison of these with the same calculations using hessian matrices for only the qm atoms (see fig 12.2) showed it was necessary for accuracy to use the larger hessians. This was in keeping with the results for aqueous secondary deuterium fractionation factors in chapter 8.

The total number of atoms in the pseudo sphere was not the same for each job (due to the truncation method). The different sizes of pseudo sphere were caused by differences in the atoms on the surface of the pseudo sphere. Therefore the consequent differences in the AS to bulk interaction term were very small. Consequently the energies of the interaction of the AS with itself plus the interaction of the AS with the bulk could be compared between jobs .

The qm/mm modelling in CHARMM reports the energy for interaction of the qm atoms with themselves plus the energy for the interaction of the qm atoms with the mm point charges. This energy is referred to as the qm/elec energy. The electrostatic effect of each active site residue was determined from changes in the qm/elec energy upon zeroing the point charges on each AS residue in turn.

A comparison of the LDH to the aqueous environment was performed by placing the geometry of the qm atoms at a saddle point in a cavity in a pre-formed 15Å radius water sphere using the TIP3P potential and stochastic boundary conditions (83). This followed the solvation method used by Barnes and Williams (16) and was much

faster than simulated desublimation (chapter 6). The first order saddle point, intrinsic reaction co-ordinate and kinetic isotope effects were computed using the same method as they were for the enzymic environment. This approach was then repeated, but with no environment (*i.e.* in the gas phase).

12.4 Results and discussion:

In the protein, all six jobs produced very similar TS and reactant structures. The pyruvate remained 'anchored' by two hydrogen bonds to Arg-171 in all the minima and saddle points of all six jobs. It seems probable that the enzymic role of Arg-171 is to align the pyruvate correctly for the reaction and consequently reduce the reorganisation energy require to go from reactants to TS.

For all six jobs the eigenvector which corresponded to the negative eigenvalue of the saddle point hessian matrix showed the motion of both the hydride (H') and proton (H") in the direction of the reaction. If these saddle points are considered to represent the transition states then all six jobs report a concerted mechanism. The IRC calculations went from the located saddle point to reactants. This confirms the concerted nature of the reaction in this model.

Table 12.1 shows that the proton transfer is very advanced at the TS where as the hydride transfer is only about half completed. This indicates that the proton and hydride transfers are kinetically coupled but dynamically uncoupled, in agreement with the results of Andrés *et al.*(80) .

The reaction model of the qm atoms in water produced an intermediate. This intermediate was formed by proton transfer preceding hydride transfer. The energy of the intermediate was such that the hydride transfer remained the rate limiting step whilst the proton transfer was the most energetic process. The IRC algorithm had a setting to control the minimum step length in femtoseconds. When it was set to 15

femtoseconds, the enzymic IRC calculations exited due to an energy increase at a structure that resembled the aqueous intermediate. Improving the accuracy of the IRC algorithm by setting the minimum step length to 1 femtosecond, caused it to follow the IRC all the way to reactants; the 'intermediate like structures' were not true intermediates. The fact that the IRC algorithm exited at these structure means that the amount of change in the potential energy hyper-surface curvature required to make them intermediates was very small.

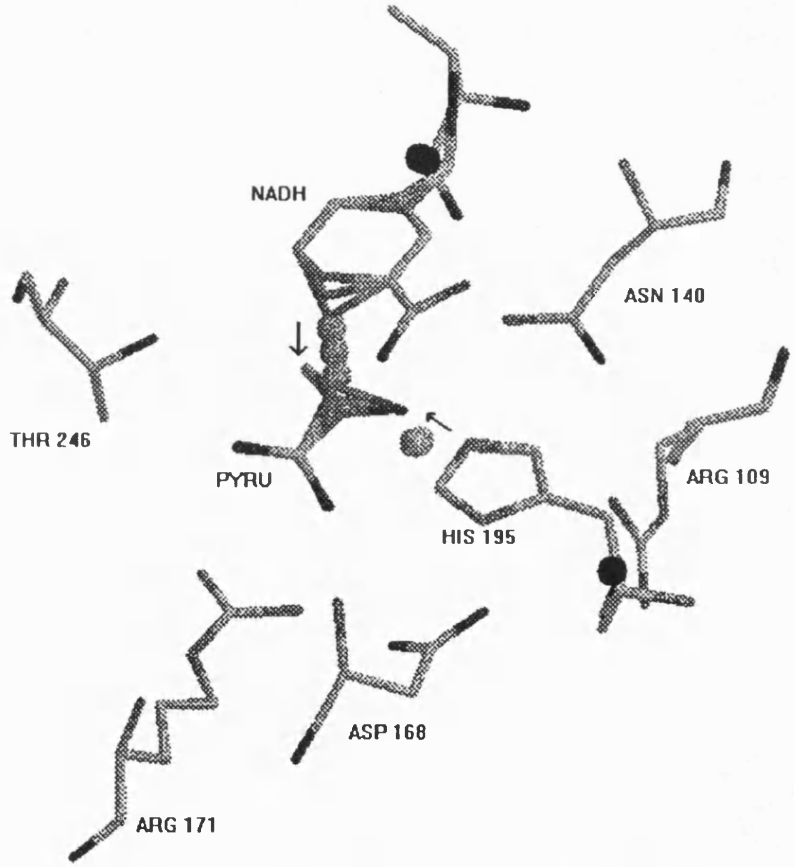

Fig 12.3: This image is of the AS atoms, for job number one, at the saddle point. Superimposed upon it are the same atoms translated by the transition eigen vector of the hessian matrix in both positive and negative directions. The golden atoms are the transferring hydride (upper) and proton (lower left). All other hydrogen atoms are left out of the image for clarity. This image shows that the motion of the transition vector is localised to only a few of the AS atoms. The black objects represent the link atoms. (In this image the ribose ring of the NADH is edge on.)

Table 12.1: Inter-atomic distances, reaction barrier heights and kinetic isotope effects of the reduction of pyruvate to lactate in LDH and of the 'qm' atoms (see method) in water and gas phase (*in vacuo*).

Distance	job number						Non enzymic	
A	1	2	3	4	5	6	aqueous‡	gas
TS Nic-H'	1.31	1.36	1.32	1.31	1.31	1.34	1.25	1.37
TS Pyr-H'	1.42	1.34	1.41	1.42	1.42	1.36	1.49	1.34
TS Nic-Pyr	2.69	2.66	2.71	2.67	2.66	2.65	2.73	2.67
R Nic-H'	1.13	1.13	1.13	1.13	1.13	1.13	-	1.13
R Pyr-H'	2.90	2.64	2.85	3.11	3.21	3.14	-	6.78
R Nic-Pyr	3.81	3.61	3.91	3.72	3.86	3.75	-	6.28
TS His-H"	2.31	1.90	1.86	1.91	2.16	2.45	1.94	2.76
TS Pyr-H"	0.99	0.99	0.99	1.00	0.99	0.98	0.99	0.99
TS-His-Pyr	3.00	2.84	2.82	2.74	2.85	3.04	2.90	3.39
R His-H"	1.00	1.00	1.00	1.00	1.00	1.00	-	1.03
R Pyr-H"	2.21	2.08	2.02	2.03	2.06	2.07	-	4.70
R His-Pyr	3.13	3.07	3.01	3.02	3.05	3.06	-	5.27
KIE *	2.79	2.71	2.84	2.72	2.72	2.63	2.40	2.96
Barrier † in kJmol^{-1}	243 247	248 243	209 197	256 247	255 246	244 243	172	188

† Difference in qm/mm energy in kJmol^{-1}. Where two figures are quoted: the upper is for the entire protein pseudo sphere and the lower the AS/AS and AS/bulk terms (see method).

‡ These figures are for hydride transfer. The quoted barrier is for the proton and hydride transfer steps combined. The hydride transfer step is rate limiting and occurs after proton transfer.

* The semi-classical primary kinetic isotope effect for deuteration of the hydride (H') for the rate limiting step.

TS Transition state

R Reactants (the minimised structure from end of the IRC calculation)

Pyr Pyruvate (see fig. 12.1)

H" Transferring proton (see fig. 12.1)

H' Transferring hydride (see fig. 12.1)

Some of the most revealing information comes from the relationships between various properties of the reactant and transition states. The essential features of the reaction show a remarkable similarity between the six jobs. The Pauling bond order for the TS pyruvate to proton bond varied by only ±0.04 for all the enzymic calculations. The TS pyruvate to hydride bond order varied by only ±0.05 (see table 12.2). Both these sets of bond orders show a remarkable similarity to the gas phase results. The bond order of the gas phase hydride transfer was equal to the largest enzymic result. The gas phase proton transfer lay within the range of the enzymic results.

Despite the similarity in the extent of hydride and proton transfer between the jobs, some other AS residues behaved quite differently in the different reaction co-ordinates. This indicates a large degree of active site flexibility. In job 1 Thr-246 was hydrogen bonded to the Pyr whilst Asn-168 was hydrogen bonded to Arg-171 and His-195 (see fig 12.3). In the rest of the jobs Asn-168 had two hydrogen bonds with His-195 and non with Arg-171. Thr-246 was not hydrogen bonded in to Pyr in jobs 2 to 6. The differences in the behaviour of Arg-109 and H_2O between jobs were similarly large and will be discussed later.

Table 12.2: The Pauling bond orders for pyruvate to proton (H") and for pyruvate to hydride (H') at the transition state in all six enzymic jobs and in the gas phase.

Bond	enzymic job number						Gas
	1	2	3	4	5	6	phase
C - H'	0.27	0.38	0.28	0.28	0.27	0.36	0.38
C - H"	0.90	0.88	0.88	0.86	0.89	0.92	0.90

Fig (12.4) shows the reactant, TS and barrier height energies for interaction of AS with AS plus AS with bulk for all six jobs. As discussed in the methods, these

interaction energies represent the contributions relevant to the active site and lack unwanted variations due to differences at the surface of the pseudo sphere.

Job 3 produced the lowest barrier height. This was due to destabilisation of the reactants. The largest barrier height was that of job 4, which was due to destabilisation of the saddle point. Despite the variation in active site conformations the barrier heights were within 40 $kJmol^{-1}$ of each other. The combination of this result with the bond order results (above) implies a 'robust' underlying reaction mechanism. A 'robust' mechanism, the essential features of which do not vary with the reaction environment, is in agreement with the calculations by Andrés *et al* (80).

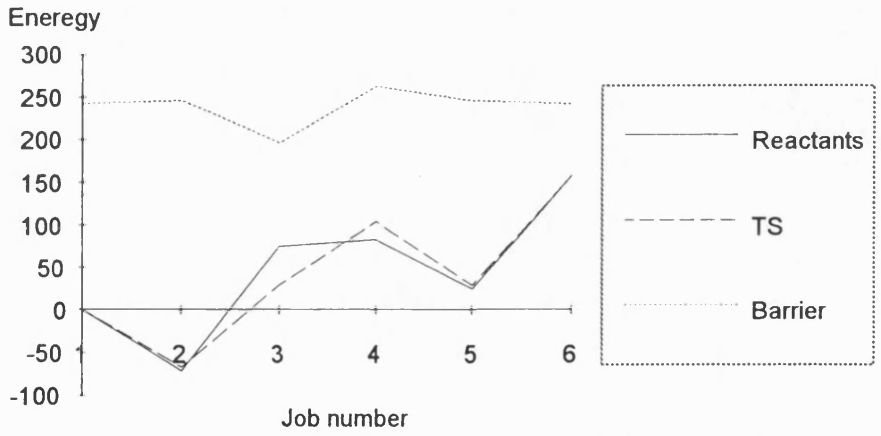

Fig 12.4: The graph shows the interaction between the AS and the AS plus the interaction energy of the AS and the bulk. The AS consists of those atoms in fig 12.1. The barrier is the difference between the reactant and TS energies. The reactant and TS energies are shown relative to those of job number one. Table 12.1 shows these barrier energies to be in close agreement with the barriers computed from the energy change for the entire protein pseudo sphere. Energies are in $kJmol^{-1}$.

The reactant and saddle point energies for job 2 were much lower than for the other jobs. A direct interpretation of this would be that the structural features of the active site in this job are the only ones that would be seen experimentally. It is certain that there are many more conformations available to the system than were sampled in this work. This would lead to many reaction co-ordinates that have not been tested here. In seems probable that conformational features seen in job 2 may be combined with

features from the other jobs in some of these 'untested' reaction co-ordinates. Consequently, the results for all the jobs are relevant, despite the lower energy of job 2.

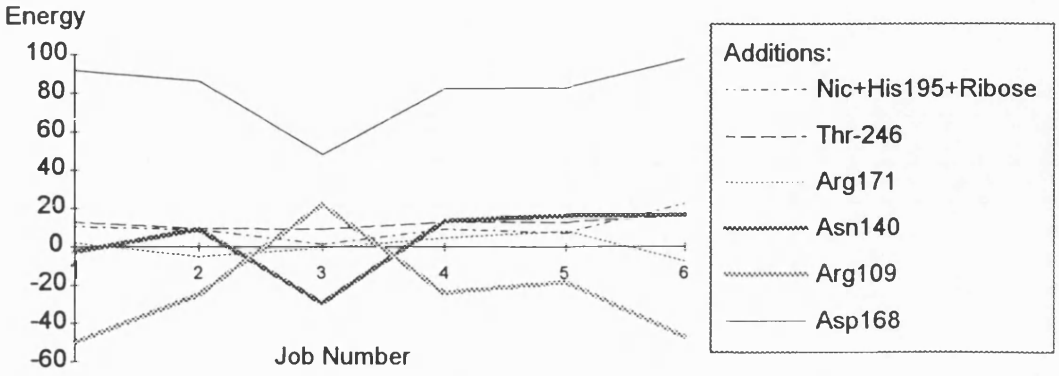

Fig 12.5: The graph shows the change in the quantum/electrostatic (see methods) component of the reaction barrier heights upon inclusion of different active site residues into single point energy calculations of the TS and reactant structures for all six jobs. Energies are in $kJmol^{-1}$.

If a residue is directly involved in catalysis, instead of playing a purely structural role, its contribution to the barrier height is likely to vary as the barrier height varies. To test this idea the contribution to barrier height energy was computed for each AS residue in each job.

As discussed in the methods, it was only possible to obtain meaningfull figures for each residue's contributions the barrier height from the quan/elec energy; deletion of a residue produced enormous molecular mechanical energy changes due to the 'bonded' energy terms that interconnected the deleted residue to the rest of the system. When this analysis was done, only Asn-140, Arg-109 and Asp-168 showed a coupling between their energy contribution and the differences in barrier height between jobs (see fig 12.5). This strongly indicates that, out of the active site residues, it is only these three, plus Nic and His-195, that have an electrostatic role in catalysis. This result is in agreement with site directed mutagenesis (87,90) and with Raman difference spectroscopy studies (86).

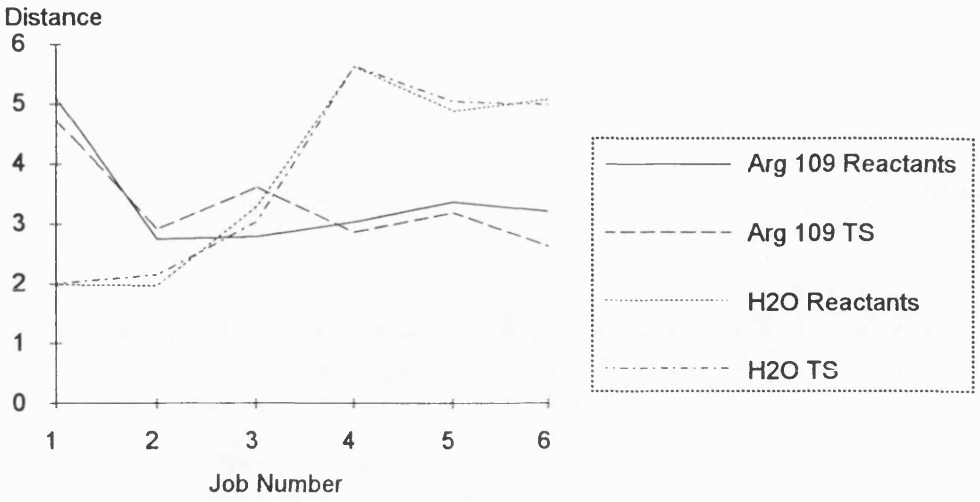

Fig 12.6: The graph shows the inter-atomic distances in Å between the carbonyl oxygen of pyruvate and the hydrogen bonding protons of H_2O and Arg-109 for all six jobs. See fig 12.1 for residue nomenclature.

In jobs one and two, H_2O was hydrogen bonded to the carbonyl oxygen of the pyruvate in both reactants and TS. In jobs four, five and six, it was Arg-109 that was hydrogen bonded to pyruvate in both reactants and TS. Fig 12.6 shows that in job three, the hydrogen bond in the reactants was to Arg-109. However, neither H_2O or Arg-109 were hydrogen bonded to Pyr in the TS of job 3. This effect is more clearly seen in fig 12.7 where the change in Arg-109 to pyruvate distance is plotted. The positive contribution to the barrier height from Arg-109 in job three (see fig 12.5) probably comes from the energy required to break its hydrogen bond to Pyr. The structural alignments that caused this situation have also reduced the reactant stabilisation from Asp-168 and Asn-140. These two effects were in opposition. As reactant stabilisation caused the greatest energy change, the barrier height was lower for job three, despite the anti-catalytic effect of Arg-109.

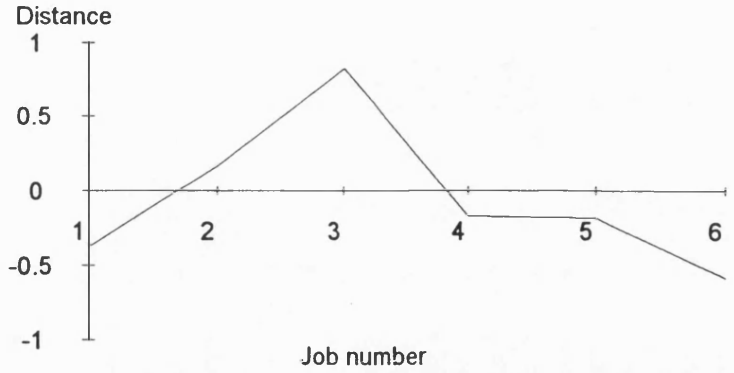

Fig 12.7: The graphs shows the change in Å of the distance between the carbonyl oxygen of pyruvate and the hydrogen bonding protons of Arg-109 (the mean of the two O··H distances) upon going from reactants to TS, for all six jobs.

Clarke *et al.* (87) reported a 200 fold reduction in the binding of pyruvate upon mutation of aspartate 168 to alanine. They conclude that the removal of the aspartate negative charge moves the equilibrium between bound pyruvate and bound lactate towards bound lactate. They also report a 100 fold reduction in k_{cat} in the mutant relative to the wild type. This would require the opposite effect on barrier height by Asp-168 than that shown in these results (see fig 12.5). The contribution to the quan/elec component of the barrier height by Asn-168 is anti-catalytic. This is probably due to the negative charge on Asn-168 decreasing the acidity of the His-195 proton donor. This would imply that mutation of Asn-168 to a residue without this negative charge would increase reaction rate by lowering the barrier. It would also destabilise the lactate products with respect to the reactants.

Williams and Wilkie (81b) showed that a dipole interacting with the proton donor will alter its p*K*. In all six jobs, Asn-168 is hydrogen bonded to His-195 and so represents such a dipole. Consequently, the qm/mm model predicts that the p*K* of His-195 will change upon mutation of Asn-168 to a less dipolar residue. Clarke *et al.* reported (87) that the p*K* of His-195 is unchanged in bound reactants by mutation or Asn-168 to alanine. This experimental result is the opposite of the theoretical prediction.

It may well be that these differences are due to deficiencies in the qm/mm model at handling the hydrogen bonding between Asp-168 and His-195. As mentioned above,

in job number one, Asp-168 is not only hydrogen bonded to His-195 but also to Arg-171. In all the other jobs both oxygens of the carbonyl group of Asp-168 were hydrogen bonded to His-195 and the proton on the nitrogen of Asp-168 auto hydrogen bonded to the carboxylate group. This indicates that there are alternatives to His-195 to which Asp-168 carboxylate oxygens can hydrogen bond.

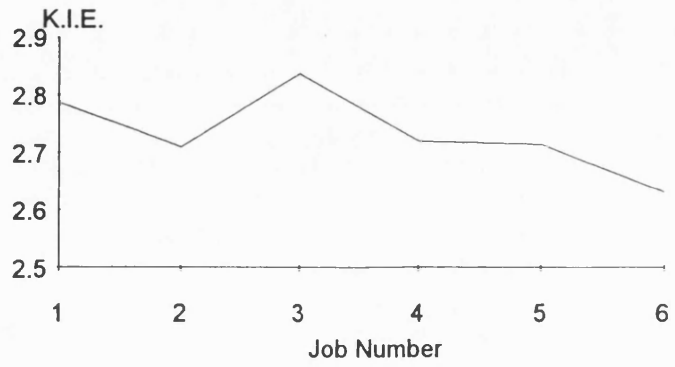

Fig 12.8: The graph shows the semi-classical primary kinetic isotope effect at 298.15K for deuteration of the transferring protide for all six jobs.

If the theoretically generated barrier heights are incorrect, there is no validity in tunnelling corrections to computed kinetic isotope effects. In light of this observation, fig 12.8 reports the semi-classical primary kinetic isotope effects for replacement of protide (H' in fig 12.1) with deuteride. The results are broadly in agreement with the those for mutant enzymes (87). It is not presently possible to compare them to wild type enzymes because hydride transfer is not the rate limiting step in the wild type(87). The peak in kinetic isotope effect (KIE) for job number three may indicate an increase in acidity of His-195. This would follow the acidity of proton donor to KIE relationship reported by Williams and Wilkie(81b). In job three, the average length of the two hydrogen bonds of Asp-168 to His-195 is shorter than for any other job. This is in agreement with the expectation that the negative charge on Asp-168 will decrease His-195 acidity (81a,87).

12.5 Conclusions:

The structure of the active site shows a large amount of flexibility. The six reaction co-ordinates that were modelled in this work probably represent only a small fraction of those that are available to the system. These six jobs have generated great deal of information concerning the different effects that are present in the enzymic reaction. To fully understand the interplay of these effects would require a much greater number of samples from the total number of possible reaction co-ordinates. This implies that the conclusions which can be made from these six jobs cannot be extended to all possible reaction co-ordinates with absolute certainty.

The model predicts a large degree of flexibility in the active site. This means that the experimentally observed reaction will probably represent an average over many different active site structural conformations. This emphasises the need to model many conformations before the nature of the enzymic catalysis will be fully understood. In contrast, the extent of proton and hydride transfer at the TS is remarkably similar between the six jobs and between the gas phase and enzymic reactions. This supports the use of gas phase modelling as the first step in the investigation of enzymic reactions.

Whilst all six jobs proceeded by a concerted mechanism, these results do not conclusively show a concerted mechanism for all possible reaction co-ordinates on the qm/mm potential surface. The potential energy hyper surface is indicative of a system on the border line between concerted and stepwise mechanisms. However, these theoretical results are a very long way indeed from predicting a mechanism where hydride transfer precedes proton transfer. In combination with the work by Andrés et al (80) and by Williams and Wilkie(81a,b) (see introduction) it seems extremely unlikely that the reaction goes via hydride transfer preceding proton transfer. In conclusion, the enzymic mechanism is probably dominated by the proton transfer energy whist the rate limiting step involves hydride transfer. If the

mechanism is stepwise, the protonated intermediate will be of high energy. Fig 12.9 depicts these the two possible reaction energy profiles.

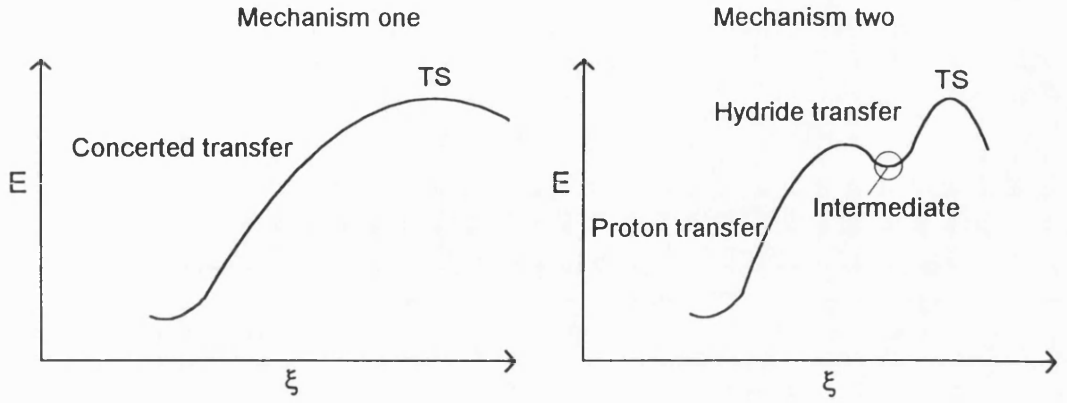

Fig 12.9: The two possible mechanisms for the reduction of pyruvate to lactate by LDH. In both mechanisms most of the energy of the overall reaction goes into the proton transfer whilst the rate limiting step involves the hydride transfer. The only difference is whether the proton transfer is nearly complete at the rate limiting TS (mechanism one) or actually complete (mechanism two). E = energy, ξ = reaction co-ordinate.

Some success has been obtained in recognising which residues are catalytically active. Arg-171 appears to be performing a purely structural role. Arg-109 performs an electrostatic stabilisation of the TS. Asn-140 may also have an electrostatic role to play in TS stabilisation, although the results are not as definitive in that regard.

These results suggest a possible role of water as an alternative to Arg-109 for hydrogen bonding to the pyruvate carbonyl. This would go some way to explain why the 400 fold reduction in k_{cat} (85) for replacement of Arg-109 by glutamine is so small.

This work raises some concerns over the CHARMM AM1 qm/mm potential energy function. In chapter 9 a comparison of high level *ab initio* qm/mm with AM1 qm/mm showed the AM1 based method to over estimate reaction barrier heights. It seems likely that this is the case here. It is also very likely that the interaction of Asn-168 with His-195 is being very poorly handled by this model. 'Suggestions for further work' gives some further consideration of these matters.

This work goes to support both the hypotheses of structural stabilisation and of electrostatic stabilisation. To that extent, it is not in conflict with the work by Warshel, even though it does not predict the same transition state.

12.6 Suggestions for further work:

The interaction between Asp-168 and His-195 requires considerable re-parameterisation of the model. It may be necessary to use either density functional or Møller Plesset perturbation theory in *ab initio* quantum mechanical calculations to find values for the charge and Van der Waals parameters to define this interaction. It may be also be worth investigating the effect of including Asp-168 in the quantum mechanics section of the qm/mm treatment.

Whilst the approach used here has investigated some of the structural permutations for the TS, there are many more available to the system. It would seem wise to devise a more systematic method of working through these permutations. One possible approach could be to estimate all possible hydrogen bond pairs for each residue and use internal co-ordinate constraints to force these pairs to form in sequence with TS location after each pair has formed.

Chapter 13 - General Discussion

Attainment of overall goals: *(see chapter 4)*

1,a:

The goal of characterising aqueous organic transition states using semi-empirical qm/mm modelling was attained. Some flaws in the nature of the AM1 semi-empirical hameltonian appears to have reduced the accuracy of the results. The implication of the results from chapter 8 on fractionation factors is that the AM1 method is accurate for a restricted number of systems. It may be that once semi-empirical qm/mm has been used to model a larger number of transition states it will be possible to make predictions as to which systems the method can handle.

Comparison of free energy barrier height calculations by J Gao (26) with the minimal sampling calculations goes a long way to support the minimal sampling method (chapter 11). The difference in reaction barrier height due to the entropy terms, which are not included in the minimal sampling method, were trivial. This might not be the case where the barrier height is much lower or the temperature much higher.

1,b:

The goal of characterising aqueous organic transition states using *ab initio* qm/mm was also attained. Once electron correlation was included in the *ab initio* method using second order Møller Plesset perturbation theory (71), the calculated kinetic isotope effects were in excellent agreement with experiment. The three sub-set qm/mm model (chapter 10), with only the first and second solvation shells polarising the solute, significantly accelerated the location of the transition states. Comparison between using this method and semi-empirical qm/mm on small molecules may prove useful for predicting for which systems semi-empirical qm/mm will be reliable.

2,a:

Some considerable success was achieved in the modelling of enzymic reactivity using semi-empirical qm/mm. Problems with the paramterisation of the qm/mm interactions, and with the semi-empirical method itsself, would appear to have made the calculation of barrier heights rather poor. The kinetic isotope effect results were encouragingly close to that expected as was the prediction of which residues are responsible for the electrostatic contribution to catalysis.

These results clearly indicate that one single transition state will not give a clear picture of enzymic reactivity. The six transition states located in this work almost certainly represent a tiny subset of those which would need to be characterised to form a statistically relevant sample.

2,b:

A significant amount of the methodology to facilitate *ab initio* qm/mm modelling of enzymic reactivity was developed in this work. The qm system in the lactate dehydrogenase work (chapter 12) contained 39 atoms. By using the three sub-set qm/mm approach developed in this work, it should be possible to model this system on the largest super-computers presently in use. It maybe that the implementation of linear scaling *ab initio* methods into the three sub-set qm/mm modelling would bring these calculations into reach of the fastest contemporary workstations.

Calculation of isotope effects:

The use of the rigid rotor harmonic oscillator (rr/ho) approximations has been broadly successful. For these calculations, the minimal sampling methods presented have been especially efficient compared to molecular dynamics methods. This is because it proved to be unnecessary to include the motions of atoms that were distant from the isotopomeric species in the rr/ho calculations.

A comparison of the semi-empirical and *ab initio* qm/mm models for isotope effect calculations only shows a benefit in using *ab initio* methods for kinetic isotope effects. Neither method proved to be decisively superior for equilibrium properties in aqueous solution. However, *ab initio* methods will allow modelling of systems with nuclei for which there are no semi-empirical parameters.

Comparisons with the COSMO solvation model:

The COSMO (27) solvation model was used extensively as a comparison to the qm/mm methods. For all vibrational and energetic properties for which the comparison was made, semi-empirical COSMO gave very similar results to semi-empirical qm/mm. COSMO has also provided a rapid way to defining geometries that were the starting point of qm/mm optimisations.

Charge fitting to the qm/mm gradient vector and three sub-set qm/mm modelling:

The concept of fitting point charges to a qm/mm gradient vector was introduced in chapter 5. The method proved to be useful for solvation, analysis and three sub-set qm/mm modelling. The presented three sub-set qm/mm method uses this form of charge fitting to approximate the electrostatic interaction of the qm atoms with the outer mm atoms to a simple point charge scheme.

For enzymic modelling, this novel form of charge fitting may be of great utility. Possible application are not only for 3 sub-set qm/mm but may also involve location of lone pairs and other off centre charges (chapters 5,6) or charge perturbations (chapter 7) within the active site. The method may also prove to be of advantage in parameterising pure mm force fields by obtaining charge distributions directly from condensed phase qm/mm structures.

Simulated desublimation:

This thesis does not have a rigorous comparison of simulated desublimation with other solvation methods. However, the results would indicate that the method is at least as good as the other methods which do not employ dynamics or global minimisation.

The partial rational function optimisation sub set algorithm:

The partial rational function optimisation (PRFO) sub-set method has proved to be very successful for exactly locating first order saddle points in systems of high dimensionality (chapter 9). Although it appears to require a large number of energy and gradient calculations for the 'environment' , this becomes less significant when it is used in conjunction with the three sub-set qm/mm model. A comparison with other saddle point search algorithms was not possible as non was found which could locate saddle points for bond making and bond breaking in qm/mm systems of high dimensionality. Two methods for preventing the optimiser missing the desired saddle point and locating a different one have been introduced. Firstly, which atoms were included in the hessian matrix can be set to maximise the overlap the transition mode between iterations of the optimiser. Secondly, the integration of mode overlap into the trust radius algorithm has been enhanced compared to previous implementations of algorithms (54,65). These two measures have proven to be successful in improving the stability of the algorithm at finding the 'correct' saddle point.

13.1 Unifying conclusion:

Minimal sampling methods have proven to be a useful addition to Montr Carlo (MC) and molecular dynamics (MD) modelling of qm/mm systems. This is especially so for *ab initio* qm/mm modelling. For vibrational spectra, isotope effects and reaction barrier heights of systems in aqueous solution, they provide a complete replacement for MC or MD . For enzymic systems, minimal sampling methods are probably best used in conjunction with MC or MD methods.

Appendix A - A method for auto-generation of redundant and non-redundant valence co-ordinates

Introduction:

In this work, valence co-ordinates are considered to be internal geometric co-ordinates which derive their nature from chemically relevant connectivity, bending and twisting of poly-atomic chemical species. The significant difference between valence co-ordinates and z-matrix co-ordinates is in the concept of atomic valence. The valence co-ordinates described here are based around the positions and motions of the atoms surrounding any given atom. Z-matrix co-ordinates are not necessarily defined in this way, but can follow any systematic series of length, angle and dihedral ordinates. The method described here is to generate a set of valence co-ordinates automatically from the minimum knowledge of cartesian co-ordinates and atomic species.

There were three major reasons for wanting to auto-generate valence co-ordinates. (i)They were required for the CAMVIB program (62) for the projection out of rotational and translational modes from cartesian hessians; (ii) they were of use in constructing internal co-ordinate constraints; and (iii) they offered a highly uncoupled co-ordinate system for geometry optimisation.

Method:

The valence co-ordinates used were of the five types described in table A.1 . The use of the 'wag' to describe out of plane position (and motion), instead of dihedral angles, was because the atomic connectivity used in a wag is more chemically relevant. This greater relevance is likely to produce a less coupled co-ordinate system.

Table A.1: Types of valence co-ordinates used in GRACE.

Co-ordinate type and subscripts	Description of relationship defined by the co-ordinate, the name generally refers to the motion with respect to that relationship.
Stretch p,q	Distance between atoms p & q
Bend p,q,r	Angle p - q - r
Torsion p,q,r,s	Either the torsion between q & r or the dihedral p - q - r - s
Wag p,q,s,r	Angle of p - r out of the plane q - r - s
Linear p,q,r,s	Angle p - q - r in plane q - r - s and orthogonal to that plane. Where s=0 => the use of xy plane instead, s=-1 (not a standard CAMVIB type) => use yz plane instead.

CAMVIB required non-redundant valence co-ordinates. The majority of the logic in the algorithm was to control redundancy and to allow the generation of totally non-redundant co-ordinates.

Generating a chemically relevant connection set (the list of inter-atomic connections defining distance in the co-ordinate set) led to the generation of chemically relevant valence co-ordinates. Two connection algorithms were used in conjunction with one another. The first was a covalent radius connection algorithm. If the square of the distance between two atoms was less than 1.3 times the square of the sum of their covalent radii, a connection was made. The radii were taken from ref(96).

Covalent radius based connections can produce a redundant connection set (in the case of ring molecules for example). There is also the possibility that a covalent connection set will not fully inter-connect the chemical system; molecules that are not covalently bonded to one another will not be connected, neither will atoms with partially made bonds. To overcome this problem a connection algorithm, which to the author's knowledge is novel, was employed to find the shortest total length non-redundant connection set that links all the atoms in an unbroken chain.

This was called the 'distance' connection algorithm because it minimised the sum of the inter-atomic distances defined by its resultant connection set.

The 'distance' connection algorithm split the atoms into two sets, a 'defined' set and an 'undefined' set. A matrix **D** of the inter-atomic distances between all atoms was computed such that element ri,cj was the distance between atoms i and j. One atom, picked arbitrarily as atom 1, was placed in the defined set, the rest were placed in the undefined set. The index of the smallest value in row 1 (except element r1,c1) of **D** gave the index of an atom to which to make the first connection. Once this connection was defined, the atom to which atom 1 was then connected was moved to the defined set.

1 ----- 4 ----- 3 ----- 2
1.0Å 1.0Å 1.0Å

r\c	c1	c2	c3	c4
r1	-	3.0	2.0	1.0
r2	3.0	-	1.0	2.0
r3	2.0	1.0	-	1
r4	1.0	2.0	1.0	-

Fig A.1: An example of distance connection.
The four atoms 1,2,3,4 are in a straight line. The matrix is the **D** matrix of inter-atomic distances. Starting with atom one, element 4 of row 1 of **D** is the row's smallest value. So the first connection is 1 - 4 and atom 4 goes into the defined set. The smallest element in either row 4 or 1 in column 2 or 3 is element r4,c3. The next connection is between atoms 4 and 3 and atom 3 is moved into the defined set. The smallest element in rows 1,3,4 and column 2 is r3,c2 so the last connection is 3 - 2. By inspection: the resultant connection set (1-4) (4-3) (3-2) defines the shortest possible unbroken chain connecting all the atoms.

On subsequent iterations of the algorithm, the smallest element of **D** for which the row index was of a defined atom and the column index of an undefined atom was found. This row and column index gave a new connection. The newly connected

undefined atom was moved into the defined set. Once all the atoms were in the defined set, the connection set was finished.

Distance connection, as presented, had the drawback that it lacked chemical relevance. Where covalent or hydrogen bonds defined the shortest distances between atoms, distance connection was chemically relevant. Properties like the partially broken bonds at saddle points could cause the algorithm to produce chemically non-relevant connection patterns. By scaling the elements of **D** defined by an existing connection set by 0.01, the algorithm was forced to use pre-existing connections in preference to minimum distance ones where ever possible. For most applications, the connection set from a covalent connection algorithm was used as the pre-existing connection set. Manual inclusion of connections defining partly made bonds was also possible. The distance connection algorithm then acted to convert the pre-defined connection set into a complete and non-redundant set.

To extend this method to very large systems, the elements of D could be computed directly as needed rather than computing them at the start and holding them in memory. Such an approach would be significantly more computer time intensive but use much less memory.

Once the connection set was defined, it could be used to generate the valence co-ordinates. This was done by first generating co-ordinates defining stretching, bending, wagging and linear bends, then connecting these up with torsions (see table A.1 for a description of these co-ordinates). The 'valence' of each atom was defined as all those atoms which have a connection to it (from the supplied connection set). The valence number was then the number of atoms in the valence. Stretches were defined as being the connections. The rules for defining

bends, wags and linear bends were rather more complex and so are outlined in turn below:

Total number of bends:

There are 2n-3 bends (including wags) around an atom where n is its valence number. This can be derived from the 3N-6 internal co-ordinates where N is the valence number plus the central atom, N=n+1 ∴ there are 3n-3 internal co-ordinates. One stretch connects each valence atom to the central atom, accounting for n co-ordinates, leaving the 2n-3 bends.

Distribution of bends

Each valence atom must be cited by at least 2 bends or wags. For example, a bend of atoms 1 and 3 about 2 cites atoms 1 and 3; a wag of atom 1-2 in the plane of 3-2-4 cites atoms 1, 3 and 4. Where one of the two valence atoms defining the plane of a wag is orthogonal the wagging atom's stretch to the central atom, this plane defining atom is not counted as being cited.

These conditions were achieved by adding in bends starting from each valence atom in turn. Once one atom was sited twice, its turn was finished or skipped. This did not guarantee that a valence atom would not be sited more than twice since, it might have made up the far end of another bend or one of the plane defining atoms of a wag.

Inclusion of wags:

A wag was defined where a valence atom was co-planar with two already defined bends, both of which started or finished with the 'wagging' atom. Co-planarity was defined as when the sum of the three possible bends of three valence atoms about the central atom was greater or equal to 359°. Fig A.1 shows how two tests were required to overcome the problem of

reflex angles. Reflex angles proved to be uncommon in covalently bonded systems, but quite usual in hydrogen bonded systems like water. An explicit test had to be included to prevent special cases where two wags were generated which defined motions which were redundant with respect to each other.

Linear bends:

If an atom was bivalent and the bend defined by its valence atoms had an angle greater than 179.0°, a linear bending co-ordinate was used. This consisted of two bends, one parallel and one orthogonal to a plane. Where the line joining the three atoms had an angle between 5° and 175° with the xy plane, this plane was used to define the two bending directions. Otherwise the algorithm searched for an atom which defined a plane with the three atoms which had an angle between 5° and 175° with the line joining those atoms. If no such atom could be found, it reported this by giving an atom number of -1 for this fourth atom so later versions of CAMVIB would be able to use the yz plane instead. Where the xy plane was to be used, the fourth atom number is reported as zero.

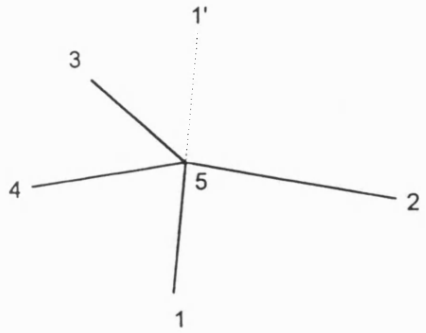

Fig A.1: Testing for wags
Atoms 1,2,3,4 are the valence of atom 5 and are co-planar. If bends 1-5-2 and 1-5-4 have been defined, bend 2-5-4 would be redundant. The sum of the angles 1-5-4, 1-5-2 and 2-5-4 would be less than 360° and so this condition would not be detected. To overcome this problem, the algorithm would have also checked the angles from the projection of the initial atom through the central atom. Angles 1'-5-2, 1'-5-4 and 2-5-4 are be exactly 360° and so, in this case, the algorithm would have generated a wag 1-5 in the plane of 2-5-4.

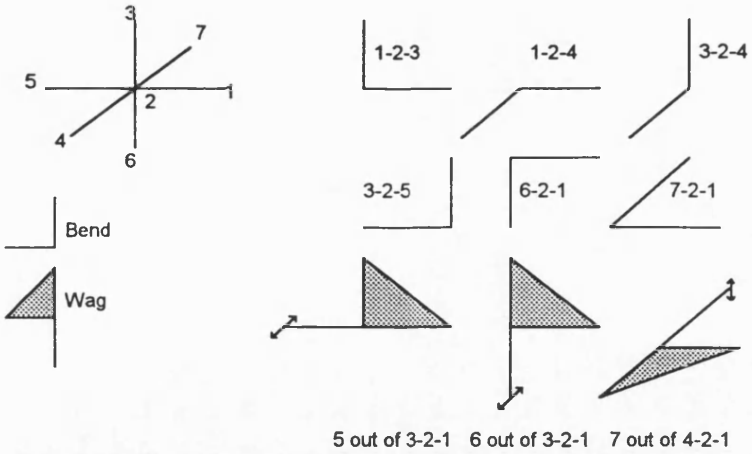

Fig A.2: The GRACE generated valence co-ordinates around an octahedral centre consisted of stretches along the 6 bonds shown, plus 6 bends and 3 wags.

Once the bends, wags and linear bends were established around every atom, torsions or dihedral angles were added to define the rotations between multi (as against uni) valent atoms. A rotation between two atoms, one of which is bivalent and linear, has no meaning. The algorithm used the list of linear bivalent centres to 'expand' the torsions to define atoms on either end of linear chains of atoms. If a linear chain is terminated with a univalent atom, no torsion was added. Once the torsion was defined, atoms in the valence shell of the atoms at each end of the torsion, which were not part of the torsion itself, were chosen to define the dihedral angle.

Suggestions for further work:

By using a redundant connection set, the valence co-ordinate set will become redundant. Such a redundant set could then form the basis of an optimisation scheme similar to that by Schlegel (52) in which the hessian matrix is stored in redundant internal co-ordinates and a step is generated by projecting a redundant co-ordinate step into non-redundant co-ordinates.

The inclusion of the connection and valence co-ordinate code into CAMVIB would significantly increase the utility of this code for general internal co-ordinate analysis of vibrational spectra.

Appendix B - GRACE

General Re-programmable Algebraic Chemistry Engine

Introduction:

Many of the challenges faced in the development of the techniques discussed in this thesis would have required more programming time than was available if approached in FORTRAN. Codes able to give the molecular mechanics terms and other codes able to give the quantum mechanics terms already existed for the *ab initio* qm/mm modelling. CHARMM24b2 already had an AM1 based qm/mm method, but lacked many of the support methods required for application to real problems of interest.

To bring all these different codes together, and to generate an 'environment' in which new developments could occur quickly, a highly structured interpreter based programming environment was developed. This environment grew to become the code now called GRACE. The name GRACE has a direct meaning relating to its function and form:

General:

The algorithms for data handling and optimisation in GRACE are, as far as possible, generally applicable. For example, instead of the optimisers being designed to optimise chemical problems, they can be used to optimise anything, and the default settings are set to be appropriate to chemical problems. This philosophy has built in the maximum amount of flexibility into the code.

Re-programmable:

The main interface with GRACE is via Tool Control Language(61). This is a structured programming language. GRACE input scripts can be re-programmed to answer a variety of different questions.

Algebraic:

Although many chemistry modelling codes attempt to interface with the user in terms of chemistry, the methods used for the modelling are all algebraic. GRACE has the facility for the user to interface with this algebra directly, rather than through a chemically oriented interface.

Chemistry Engine:

GRACE is far from being a mathematical programming language. Its functions are oriented to the needs of qm/mm modelling of chemical phenomena.

Grace - a qm/mm modelling brain

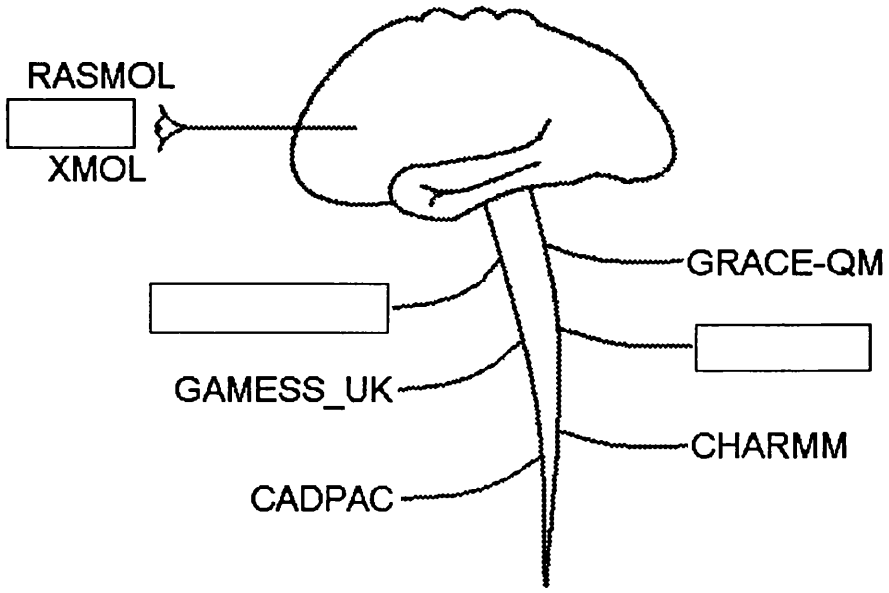

Fig B.1: GRACE can be viewed as a qm/mm modelling brain. The quantum mechanical, molecular mechanical and visualisation codes are not part of GRACE. The algorithms and structures in GRACE allow control over these external programs to facilitate a synergy between them and allow novel modelling approaches. The blank boxes represent future interfaces with other codes. GRACE-QM is a possible future extension of GRACE to have a native semi-empirical qm/mm method instead of using that from CHARMM.

As depicted in fig B.1, GRACE can be viewed as a qm/mm modelling brain. The code contains very few energy functions; the majority come from external codes. What it provides is a more sophisticated control system than is available in the codes it calls, plus access to the range of optimisation and analysis tools built into GRACE.

The code having by far the most sophisticated built-in user interface, and which is called by GRACE, is CHARMM. Largely because of this, the interface between GRACE and CHARMM is the most sophisticated of the interfaces present in GRACE. When GRACE is using CHARMM, CHARMM is run as a child (in the UNIX sense) process to TCL. By routing all commands that are unrecognised by TCL into CHARMM, and all commands that start with a capital letter into CHARMM, the programming language of CHARMM is completely integrated into the TCL language.

CHARMM data structures, such as the position and gradient arrays are 'reflected' into TCL arrays. When these arrays are accessed in TCL, GRACE keeps track of whether the TCL arrays need updating from CHARMM. In the reverse direction, before CHARMM performs any task, GRACE will check if it needs to update CHARMM's data structures from TCL. This means that the CHARMM data structures can be seamlessly interfaced with the optimisers and analysis tools in GRACE.

The interfaces with CADPAC and GAMESS are less sophisticated. They operate as part of the *ab initio* qm/mm modelling method in GRACE. When the energy and gradient of a qm/mm system is required, GRACE constructs an appropriate input deck for either GAMESS or CADPAC, runs the code and parses out the energy and gradients from either the punch file or the log file. The molecular mechanics components of the qm/mm function are then constructed via the interface with CHARMM. None of this requires any interface with the qm/mm methodologies in CHARMM.

In the work where the AM1 based qm/mm method in CHARMM has been used, GRACE has treated both the molecular mechanics and quantum mechanics atoms

identically. It has been the job of CHARMM to generate the appropriate qm/mm function and gradient.

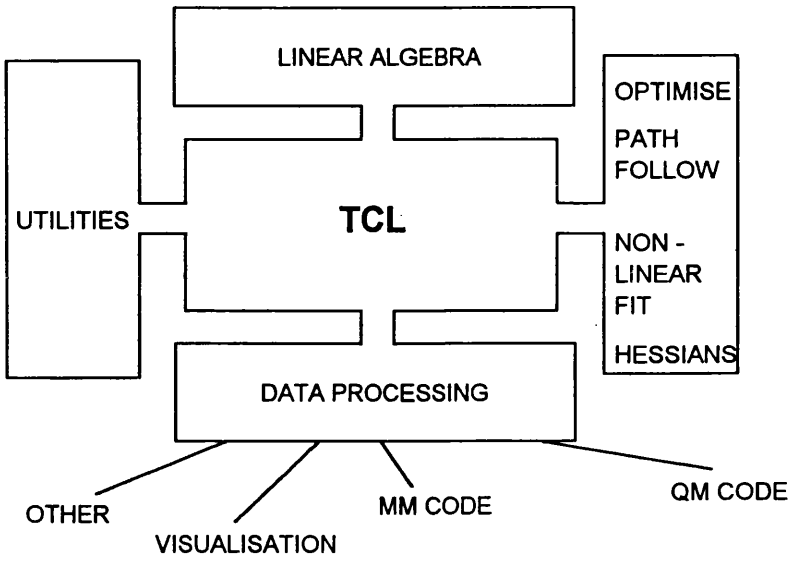

Fig B.2: A pictorial representation of the conceptual divisions in GRACE. The core is Tool Control Language. This controls the internal functions of utilities (disk handling *etc.*) linear algebra, optimisation and analysis. TCL uses the data processing algorithms to interface with external codes.

The interface with RASMOL (63) is of a similar type to that with CHARMM. This allows a 'programmable' visualisation method. The interface lets the RASMOL images be updated as the GRACE code runs. This way the evolution of the chemical model can be viewed interactively.

The interface with Xmol(64) is via writing out pdb files which Xmol can then read. The major purpose behind this is to take advantage of the animation and measuring facilities in Xmol. GRACE can produce a pdb file containing several structures. Xmol can show these structures as an animation. This method has been used heavily for the viewing of eigen vectors of the hessian matrix during saddle point location by the PRFO-SS method (see chapter 6).

la - a stand alone interpreter:

One of the programs launched by GRACE is la. This code is a stand alone interpreter written in FORTRAN. It contains most of the linear algebra and optimisation methods plus some other function. The TCL part of GRACE controls la by launching it as a child process, as it does CHARMM. TCL sends instructions to la as a simple alpha–numeric data stream. la returns TCL executable code which instructs the TCL interpreter to fill its arrays with information or to perform various functions, like acquiring energies and gradients.

The transfer of many of GRACE's vital algorithms to la makes these functions available to programs written in other languages. This should improve the long-term viability of these algorithms in the event that TCL becomes obsolete.

in_core - information-flow management:

To avoid problems with compiling code written in C with that written in FORTRAN, the communication between CHARMM and TCL is handled using UNIX pipes. Under UNIX, FORTRAN unit 5 is always allocated to the standard input pipe and unit 6 to standard output. This method creates a problem of flow control. If TCL is trying to write to CHARMM's input whilst CHARMM is trying to write to its output, CHARMM's output pipe will not be read by TCL. This will cause the CHARMM process to be halted at which point it will perform no more reading, and so the TCL process will also be halted.

in_core prevents this by acting as a memory buffer between TCL and CHARMM. TCL communicates to in_core's standard input whilst in_core's standard output talks to CHARMM's standard input. in_core stores the information from TCL in memory until it is sent a special instruction to flush this information to CHARMM. This allows TCL and CHARMM to run asynchronously. As in_core is a separate process to CHARMM, it could be

written in C without compiler portability problems. C allows it to take advantage of dynamic memory management to store considerable amounts of data storage. Memory is allocated exponentially to avoid excessive calls to `malloc`.

Making GRACE available to other users:

It is very hard to write an input script for any interpreter based chemical modelling package without a great deal of experience with that particular package. This is because of the very large number of individual facts that the user must know and understand in order to control the program. Interfacing with GRACE at this level can be seen as writing a 'unique' script (see fig B.3).

Once such a script has been written for a particular chemical problem, then it can be used as an example for later scripts. A user who has not had the time to learn how to write a unique script is much more likely to be able to edit an example script to their needs. 'Editable examples' have been the main way the author's co-workers have controlled GRACE.

For some chemical questions, that are always asked the same way, there is no need for the user to interface with the algebraic interpreter part of GRACE. Questions can be asked in a purely chemical way. A GRACE command script can be written that reads an input deck and writes out a log file mimicking the way other popular chemical modelling codes work. The input deck can then hold purely chemical information. The script that made GRACE behave in this way can be called an 'application script'. A good example of an application script is one that takes z-matrix description of the chemical, minimises its structure and finds the vibrational frequencies using the AM1 hamiltonian.

Some new methods are far too computationally demanding to be coded in TCL. TCL is an interpreted language and so is very much slower than compiled

languages such as FORTRAN or C. Such methods can be compiled into the FORTRAN (or to a lesser extent C) parts of GRACE. GRACE has a subroutine library for inter-communication between FORTRAN and TCL. New applications can call these library subroutines and so be interfaced quickly and simply. FORTRAN internal memory management is via allocation of sections of a large array stored in a common block. This sort of memory storage is often referred to as a 'stack'. If new applications use the GRACE memory management routines `stalloc` (allocate stack space) and `stdalloc` (de-allocate stack space) their memory requirements will not interfere with that of other routines in GRACE.

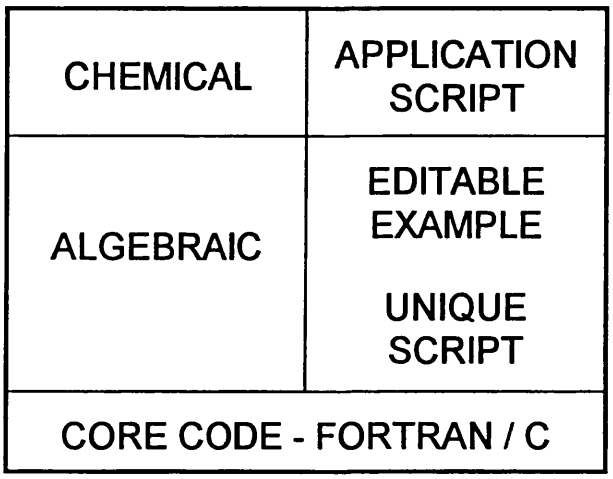

Fig B.3: The levels at which the user can interface with GRACE. Chemically oriented input decks can be passed to application scripts. For more control, algebraic instructions can be passed to GRACE by editing a prepared example script or writing a unique script from scratch. Methods that involve a computationally demanding algorithm not present in GRACE may require the editing of the C or FORTRAN parts of GRACE.

Suggestions for further work:

The major limiting factor in the future of GRACE is the inefficient way it performs calculations. The problem is that *ab initio* codes are re-launched for every single-point calculation and the CHARMM to GRACE communication method is very slow for the transfer of array data. If the input and output utility routines from GRACE were compiled into CHARMM, then the interface with CHARMM would be very fast. A simple alteration to the GAMESS_UK and

CADPAC codes would allow them to receive updated structures and recompute the energy and gradient, rather than being re-launched.

These efficiency improvements would allow GRACE to perform molecular dynamics of qm/mm systems and then start to realise the 'dynamics or rare events' ideas covered in the literature review of this thesis.

The implementation of the three layer polarised qm/mm model (see chapter 7), using semi-empirical quantum mechanics, would give a very fast, near-linear-scaling, qm/mm model. This would prevent the need for some of the elaborate molecular truncations that were used for the lactate dehydrogenase work discussed in this thesis (see chapter 9).

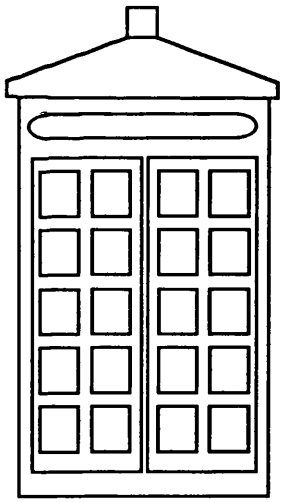

- *AB-INITIO* QM/MM
- STRUCTURED PROGRAMMING
- INTERNAL CO-ORDINATE GENERATION
- LOAN PAIR LOCATION
- SADDLE SEARCH
- IRC CALCULATION
- HESSIAN GENERATION
- VIBRATIONAL FREQUENCIES
- ISOTOPE EFFECTS
- PARTIAL CHARGE FITTING
- DATA HANDLING
- LINEAR ALGEBRA

Fig B.4: Like the 'Tardis' from the popular T.V. series Dr. Who, GRACE is 'bigger on the inside than the outside'. At the time of writing GRACE consists of about 40 000 lines of code (not including the TCL interpreter its self). This relatively small program offers all the listed features and so goes far beyond the abilities of the programs it controls.

References

The format of references is:

Authors

'Title'

Journal, volume,(binding)$_{\text{(if quoted)}}$*,page/s* $_{\text{(if quoted)}}$ *, (year)*

1 **H. Eyring and M. Polanyi,**

'Über einfache Gasreaktionen'

Z. Phys. Chem. B, 12,(4),279-311(1931)

2 **J.A. Barnes, J. Wilkie and I.H. Williams**

'Transition-state structure variation and mechanistic change'

J. Chem. Soc., Faraday Trans. 90,(12), 1709-1714,(1994)

3 **K. Fukui,**

'The path of chemical reactions - the IRC approach'

Acc. Chem. Res. 14,(12), 363-368,(1981)

4a **K. Muller and L.D. Brown**

'Location of saddle points and minimum energy paths by a constrained

simplex optimisation procedure'

Theoret Chim. Acta 57,75-93, (1979)

b. **R.S. Berry, H.L. Davis and T.L. Beck**

'Finding saddles on multi-dimensional potential surfaces'

Chem. Phys. Letters 147,(1),13-17,(1988)

5 **I.H. Williams**

"Interplay of theory and experiment in the determination of transition-state structure'

Chem. Soc. Rev. 22,(4), 277-283,(1993)

6 **D.M. Hirst,**

'A Computational Approach to Chemistry'

Blackwell Scientific Publishing, Oxford, 1990

7 **D.G. Truhlar, B.C. Garrett and S.J. Klippenstein**

'Current status of transition state theory'

J. Phys. Chem. 100,(31),12771-12800,(1996).

8 **M.J. Pilling and P.W.Seakins**

'Reaction Kinetics'

Oxford University Press, Oxford, 1995

9a **M. Strnad, M. T. C. Martins-Costa, C. Millot, I. Tunon, M. F. Ruiz-Lopez and J.-L. Rivail**

'Molecular dynamics simulations of elementary chemical processes in liquid water using combined density functional and molecular mechanics potentials .2. Charge separation processes'

J. Chem. Phys. 106,(9),3643-3657,(1997)

9b **E.A. Carter, G. Ciccotti, J.T. Hynes and R. Kapral**

'Constrained reaction coordinate dynamics for simulation of rare events'

Chem. Phys. Lett. 156,(5),472,(1989)

10 **A. Warshel**

'Computer Modeling of Chemical Reactions in Enzymes and Solutions'

John Wiley & Sons, New York, 1986

11 **W.D. Gwinn**

'Normal Coordinates: General Theory, Redundant Coordinates, and General Analysis Using Electronic Computers'

J. Chem. Phys. (1971)

12 **C. Doubleday, J. McIver, M Page and T. Zielinski**

'Temperature-dependence of transition-state structure for the disproportionation of hydrogen-atom with ethyl-radical.

J. Am. Chem. Soc. 107,(20),5800-5801,(1985)

13a **A. J. Bennet and M. L. Sinnott**

'Complete kinetic isotope effect description of transition-states for acid catalysed hydrolysis of methyl alpha-glucopyranosides and beta-glucopyranosides'

J. Am. Chem. Soc. 108,(23),7287-7294 (1986)

b **D. Tull and S. G. Withers**

'Mechanisms of cellulases and xylannases -

a detailed kinetic study of the exo-beta-1,4-glycannase from Cellulomnas Fimi'

Biochemistry, 33,(20),6363-6370 (1994)

14a **U.C. Singh, F.K. Brown, P.A. Bash and P,A, Kollman**

'An approach to the application of free-energy perturbation-methods using molecular dynamics-application to the transformation of CH_3OH-CH_3CH_3, H_3O - NH_4, Glycine-alanine, and alanine-phenyl alanine in aqueous solution and to $H_3O(H_2O)_3$ - $NH_4(H_2O)_3$ in the gsa phase'

J. Am. Chem. Soc. 109,(6), 1607-1614,(1987)

b **P. Cieplak, P.A. Bash, U.C. Singh and P.A. Kollmans**

'A theoretical study of tautomerism in the gas phase and aqueous solution - a combined use of state of the art ab-initio quantum mechanics and free energy perturbation methods'

J. Am. Chem. Soc. 109,(20), 6283-6289,(1987)

c **D.A. Pearlman and P.A. Kollman**

'The lag between the hamiltonian and the system configuration in free energy perturbation calculations'

J. Chem. Phys. 91,(12), 7831-7839,(1989)

15 **M.C. Flanigan, A. Komornicki and J. W. McIver**

'Theoretical chemistry, vol 8 Semiempirical methods of electronic structure theory, Part B: Application', ed. G A Segal

Plenum Press, New York 1977 p.1.

16 **J. A. Barnes and I. H. Williams**

'Theoretical modeling of kinetic isotope effects for glycoside hydrolysis in aqueous solution by a qm/mm method'

J. Chem. Soc., Chem. Commun. (2),193-194,(1996)

17 **I. H. Williams**

'Deuterium fractionation factors for carbon - hydrogen bonds. Calculations using scaled quantum-mechanical force constants'

J. Phys. Org. Chem., 3, 181-190 (1990)

18a **M. C. Strain, G. E. Scuseria and M. J. Frisch**

'Achieving linear scaling for the electronic quantum coulomb problem'

Science, 271, (5245), 51-53 (1996)

b **S. L. Dixon and K. M. Merz**

'Semi empirical molecular orbital calculations with linear system size scaling'

J. Chem. Phys., 104,(17),6643-6649 (1996)

c **R. T. Gallant and A. St Amant**

'Linear scaling for the charge-density fitting procedure of the linear combination of gaussian-type orbitals density functional method'

Chem. Phys. Letters., 256,(6),569-574 (1996)

19 **J.M. Millam and G. E. Scuseria**

'Linear scaling conjugate gradient density matrix search as an alternative to diagonalisation for first principles electronic structure calculations'

J. Chem. Phys. 106,(13),5569-5577 (1997)

20 **D. B. Boyd**

'Reviews of computational Chemistry, vol 1'

Ed. K. B. Lipkowitz and D. B. Boyd

VCH New York, 1990

21 **M. J. S. Dewar, W. Thiel**

'Ground states of molecules. 38. The MNDO method . Approximations and parameters'

J. Am. Chem. Soc., 99,(15), 4899-4917, (1977).

22 **M. J. Field, P. A. Bash and M. Karplus**

'A combined quantum mechanical and molecular mechanical potential for molecular dynamics simulations'

J. Comput. Chem. 11,(6),700-733, (1990)

23 **A. Warshel and M. Levitt**

'Theoretical studies of enzymic reactions:

Dielectric, electrostatic and steric stabilization of the carbonium ion in the reaction of lysozyme.

J. Mol. Biol. 103,(2), 227-249 (1976)

24 **J. Wang, R. J. Boyd and A. Laaksonen**

'A hybrid quantum mechanical force field molecular dynamics simulation of liquid methanol: Vibrational frequency shifts as a probe of the quantum mechanical/molecular mechanical coupling'

J. Chem. Phys, 104 (18),7261-7269 (1996)

25 **I. Tuñón, M. T. C. Martins-Cosnta, C. Millot,**

M. F. Riuz-Lopez and J. L. Rivail

'A coupled density functional-molecular mechanics monte carlo simulation method:

The water molecule in liquid water'

J. Comput. Chem, 17,(1),19-29 (1996)

26 **J. Gao**

'Hybrid quantum and molecular mechanical simulations:

An alternative avenue to solvent effects in organics chemistry'

Acc. Chem. Res. 29,(6),298-305(1996)

27 **A. Klamt and G. Schüürmann**

'COSMO - a new approach to dielectric screening in solvents with explicit expressions for the screening energy and its gradient.'

J. Chem. Soc., Perkin Trans. 2,(5),799-805,(1993)

28 **V. Dillet, D. Rinaldi, J Bertrán and J-L Rivail**

'Analytic energy derivatives for a reaclistic continuum model of solvation - application to the analysis of solvent effects on reaction paths'

J. Chem. Phys. 104,(23),9437-94444,(1996)

29 **C. J. Cramer and D.G. Truhlar**

'A scf solvation model for the hydrophobic effect and absolute free energy of aqueous solvation'

Science 256,(5054),213-217,(1992)

30a **B. R. Brooks, R. E. Bruccoleri, B. D. Olafson, D. J. States S. Swaminathan and M. Karplus**

'CHARMM: A program for macromolecular energy, minimisations and dynamics calculations'

J. Comput. Chem. 4,(2),187-217,(1983)

b CHARMM24b2- **M. Karplus**

Harvard University. 1996

31 **Gaussian 94**

M. J. Frisch, G. W. Trucks, M. Head-Gordon, P. M. W. Gill, M. W. Wong, J. B. Forman, B. G. Johnson, H. B. Schlegel, M. A Robb, E. S. Replogle, R. Gomperts, J. L. Andres, K. Raghavachari, J. S. Binkley, C. Gonzalez, R. L. Martin, D. J. Fox, D. J. Defrees, J. Baker, J. J. P. Stewart and J. A. Pople, Gaussian, Inc., Pittsburgh PA, 1994.

32 **The Cambridge Analytical Derivatives Package Issue 6**

Cambridge 1995.

R. D. Amos

Contributors:

I. L. Alberts, J. S. Andrews, S. M. Colwell, N. C. Handy, D. Jayatilaka, P. J. Knowles, R. Kobayashi, K. E. Laidig,

G. Laming, A. M. Lee, P. E. Maslen, C. W. Murray,

J. E. Rice, E. D. Simandiras, A. J. Stone, M. -D. Su and

D. J. Tozer.

33 **GAMESS-UK is a package of *ab initio* programs written by**

M. F. Guest, J. H. van Lenthe, K. Schoffel, P. Sherwood,

and R. J. Harrison.

Contributors:

R. D. Amos, R. J. Buenker, M. Dupuis, N. C. Handy, I. H. Hillier,

P. J. Knowles, V. Bonacic-Koutecky, W. von Niessen,

V. R. Saunders and A. J. Stone. The package is derived from the

origiinal GAMESS code due to M. Dupuis, D. Spangler and

J. Wendoloski.

Daresbury Laboratories (1995-7)

34 **K. M. Merz and L. Banci**

'Binding of bicarbonate to human carbonic anhydrase II:

A continuum of binding sites'

J. Am. Chem. Soc. 119,(5),863-871,(1997)

35 **P. D. Lyne, A. J. Mulholland and W. G. Richards**

'Insights into chorismate mutase catalysis from a combined qm/mm simulation of the enzyme reaction'

J. Am. Chem. Soc. 117,(45),11345-11350,(1995)

36 **A. J. Mulholland and W. G. Richards**

'Acetyl-CoA enolization in citrate synthase: A quantum mechanical/molecular mechanical (qm/mm) study'

Proteins: Structure, Function, and Genetics 27,(1),9-25,(1997)

37 **P. A. Kollman**

'Theory of enzyme mechanisms'

Current Opinion in Structural Biology 2,765-771,(1992)

38 **M.J. Harrison, N. A. Burton, I. H. Hillier and I. R. Gould**

'Mechanism and transition state structure for papain catalysed amide hydrolysis, using a hybrid qm/mm potential'

J. Chem. Soc., Chemical Communications (24),2769-2770,(1996)

39a **Binkley, Pople and Hehre**

J. Am. Chem. Soc 102,939,(1980)

b **Gordon, Binkley, Pople, Pietro and Hehre**

J. Am. Chem. Soc. 104,2797,(1982)

c **Ditchfield Pople and Hehre**

J. Chem. Phys., 54,724,(1971)

d **Pople and Hehre**

J. Chem. Phys., 56,4233,(1972)

e **Krishnan, Binkley, Seeger and Pople**

J. Chem.Phys., 72,650,(1980)

40 **M. A. Thompson**

'Molecular-dynamics study of new rigidified 18-crown-6 derivative using qm/mm modeling'

Int. J. Quantum Chem, 60,(6),1133-1141,(1996)

41 **T. Kerdcharoen, K. R. Liedl and B. M. Rode**

'A qm/mm simulation method applied to the solution of Li^+ in liquid ammonia'

Chemical Physics, 211,(1-3),,313-323,(1996)

42a **F. Maseras and K. Morokuma**

'IMOMM: A new integrated *ab initio* + molecular mechanics geometry optimisation scheme of equilibrium structures and transition states'

J. Comput. Chem. 16,(9),1170-1179,(1995)

b **M. Svensson, S. Humbel, R. D. J. Froese, T. Matsubara, S. Sieber and K. Morokuma**

'ONIOM: A multilayered integrated MO + MM method for geometry optimisation and signle point energy predictions. A test for Diels-Alder reactions and $Pt(P(t\text{-}But)_3)_2$ + H_2 oxidative addition'

J. Phys. Chem,100,(50),19357-19363,(1996)

43a **M. M. Francl and L. E. Chirlian**

'Atomic charges derived from electrostatic potentials - a detailed study'

J. Comput. Chem. 8,(6),894-905(1987)

b **C. M. Breneman and K. B Wilberg**

'Determining atom-centered monopoles from molecular electrostatic potential - the need for high sampling density in foramide conformational-analysis'

J. Comput. Chem. 11,(3),361-373,(1990)

44 **M. M. Francl, C. Carey, L. E. Chirlian and D. M. Gange**

'Charges fit to electrostatic potentials .2. Can atomic charges be unambiguously fit to electrostatic potentials?'

J. Comput. Chem. 17,(3), 367-383,(1996)

45 **B.H. Besler, K.M. Merz Jr. and P.A. Kollman**

'Atomic Charges Derived from Semi-empirical Methods'

J. Comput. Chem., 11,431-439,(1990)

46 **C.A. Reynolds, G.G. Ferenczy and W.G. Richards**

'Methods for determining the reliability of semi-empirical electrosstatic potentials and potential derived charges'

Theochem- J. Mol. Struct. 88,249-269,(1992)

47 **D. Bakowies and W. Thiel**

'Semiempirical treatment of electrostatic potentials and partial charges in combined quantum mechanical molecular mechanical approaches'

J. Comput. Chem., 17,(1),87-108,(1996)

48 **W.H. Press *et al.***

'Numerical recipes: the art of scientific computing'

Cambridge University Press: Cambridge (1986)

49 **H. B. Schlegel**

'Optimisation of equilibrium geometries and transition structures'

J. Comput. Chem. 3,(2),214-218 (1982)

50 **D.C. Liu and J. Nocedal**

'On the limited memory BFGS method for large scale optimisation'

Mathematical Progamming 45,(3),503-528,1989

51 **H. B. Schlegel**

'A comparison of geometry optimisation with internal, cartesian and mixed co-ordinates'

Int. J. Quantum Chem., Quantum Chem. Symp. 26,243-252 (1992)

52 **C.Y. Peng, P Y. Ayala and H. B. Schlegel**

'Using redundant internal co-ordiantes to optimise equilibrium geometries and transition states'

J. Comput. Chem. 17,(1),49-56 (1996)

53 **S. Bell and J. S. Crighton**

'Locating transition states'

J. Chem. Phys. 80,6,2464 (1984)

54 **J. Baker**

'An algorithm for the location of transition states'

J. Comput. Chem. 7,4,3850395 (1986)

55 **A. Banerjee, N. Adams, J. Simons and R. Shepard**

'Search for stationary-points on a surface'

J. Phys. Chem., 89,(1),52-57 (1985)

56 **C. J. Cerjan and W. H. Miller**

'On finding transition states'

J. Chem. Phys. 75,(6),2800-2806 (1981)

57 **S. S-L. Chiu, J. W. McDouall and I. H. Hillier**

'Prediction of whole reaction paths for large molecular systems'

J. Chem. Soc. Faraday Trans. 90(12),1575-1579(1994)

58 **M. J. S. Dewar, E. F. Healy and J. J. P. Stewart**

'Location of transition states in reaction mechanisms'

J. Chem. Soc., Faraday Trans. 2,(3),227-233 (1984)

59 **S. F. Fischer and M. Karplus**

'Conjugate Peak refinement: an algorithm for finding reaction paths and accurate transition states in systems with many degrees of freedom'

Chemical Physics Letters 194,(3),252-261 (1992)

60a **J.J.P. Stewart and Fujitsu Limited**

MOPAC 93

Tokyo, (1993)

b **J. J. P. Stewart**

'MOPAC 6'

(QCPE455),QCPE Bull. 10,86,(1990)

61 **J.K. Ousterhout.**

'Tcl and Tk toolkit'

Addison Wesley (1994) ISBN 0-201-6337-X

62 **I. H. Williams**

'CAMVIB and CAMISO'

Chem. Phys. Lett., 88,(5),462-466,(1982)

Theochem - J. Mol. Struct., 11,(3-4),275-284,(1983)

63 **R. Sayle**

'RasMol v2.5: A molecular visualisation Program'

Biomolecular Structure, Glaxo Research and Development, Greenford, Middlexsex, UK.

64 **dba Minnesota Supercomputer Center Inc.**

'Xmol version 1.3.1'

65 **P. Culot, G Dive, V. H. Nguyen and J. M. Ghuysen**

'A quasi-newton algorithm for 1st order saddle-point location'

Theoret. Chimi. Acta 82,(3-4),189-205(1992)

66 **K.T. Leffek and J.W. Maclean**

'Secondary kinetic isotope effects in biomolecular nucleophilic substitutions

II, α- Deuterium effects in Measchutkia reactions of methyl iodide'

Canad. J. Chem. 43,40-46(1965)

67 **J.A. Llewellyn, R.E. Robertson and J.M. Scott**

'Some deuterium isotope effects: I. Water solvolysis of methyl-d, esters'

Canadian J. Chem. 38,222-232,(1960)

68 **M. J. D. Powell**

'Restart procedures for the conjugate gradient method'

Mathematical Programming 12,241-254(1977)

69 **K. Okamoto, S. Fukui, I. Nitta and H. Shingu**

Bull. Chem. Soc. Jpn. 40, 2354 (1967)

70 **J. Wilkie and I. H. Williams**

'Transition-state structural variation in a model for carbonyl reduction by lactate dehydrogenase: Computational validation of empirical predictions based upon Albery-More O'Ferrall-Jencks diagrams'

J. Am. Chem. Soc. 114,(13),5423-5424,(1992)

71 **C.Møller and M.S. Plesset**

Physical Review, 46,618,(1934)

72 **N.L. Allinger and Y. Yuh**

'MM2'

Q.C.P.E., 12,395(1980)

73 **N.L. Allinger**

'MM3'

Q.C.P.E. (1992)

74 **DGELSS**

Univ. of Tennessee, Univ. California Berkley, NAG Ltd.,

Courant Institute, Argonne National Lab and

Rice Univ. ; Sept. 30, 1994

75 **W.L. Jorgensen, J. Chandrasekhar, J.D. Madura, R.W. Impey and M.L. Klein**

Chemtracts: Org. Chem, 4,91,(1991)

76 **Dr T. Dafforn (University of Bristol),**

personnal communication to Prof. I. H. Williams

September 1996

77a **A.D. Mackerell Jr.**

'Developmental parameter file for proteins'

Unplublished work, (1996)

b **J.J. Pavelites, J Gao, P.A. Bash and A.D. Mackerell Jr.**

'A molecular mechanics force field for NAD^+, NADH, and the pyrophosphate groups of nucleotides'

J. Comput. Chem. 18,(2),221-239,(1997)

78 **D.J. States, M. Karplus and M.J. Field**

Unpublished work

79 **M.J.S. Dewar, E.G. Zoebisch, E.F. Healy and J.J.P. Stewart**

'AM1: A new gneral purpose quantum mechanical molecular model'

J. Am. Chem. Soc., 107, 3902-3909,(1985)

80 **J. Andrés, V. Moliner, J. Krechl and E. Silla**

'Transition state structures for the molecular mechanism of lactate dehydrogenase enzyme'

J. Chem. Soc. Perkin Trans. 2,1551-1558,(1995)

81a **J. Wilkie and I.H. Williams**

'Geometrical preferences for general acid-catalysed hydride transfer: comparative theoretical study of transition structures for reduction of formaldehyde'

J. Chem. Soc. Perkin Trans., 2,1559-1567,(1995)

b **J. Wilkie and I.H. Williams**

'Transition-state structural variation in a model for carbonyl reduction by lactate dehydrogenase: Computational validation of the empirical predictions based upon Albery-More O'Ferrall-Jencks diagrams'

J. Am. Chem. Soc., 144,5423-5425,(1992)

82 **A. Yadav, R.M. Jackson, J.J. Holbrook and A. Warshel**

'Role of solvent reorganisation energies in the catalytic activity of enzymes'

J. Am. Chem. Soc., 113,4800-4805,(1991)

83 **C.L. Brooks and M. Karplus**

J. Mol. Biol. 208,159-181,(1989)

84 **S. Nakagawa, A.H. Yu, M. Karplus and H. Umeyama**

Proteins 16,172-194,(1993)

85 **D.B. Wigley, S.J. Gamblin, S.P. Turkenburg, E.J. Dodson, K. Piontek, H. Muirhead and J.J. Holbrook**

J. Mol. Biol. 223, 317,(1992)

86 **H. Deng, J. Zheng, A. Clarke, J.J. Holbrook, R. Callender and J.W. Burger**

'Source of catalysis in the lactate dehydrogenase system. Ground-state interactions in the enzyme-substrate complex'

Biochemistry, 33,(8),2297-2305,(1994)

87 **A.R. Clarke, H.M. Wilks, D.A Barstow, T. Atkinson, W.N. Chia and J.J. Holbrook**

'An investigation of the Contribution made by the carboxylate group of an active site histidine-aspartate couple to binding and catalysis in lactate dehydrogenase.'

Biochemistry, 27,1617-1622,(1988)

88 **L. Verlet**

Phys. Rev. 159,98,(1967)

89 **C.J. Cramer and D.G. Truhlar**

Science,256,213,(1992)

90 **A.R. Clarke, H.M. Wilks, D.A Barstow, T. Atkinson,**

W.N. Chia and J.J. Holbrook

'Site-directed mutagenesis reveals role of mobile arginine residue in lactate dehydrogenase catalysis'

Nature, 334,(18/25),699-702,(1986)

91 **M.L. Connolly**

'Solvent-accessible surfaces of proteins and nucleic acids'

Science, 221,709,(1983)

92 **A.K. Soper and M.G. Phillips**

Chem. Phys., 67,47,(1986)

93a **C.G. Broyden**

J. Inst. Math. Appl., 6,76,(1970)

b **R. Fletcher**

Comput. J., 13,317,(1970)

c **D. Goldfarb,**

Math. Comput., 24,23,(1970)

d **D.F. Shanno**

Math. Comput., 24,647,(1970)

94a **A.J. Kresge, R.F. More O'Ferral and M.F. Powell**

'Isotopes in organic chemistry'

edited by E. Buncel and C.C Lee

Vol 7. Elsevier, Amsterdam, 177,(1986)

b **W.W Cleland**

Methods Enzymol. 64,104, (1980) & 87,625,(1982)

c **C.A. Lewis and R. Wolfenden**

Biochemistry, 16,4886,(1977)

d **H.P. Meloche, C.T. Monti and W.W Cleland**

Biochim. Biophys. Acta, 480,517,(1977)

95 **R.P. Bell**

'The Tunnel Effect in Chemistry'

Chapman and Hall, London, 1980

96 **M.J.D Powell**

Mathematical Programming, 1,26,(1971)

97 **V. Moliner, A.J. Turner and I.H. Williams,**

'Transition-state structural refinement with GRACE and CHARMM:

realistic modelling of lactate dehydrogenase using a combined

quantum/classical method'

J. Chem. Soc., Chem. Commun. (1997) issue 14, 1271 - 1272

Acknowledgements

I present a woefully inadequate list of those to whom I owe many thanks for helping me achieve the creation of this thesis and the research that went into it.

Institutions:

BBSRC

For financial support through the award of a CASE studentship.

CLRC Daresbury Laboratory:

For sponsorship of my studies through the CASE scheme.

University of Bath

For the provision of research facilities.

SmithKline Beecham

For the donation of a computer workstation for my personal use.

Individuals:

Amongst so many-

Prof. I.H. Williams, for his excellent supervision.

Dr P. Sherwood, for many hours of patient tuition.

Dr T. Mitchell, for an introduction to CHARMM programming.

Dr C.F. Rodriquez, for unfailing support, especially during my defence.